HEAT-TRANSFER ANALYSIS OF DOUBLE-PIPE HEAT EXCHANGERS FOR INDIRECT-CYCLE SCW NPP

by

Harwinder Thind

A Thesis Submitted in Partial Fulfillment

of the Requirements for the Degree of

Master of Applied Science

Nuclear Engineering

The Faculty of Energy Systems and Nuclear Science

University of Ontario Institute of Technology

April, 2012

ABSTRACT

SuperCritical-Water-cooled Reactors (SCWRs) are being developed as one of the Generation-IV nuclear-reactor concepts. SuperCritical Water (SCW) Nuclear Power Plants (NPPs) are expected to have much higher operating parameters compared to current NPPs, i.e., pressure of about 25 MPa and outlet temperature up to 625 ^{o}C. This study presents the heat transfer analysis of an intermediate Heat exchanger (HX) design for indirect-cycle concepts of Pressure-Tube (PT) and Pressure-Vessel (PV) SCWRs. Thermodynamic configurations with an intermediate HX gives a possibility to have a single-reheat option for PT and PV SCWRs without introducing steam-reheat channels into a reactor. Similar to the current CANDU and Pressurized Water Reactor (PWR) NPPs, steam generators separate the primary loop from the secondary loop. In this way, the primary loop can be completely enclosed in a reactor containment building.

This study analyzes the heat transfer from a SCW primary (reactor) loop to a SCW and Super-Heated Steam (SHS) secondary (turbine) loop using a double-pipe intermediate HX. The numerical model is developed with MATLAB and NIST REFPROP software. Water from the primary loop flows through the inner pipe, and water from the secondary loop flows through the annulus in the counter direction of the double-pipe HX. The analysis on the double-pipe HX shows temperature and profiles of thermophysical properties along the heated length of the HX.

It was found that the pseudocritical region has a significant effect on the temperature profiles and heat-transfer area of the HX. An analysis shows the effect of variation in pressure, temperature, mass flow rate, and pipe size on the pseudocritical region and the heat-transfer area of the HX. The results from the numerical model can be used to optimize the heat-transfer area of the HX. The higher pressure difference on the hot side and higher temperature difference between the hot and cold sides reduces the pseudocritical-region length, thus decreases the heat-transfer surface area of the HX.

ACKNOWLEDGEMENTS

First and foremost, I am deeply grateful to my supervisors, Dr Pioro and Dr Harvel, for their contributions of time and ideas to make my research experience productive and stimulating. I sincerely appreciate their constant guidance and support during the period of this work and most of all, their patience and understanding. It has been an honour to work with them.

I would also like to thank my colleagues Jeffrey Samuel, Andrew Lukomski, Eugene Saltanov, Wargha Peiman, and Lisa Grande who contributed immensely through their valuable analytical discussions. The group has been a source of friendships as well as good advice and collaboration.

I gratefully acknowledge the financial support from the NSERC/NRCan/AECL Generation IV Energy Technologies Program that made this effort easier.

Finally, I would like to thank my family, especially my father and brother for all their encouragement. And most of all for the loving support and patience of my wife and sons throughout this research endeavour.

TABLE OF CONTENTS

LIST OF FIGURES

LIST OF TABLES

NOMENCLATURE

A	area, m^2
Cp	specific heat, J/kg·K
$\overline{Cp}$	average specific heat, J/kg·K $\left(\frac{H_w - H_b}{T_w - T_b}\right)$
D	diameter – outer pipe, m
d	diameter – inner pipe, m
E	Young's modulus of elasticity, Pa
G	mass flux, kg/m^2s
H	enthalpy, J/kg
HTC	heat transfer coefficient, W/m^2K
k	thermal conductivity, W/m·K
L	length, m
$\dot{m}$	mass-flow rate, kg/s
N	number of tubes
n	node
P	pressure, Pa
Q	total heat transfer rate, W
$\dot{Q}$	heat transfer per unit mass, J/kg
q	heat flux, W/m^2
R	thermal resistance, K/W
S	entropy, J/kg·K
s	maximum allowable stress in tension, MPa
T	temperature, ^oC or K
U	overall heat transfer coefficient, W/m^2K
$\dot{W}$	work per unit mass, J/kg

Greek Letters

$\triangle$	difference
δ	thickness, m
η	efficiency

μ	viscosity, Pa·s
ν	Poisson's ratio
ρ	density, kg/m^3

Dimensionless numbers

Nu	Nusselt number $\left(\frac{HTC \cdot D}{k}\right)$
Pr	Prandtl number $\left(\frac{\mu \cdot C_p}{k}\right)$
$\overline{\mathbf{Pr}}$	average Prandtl number $\left(\frac{\mu \cdot \bar{C}_p}{k}\right)$
Re	Reynolds number $\left(\frac{G \cdot D}{\mu}\right)$

Subscripts and Superscripts

b	bulk
c	cold
cr	critical
el	electric
h	hot
hy	hydraulic
i	inner
n	node
o	outer
pc	pseudocritical
th	thermal
w	wall

Acronyms

ACR	Advanced CANDU Reactors
AECL	Atomic Energy of Canada Limited
BWR	Boiling Water Reactor

CANDU	CANada Deuterium Uranium
ChUWR	Channel-type Uranium-graphite Water Reactor
DHT	Deteriorated Heat Transfer
GEN-IV	Generation IV
GFR	Gas cooled Fast Reactor
GIF	Generation IV International Forum
HP	High Pressure
HWR	Heavy Water Reactor
HX	Heat exchanger
IAEA	International Atomic Energy Agency
INEEL	Idaho National Engineering and Environmental Laboratory
IHT	Improved Heat Transfer
IP	Intermediate Pressure
LFR	Lead-Cooled Fast Reactor
LP	Low Pressure
LWR	Light Water Reactor
MATLAB	MATrix LABoratory
MSR	Molten Salt Reactor
NHT	Normal Heat Transfer
NIST	National Institute of Standards and Technology
NPD	Nuclear Power Demonstrator
NPP	Nuclear Power Plant
NRCan	Natural Resources Canada
NSERC	Natural Sciences and Engineering Research Council
PT	Pressure-Tube
PV	Pressure-Vessel
PVWR	Pressure-Vessel Water Reactor
PWR	Pressurized Water Reactor
REFPROP	REFerence fluid thermodynamic and transport PROPerties
RMS	Root Mean Square
SC	SuperCritical

SCLWR-H	SuperCritical Light Water Reactor with High temperature
SCW	SuperCritical Water
SCWR	SuperCritical-Water-cooled Reactor
SFR	Sodium-Cooled Fast Reactor
SG	Steam Generator
SHS	Super-Heated Steam
USA	United States of America
VHTR	Very-High-Temperature Reactor
WNA	World Nuclear Association

CHAPTER 1 - INTRODUCTION

Currently there are about 2 billion people having no access to electricity and as predicted by the International Atomic Energy Agency (IAEA) the world population is going to increase from 6.6 billion in 2007 to 8.2 billion by 2030 (Hore-Lacy, 2003). The increasing standard of living in developing countries and population growth will require strong growth in electricity and energy consumption. The current worldwide electricity source, consists of approximately coal: 41%, gas 20%, oil 6%, nuclear 15%, and hydro and renewable together 18%.

According to scientists the green house effect needs to be reduced to avoid catastrophic change in our planet climate system. China is planning tremendous development of nuclear power construction to achieve low carbon economy (Lu *et al*. 2011). Power can be achieved by reducing dependency on coal and using other technologies in abundance such as nuclear and other renewable energy sources. Renewable energy sources are more suitable for small localized supply or intermittent supply of electricity due to variability in production. Figure 1.1 shows load curves for a typical electric grid for electricity demand in a given day. The base load typically represents 60-75% of the peak value depending upon the season. Conservation and load shifting will be important contributors, but are not expected to make significant changes to the cycles in the near term. Thus, variable energy sources are best used for the cyclic load. On the other hand, the nuclear energy option is capable of handling continuous base-load supply of electricity with minimum green house emissions; hence nuclear is an optimal technology for the base load. Nuclear technology at present is considered to be inexpensive and moderately efficient when compared with current coal plant technology.

To make nuclear power plants more efficient and more economical, research activities are being conducted around the world to develop Generation-IV nuclear reactors concepts. Although existing nuclear reactor designs, (denoted as Generation II and III reactors) provide a reliable, economic, and publicly acceptable supply of electricity in existing markets, further advances in nuclear energy system design can broaden the

opportunities for the use of nuclear energy. The thermal efficiency of existing Nuclear Power Plants (NPPs) are modest (30-35%), whereas the thermal efficiency of Generation IV type reactors is expected to be approximately 45-50%, closer to that of modern thermal (coal) power plants.

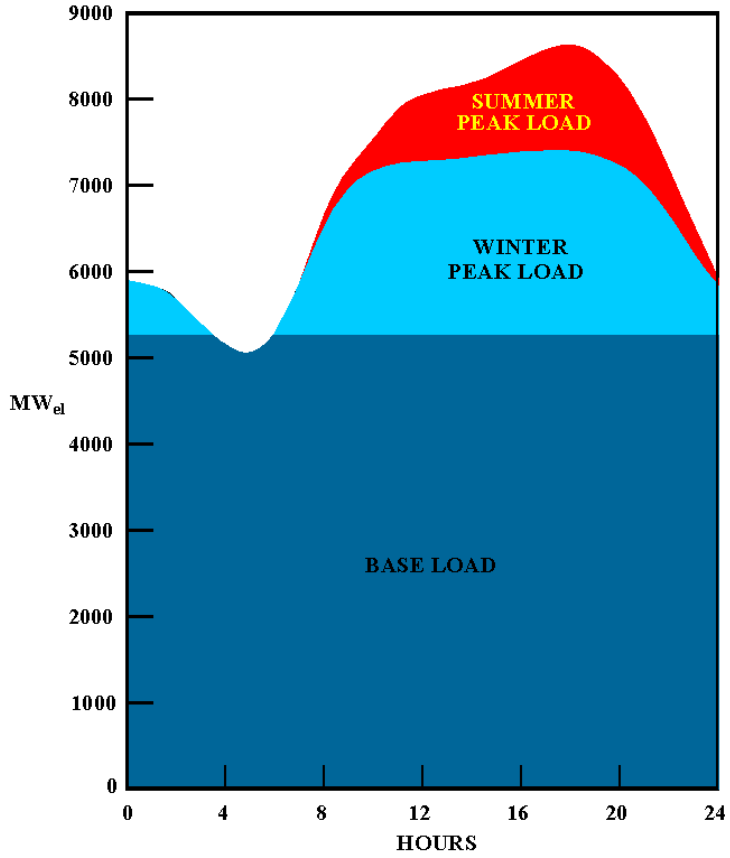

Figure 1.1: Load curves for typical electric grid for two seasons (WNA, 2010).

Since the characteristics of Generation IV NPPs differ significantly from those of current Generation II and III NPPs, the economic competitiveness of Generation IV NPPs are not compared with alternative nuclear technologies or systems, but rather are compared to advanced fossil alternatives. Apart from thermal efficiency and economic competitiveness, other benefits for Generation IV reactors are to provide continued sustainability, safety and reliability, and proliferation resistance.

There are six Generation IV nuclear reactor design concepts being considered by the Generation IV International Forum (GIF). Chapter 2 briefly discusses the characteristics

of these concepts. Most of these designs are not expected to be available for commercial construction before 2030. One of these six concepts is the Super-Critical Water-Cooled Reactor (SCWR) design. The SCWR concept was first investigated near the end of the 1950s and at the beginning of the 1960s. After almost 30 years, SCWR concepts became popular for research and development due to the requirement to have better performance in the thermal efficiency. Several concepts of SuperCritical Water-cooled nuclear Reactors were subsequently developed (Pioro and Duffey, 2007). At present, several countries including Canada, Japan, China and Russia are further investigating and developing the SCWR concept.

Super-Critical Water (SCW) NPPs are expected to have much higher operating parameters compared to current NPPs (i.e., pressure of about 25 MPa and outlet temperatures up to 625^{o}C.). Due to higher operating temperatures, SCWRs can facilitate an economical co-generation of hydrogen through thermo-chemical cycles or direct high-temperature electrolysis. The SCWR concepts (Pioro and Duffey, 2007) follow two main types: (a) A large reactor Pressure Vessel (PV) with a wall thickness of about 0.5 m to contain the reactor-core heat source, analogous to conventional Light Water Reactors (LWRs); or (b) Pressure Tubes (PTs) or fuel channels analogous to conventional Heavy Water Reactors (HWRs). Within these two main classes (PV and PT), PT reactors are more flexible with respect to flow, flux and density changes than the PV reactors. A design whose basic element is a channel has an inherent advantage of greater safety than large vessel structures at supercritical pressures. Also as compared to PV reactors, the PT reactor design gives the flexibility of accommodating a single reheat option, which will include the addition of nuclear steam reheat to the reactor. However the addition of the steam-reheat option will increase the complexity of the reactor core design.

Single steam reheat cycles are widely used in both supercritical and subcritical steam cycles in fossil-fueled plants as an economical way to improve cycle efficiency. As a side benefit, it reduces the steam flow required for a given power output (and hence, reduces equipment size), and moreover, it reduces the steam moisture content in the Low Pressure (LP) turbine and eliminates the need for moisture-removal equipment (Duffey et al., 2008b). Also the vast majority of the modern and upcoming supercritical turbines are

single-reheat-cycle turbines. Due to the maturity and the high efficiency of a single reheat steam-cycle in modern thermal plants, the option of using similar technology in SCWR appears more practical.

In fossil-fuel plants the fuel is coal and in nuclear power plants the fuel is radioactive material, with safety being the highest priority in nuclear power plants, extra steps are taken during nuclear power plant design to avoid any radiation exposure. Hence different thermodynamic-cycles such as direct, dual and indirect cycle are being evaluated for SCWR concepts to help optimize these concepts in terms of safety, economics, and efficiency.

In a direct cycle SCW the supercritical steam is fed directly into the turbines. This may be the simplest approach with higher thermal efficiency and lower capital costs. This concept is also used for some Boiling Water Reactor (BWR) NPPs, in which the steam is fed directly into the turbines. However, at a BWR NPP, pressure and temperature parameters are significant lower than for a SCWR. (Pioro *et al*., 2010). Also the savings from the Steam Generator (SG) elimination in a BWR are offset to a certain extent by the extra safety shielding and access control required around the steam turbine during normal operations due to the potential radiation levels arising from the steam entering directly from the reactor core.

Both the dual and indirect cycles provide more safety and better control for nuclear reactor and turbine plant operations. These cycles have lower thermal efficiency compared to that of the direct cycle, but have increased safety in terms of an extra barrier between the reactor primary coolant, which may contain a certain level of radioactivity, and clean NPP equipment such as the turbine, feedwater heaters, circulation pumps, etc. In addition, the primary coolant may contain unwanted substances, which will deposit on turbine blades and other equipment.

Hence, the intermediate SCW Heat exchanger (HX) is investigated, as this will allow us to use the single-reheat option in both PV reactors and in PT reactors and it will reduce further complexity in the reactor core design. The HX will separate the primary loop from the secondary loop. The primary loop can be completely enclosed in the reactor

containment building, similar to the current CANada Deuterium Uranium (CANDU) and Pressurized Water Reactor (PWR) NPPs, in which the SG separates the primary loop from the secondary loop. The nuclear activities stay within the reactor containment building, and there is a reduced probability for radioactive contamination of equipment in the turbine building, thus reducing the chances of human interaction with radioactive materials. The separation of the primary and secondary loop will also allow control of the chemistry of both the loops independently.

As SCW NPPs will have much higher operating thermal hydraulic parameters, it is necessary to analyze the technical challenges and higher costs associated with SCW HXs, e.g., the material to be used for the HX, hydraulic resistance, heat transfer surface area, size of the HX, and number of units required. The higher cost and larger size of the HX might make it impractical to implement the indirect cycle for the SCW reactor.

1.1 Objective

The main objective of this work is to develop double pipe HX concepts for SCW applications and determine the technical viability of the indirect cycle. As mentioned above, the indirect cycle will allow the nuclear activity to stay within the reactor containment building, and allow for the implementation of the single reheat option in both PV and PT reactor concepts (PT reactors core design will be less complex).

Various sub-objectives need to be met to determine the technical viability of SCW HX concepts:

1. Develop SCW NPP layout options for indirect and single-reheat cycles for both PT and PV type nuclear reactors.

2. Determine operating parameters for SCW to SCW HX and SCW to Super-Heated Steam (SHS) HX based on reactor limitations and to match with availability of the vast majority of modern and upcoming Super Critical (SC) turbines.

3. Determine the appropriate correlation to predict accurate results for heat transfer calculations for a given parameter set of the SCW HX.

4. Develop a heat transfer model and analysis for double pipe heat HX for SCW to SCW and SCW to SHS.

5. Compare results of at least two types of SCW HX to determine their limitations.

6. Optimization and sensitivity analysis of the double pipe SCW HX design.

7. Determine the heat transfer surface area, number of units, approximate physical size of units.

Generation IV nuclear reactor concepts and types of HX are discussed in Chapter 2. SCW fluid properties and correlations are discussed in Chapter 3. SCWR concepts, SCW Turbines and SCWR cycles options are discussed and analyzed in Chapter 4. The methodology and system model is described in Chapter 5. The sensitivity analysis was performed on double pipe HX against various variables for e.g. pressure, temperature, pipe diameter, and mass flow rate to optimize the system performance and are described in Chapter 6.

CHAPTER 2 - LITERATURE REVIEW

This chapter briefly discusses relevant research and design activities on nuclear reactor systems starting from generation I to generation IV, and for heat exchangers for nuclear power plants. The six generation IV nuclear reactor systems under the Generation IV International Forum are highlighted and the main driving forces behind them are discussed. Various types of heat exchangers are evaluated to narrow down the choice of design based on the operating parameters limitations.

2.1 Generation IV Nuclear Reactor Concepts

At present the Generation IV (GEN-IV) International Forum (GIF) is a collaboration of 13 countries. GIF was formally founded in 2001 and selected six GEN-IV nuclear reactor concepts for further research and development. The objective of GEN-IV nuclear reactor systems is to provide safe, sustainable, economical, proliferation resistant, and physically secure solutions for future commercial development. Most of these designs are not expected to be available for commercial construction before 2030 (GIF, 2002).

Figure 2.1 shows the evolutionary path of nuclear reactor systems from generation I to generation IV in Canada. The generation I early prototype reactors/research, i.e., NPD (Nuclear Power Demonstrators) and Douglas Point reactor advances in 1950s and 1960s demonstrated the practicality of the CANDU system. In 1970, the generation-II reactors started development for large commercial power plants and most are still operating today. The CANDU 6 was the first commercial scale nuclear reactor built by AECL (Atomic Energy of Canada Limited) under generation-II. Generation III and generation III+ reactor developments in 1990s offer proven design, construction and operation. Advanced CANDU reactors, such as the Enhanced CANDU 6 and ACR 1000 are near term deployment plants. For Generation-IV plants, the expected operational time is year 2030 and beyond, these plants are expected to have thermal efficiency very close to modern fossil thermal power plants.

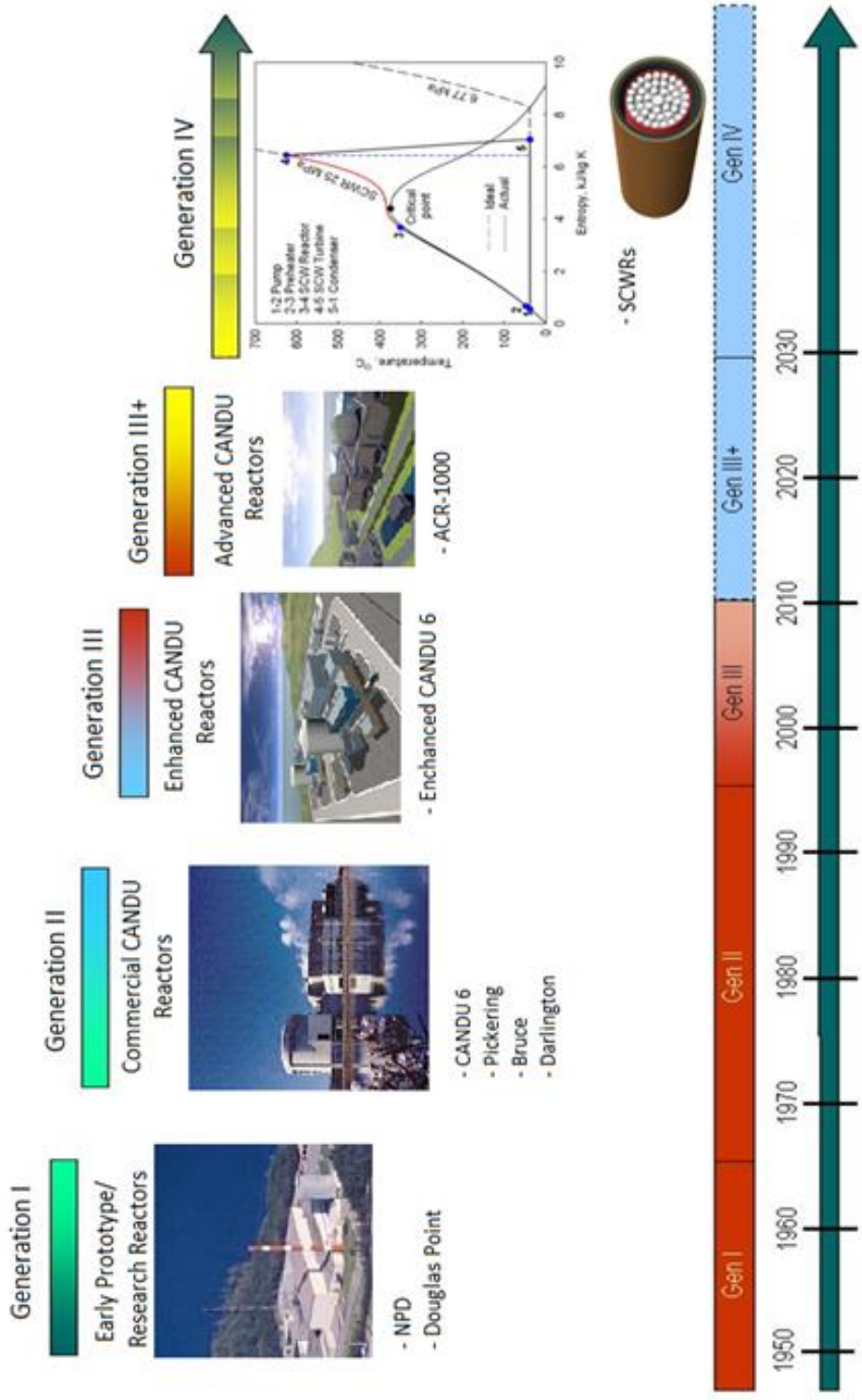

Figure 2.1: Evolution path of Canadian Nuclear Reactor Systems (courtesy of AECL and J. Samuel).

GIF (GIF 2002) defined eight goals for Generation IV program, in the four broad areas of: sustainability; economics; safety and reliability; and proliferation resistance and physical protection. Details of these areas are:

Sustainability

1. Gen- IV systems will provide sustainable and meet clean air objectives. These systems will provide effective fuel utilization and long-term availability of worldwide energy production.
2. Gen- IV systems will have minimum nuclear waste, thus improving the protection of environment and public health.

Economics

3. Gen-IV y systems will provide a better life-cycle cost over other energy sources.
4. Gen-IV systems will have less financial risk compared to other energy projects..

Safety and Reliability

5. Gen-IV systems will excel in safety, reliability and have a very low degree of reactor core damage thus eliminate the need for offsite emergency response.

Proliferation Resistance and Physical Protection

6. Gen- IV systems will be an unattractive and the least desirable route for diversion or theft of weapons-usable materials, hence provide increased physical protection against acts of terrorism.

Note that not all goals may be fully achieved in any particular design. Investigation done in this thesis is relevant to (above mentioned) items #3 and #5. Addition of a HX between the primary and secondary loop gives the flexibility to add a single-reheat option for PV and PT reactors design without introducing single-reheat channels into the reactor. The HX adds a safety layer between the reactor containment building and the turbine building. The nuclear operational activities stay within the reactor containment building,

and there is a reduced possibility for radioactive contamination of equipment in the turbine building. It also allows for better control of the chemistry in the primary and secondary loop.

Six Generation IV nuclear concepts under GIF (GIF, 2002):

More than one hundred technical experts from ten countries reviewed several concepts under Gen-IV nuclear reactor systems. The committee of experts selected six reactor types that best suited the GIF objective - sustainability, economics, safety, reliability, proliferation resistance and physical protection. These six reactors are as follows:

1. Sodium-Cooled Fast Reactor

The Sodium-Cooled Fast Reactor (SFR) system features a fast-spectrum reactor and closed fuel-recycle system as shown in Figure 2.2 (GIF, 2002). The primary mission for the SFR is to produce electricity and manage of high-level wastes.

Characteristics:

Coolant - Sodium

Outlet temperature – 550 ^{o}C

Large size – 600 to 1500 MW_{el}

Intermediate size – 300 to 600 MW_{el}

Efficiency ~ 40%

Benefits:

High thermal efficiency

Consumption of LWR actinides

Efficient fissile material generation

Concerns:

High cost

Sodium is combustible when in contact with water or air

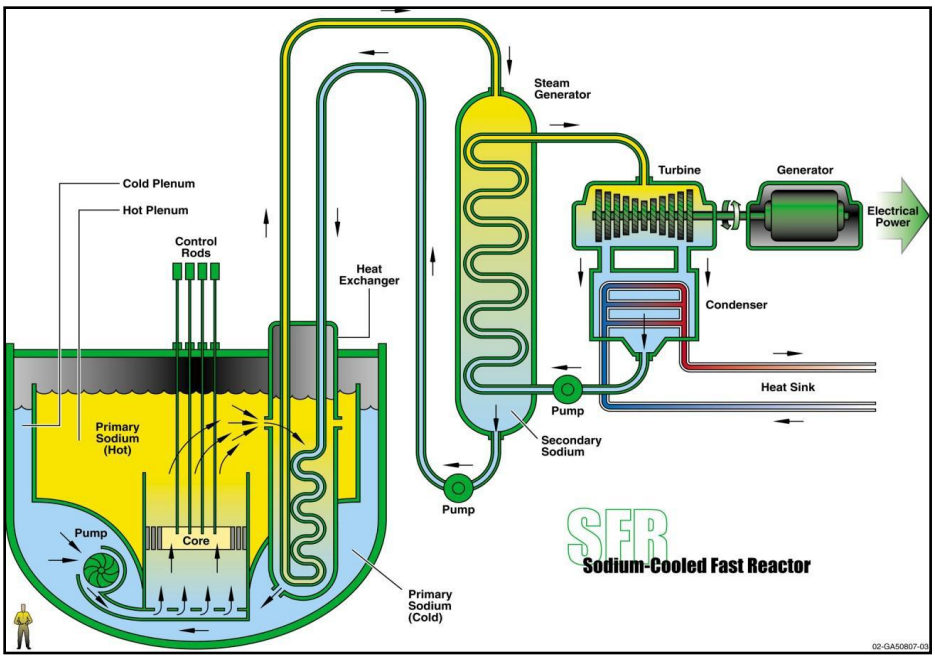

Figure 2.2: Sodium-Cooled Fast Reactor (GIF, 2002).

2. Very-High-Temperature Reactor

The Very-High-Temperature Reactor (VHTR) is a graphite-moderated, helium-cooled reactor shown in Figure 2.3 (GIF, 2002). Co-generation of heat and power makes the VHTR an attractive heat source for large industrial complexes.

Characteristics:

Coolant – Helium (He)

Outlet temperature – 1000 ^{o}C

Power - 600 MW_{th}

Efficiency ~50%

Benefits:

Hydrogen co-production

High degree of passive safety

High thermal efficiency option

Concerns:

Low thermal conductivity of Helium

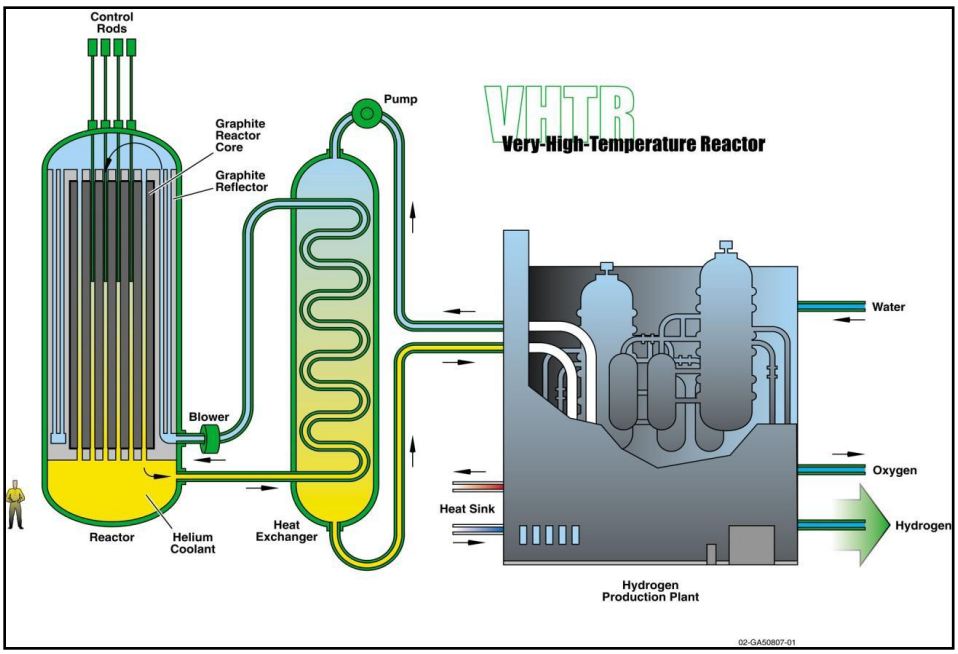

Figure 2.3: Very-High-Temperature Reactor (GIF, 2002).

3. Gas-Cooled Fast Reactor

The Gas-Cooled Reactor system (GFR) features a fast-spectrum helium-cooled reactor and closed fuel cycle as shown in Figure 2.4 (GIF, 2002). The GFR uses a direct-cycle helium turbine for electricity and can use process heat for thermo-chemical production of hydrogen.

Characteristics:

Coolant - Helium

Outlet temperature – 850 ^{o}C

Pressure – 9 MPa

Power - 2400 MWth / 1100 MW_{el}

Efficiency ~ 48%

Benefits:

High efficiency

Waste minimization and efficient use of uranium resources

Concerns:

Low thermal conductivity of Helium

Fast neutron damage

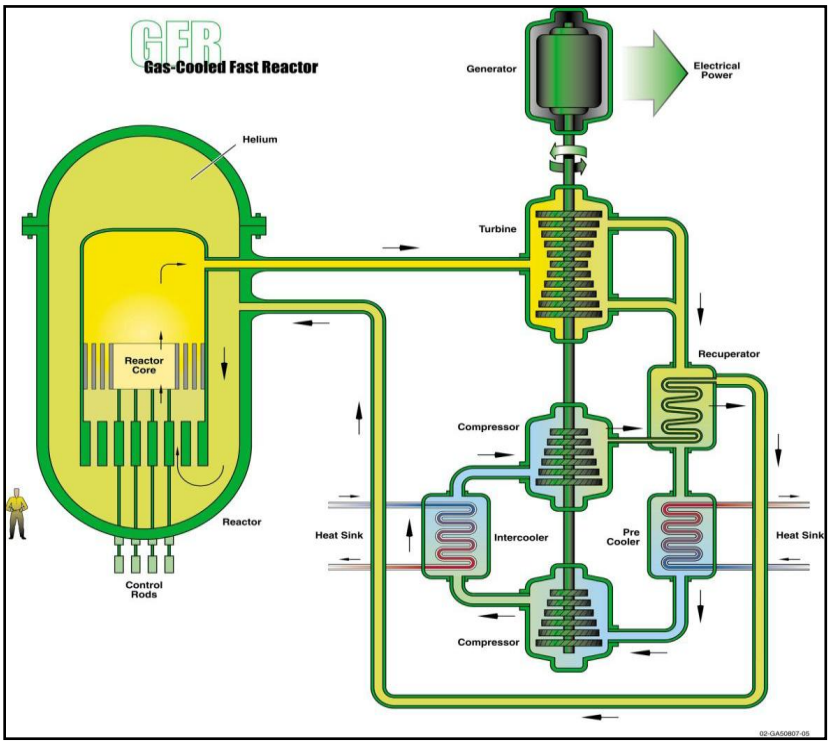

Figure 2.4: Gas-Cooled Reactor (GIF, 2002).

4. Lead-Cooled Fast Reactor

Lead-Cooled Fast Reactor (LFR) systems are lead or lead-bismuth eutectic coolant reactors with a fast-neutron spectrum and closed fuel cycle as shown in Figure 2.5 (GIF, 2002). LFR includes a range of plant ratings.

Characteristics:

Coolant - Pb or Pb/Bi coolant

Outlet temperature – 550 to 800 ^{o}C outlet temperature

Small transportable system – 50 to150 MW_{el}, and

Larger station – 300 to 1200 MW_{el}

Core life options – 15 to 30 years

Efficiency ~ 44%

Benefits:

Distributed electricity generation

Hydrogen co-production

Replaceable core for regional fuel processing

High degree of passive safety

Proliferation resistance through long-life core

Concerns:

Requires a great deal of research and development to become mainstream

New fuel needs to be analyzed for performance specification

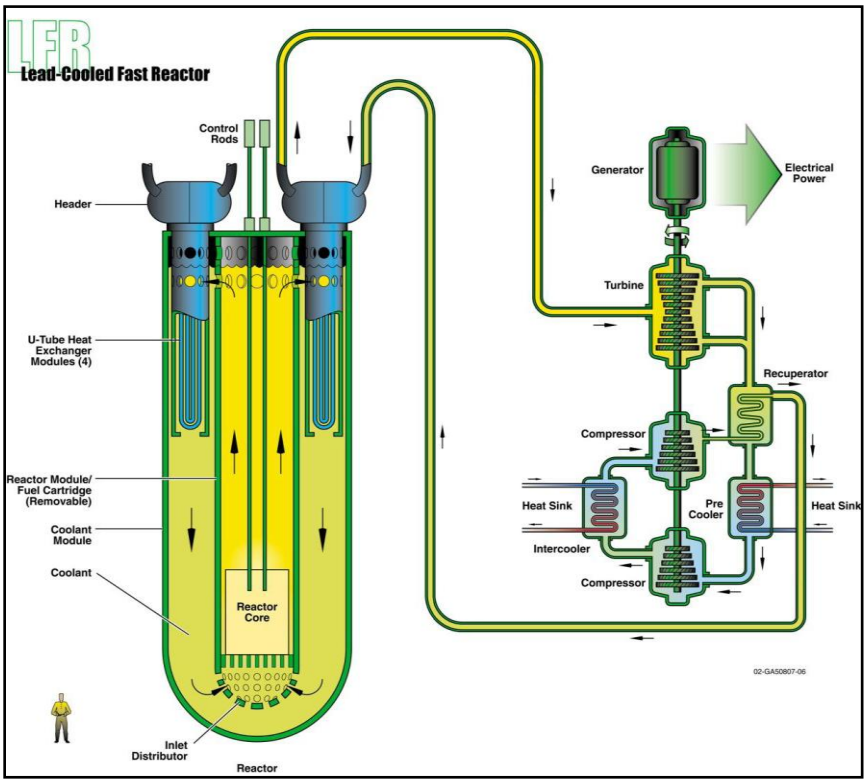

Figure 2.5: Lead-Cooled Fast Reactor (GIF, 2002).

5. Molten Salt Reactor

The Molten Salt Reactor (MSR) shown in Figure 2.6 (GIF, 2002). MSRs are fueled with uranium or plutonium fluorides dissolved in a mixture of molten fluorides. MSR high-temperature operation holds the potential for thermo chemical hydrogen production.

Characteristics:

Fuel - Liquid fluorides of U and Pu

Outlet temperature – 700 to 800 ^{o}C

Power - 1000 MW_{el}

Pressure (<0.5 MPa)

Efficiency ~ 44 - 50%

Benefits:

Waste minimization

Avoids fuel development

Proliferation resistance through low fissile material inventory

Concerns:

High corrosion potential

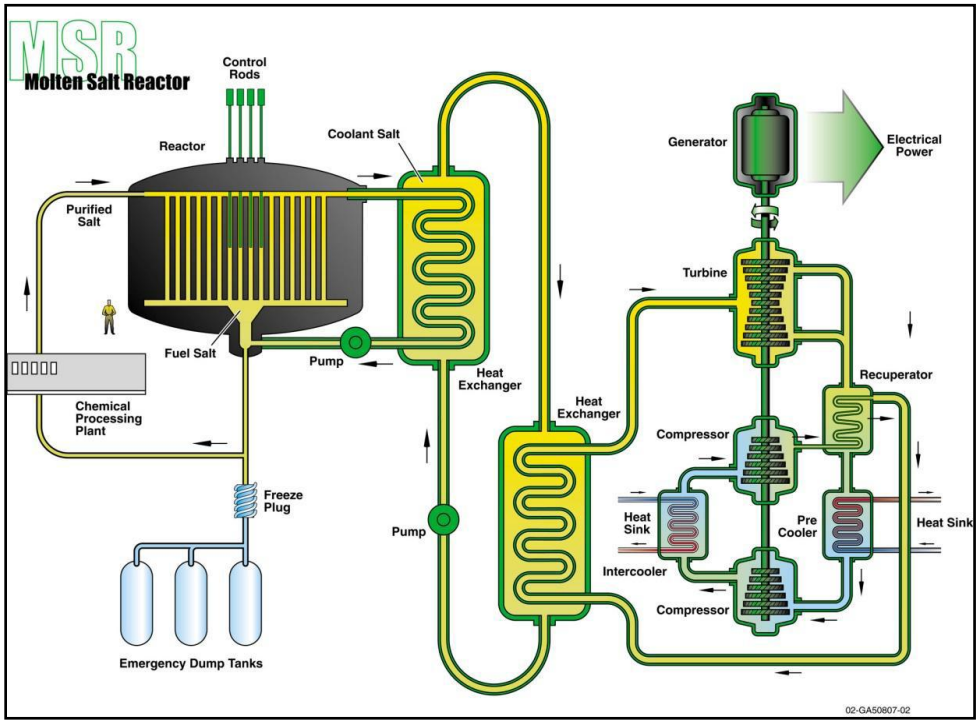

Figure 2.6: Molten Salt Reactor (GIF, 2002).

6. Supercritical-Water-Cooled Reactor

The SCWRs will have high-temperature, high-pressure that operate above the thermodynamic critical point of water. The Figure 2.7 shows the PV reactor and figure 2.8 shows the PT reactor layout of a SCWR system. Depending on the core design, these systems may have a thermal or fast-neutron spectrum.

Characteristics:

Coolant - Water above supercritical conditions (374 ^{o}C, 22.1 MPa)

Outlet temperature – 510 to 625 ^{o}C

Power - 1500 MW_{el}

Reactor options - Pressure tube or Pressure vessel

Efficiency ~ 45%

Benefits:

Efficiency near 45% with excellent economics

Leverages the current experience in operating fossil-fueled supercritical steam plants

Configurable as a fast or thermal-spectrum core

Concerns:

High pressure of water creates greater chance for a loss of coolant accident (LOCA)

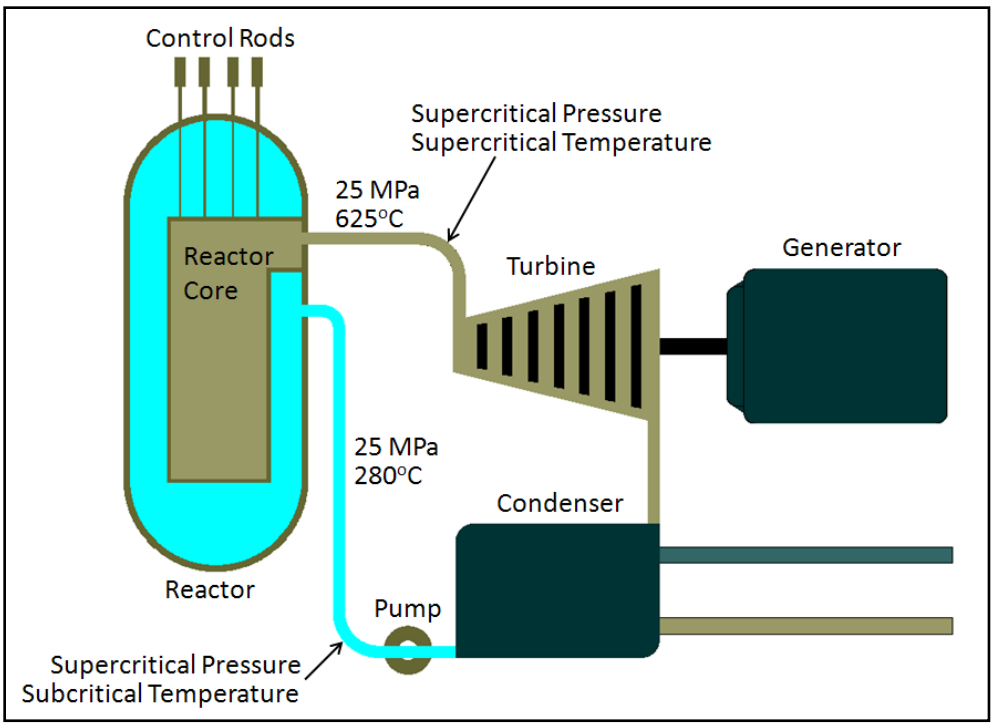

Figure 2.7: Pressure Vessel SCWR - Direct Cycle Type.

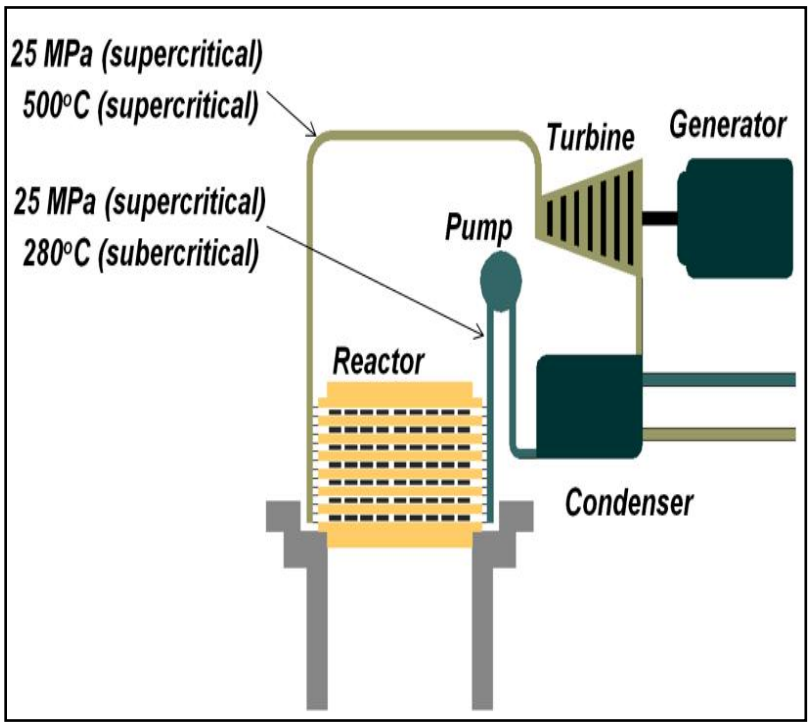

Figure 2.8: Pressure Channel SCWR - Direct Cycle Type.

The operating parameters of SCWRs are quite high as compared to present nuclear reactor systems, which make it more vulnerable to unforeseen scenarios. Also, due to the radioactive nature of the fuel on the reactor side, an extra safety (HX) layer is needed to confine radio activity within the containment building and personnel access to the steam turbine building during normal operations.

In most of these six concepts an intermediate HX is required to isolate the reactor side from the turbine side for both safety and material screening. HX materials screening is needed for potential intermediate loop fluids, e.g., molten salt, He, CO_2, and molten sodium.

2.2 Types of Heat Exchangers

Selection of the heat exchanger involves consideration of a number of factors such as thermal and hydraulic requirements, compatibility with fluids and operating conditions, maintenance, availability, and economics. Different types of heat exchangers are available and the selection need to study its capabilities and limitations (Shah and Sekulic, 2003).

Heat exchangers are typically classified according to flow arrangement and type of construction as follows:

1. Tubular Heat Exchangers
2. Plate Heat Exchangers
3. Extended Surface Heat Exchangers

2.2.1 Tubular Heat Exchangers

Tubular heat exchangers (Shah and Sekulic, 2003) are generally built of tubes. One fluid flows inside the tubes and the other fluid flows on the outside of the tubes. They can be further classified as follows:

Shell and Tube Heat Exchanger

Shell and tube heat exchangers are built of round tubes mounted in large cylindrical shells with the tube axis parallel to that of the shell. They are widely used as steam

generators in nuclear power plants. One fluid stream flows through the tubes while the other flows on the shell side, across or along the tubes. Baffles are used in shell and tube heat exchangers to promote a better heat transfer coefficient on the shell side and to support the tubes. Shell and tube heat exchangers are designed on a custom basis for any capacity and operating condition, from high vacuum to ultrahigh pressure over 100 MPa, from cryogenics to temperatures near 1100^{o}C, and are restricted only by the material of manufacturing. The existing steam generators, a type of shell and tube HX for CANDU and PWR nuclear power plants, operate at pressures of approximately 10 MPa and 15 MPa respectively, and temperature ranges of 250-350 ^{o}C.

Double Pipe Heat Exchangers

Double pipe heat exchangers consist of one pipe placed concentrically inside another pipe of larger diameter. The flow in the pipes can be in same or opposite directions. They are more suitable when one or both fluids are at high pressure, and cleaning can be done very easily by disassembly.

2.2.2 Plate Heat Exchangers

Plate heat exchangers (Shah and Sekulic, 2003) use thin plates to transfer heat through flow channels. The plates can be flat or corrugated to enhance the heat transfer. Plate heat exchangers can be further classified based on their construction.

Gasket Plate Heat Exchanger

A gasket plate heat exchanger consists of a series of thin plates with corrugations or a wavy surface that separates the fluids. The plates come with corner parts arranged so that the two media between which heat is to be exchanged flow through alternate spaces. They are suitable for pressure below 3 MPa and temperature up to 260 ^{o}C.

Welded Plate Heat Exchangers

Welded plates HX are designed to overcome the temperature, pressure, and fluid limitation of gasket behavior (gasket plate heat exchanger). Plate size in welded plate HXs is usually large to reduce welding cost. Welding of the plate increases the operating parameters of the HX to pressures of 4 MPa and temperatures 350 ^{o}C by improving the seal at the edges, but it takes away the flexibility of disassembling at the welded joints.

Spiral Plate Heat Exchanger

Spiral heat exchangers consist of two long parallel plates rolled into a spiral over a mandrel and adjacent plates are welded at the edges to form channels. The maximum operating pressure and temperature is 1.5 MPa and 500 ^{o}C, respectively. It is best suited for handling sludge, viscous liquids, and slurries in suspension.

Lamella Heat Exchanger

The lamella type of heat exchangers consists of a set of parallel welded, thin plate channels or lamellae. It is a modification of the floating head type shell and tube heat exchanger. The lamellae do not foul easily because of high turbulence, uniformly distributed flow, and smooth surfaces. The plate bundle can be easily removed for inspection and cleaning. Lamella heat exchangers are capable of pressure up to 3.5 MPa and temperature of 500 ^{o}C, depending on the type of gasket used.

2.2.3 Extended Surface Heat Exchangers

Extended surface heat exchangers (Shah and Sekulic, 2003) are types with fins on the primary heat transfer surface to increase heat transfer area. They are extensively used in gas-to-gas and gas-to-liquid heat exchangers, where the heat transfer coefficient needs to be increased on one or both sides of HX. These types of heat exchangers are usually quite compact. The operating pressure of commercial extended surface HXs is usually 8.3 MPa. In some of the automotive applications operating pressure of these HX is 14 MPa. The temperature on these HXs depends on the type of bonding and material used.

2.3 Selection of Optimum Heat Exchanger

Initial investigation suggests the shell and tube, and double-pipe types of HX are the most suitable for the operating parameters of on SCW nuclear reactor system. Both the options are investigated further in Appendix A as preliminary study to further narrow down the selection to one for this research.

CHAPTER 3 - SUPERCRITICAL WATER FLUID PROPERTIES AND CORRELATIONS

In this chapter behaviour of the supercritical water fluid and SCW correlations are discussed. Understanding supercritical water fluid behaviour above the critical point is key to developing efficient and safe SCWRs.

3.1 Critical Point, General Terms and Definitions

Prior to any discussion on supercritical water fluid properties, it is important to know what the critical point is: with an increase of temperature and pressure of a fluid, the vapour phase becomes denser while the liquid phase expands and density decreases. Eventually the density of both liquid and vapour phase becomes equal at critical point. The pressure and temperature at the critical point are called the critical pressure P_{cr} and the critical temperature T_{cr}. The fluid above the critical point is called a supercritical fluid. Figure 3.1 graphical illustration of liquid and gas density variation with pressure and temperature. The meniscus between the liquid phase and the gas phase disappears at the critical point (Clifford, 1999). At stage I, when the pressure and temperature are low, there is significant density difference between the liquid and the gas. At stage II, near the critical point, the density difference between the liquid and gas is small. At stage III, at and above the critical point, the densities of the liquid and the gas have become equal. The Figure 3.1 is for pictorial purpose only to show the different phase of the water. The physical phenomena Pseudo-boiling similar to subcritical pressure nucleate boiling may appear at supercritical fluid with a bulk fluid temperature below the pseudocritical temperature (high-density fluid, i.e., “liquid”), some layers near a heating surface may attain temperature above the pseudocritical temperature (low-density fluid, i.e., “gas”). This low-density “gas” leaves the heating surface in the form of variable density (bubble) volumes.

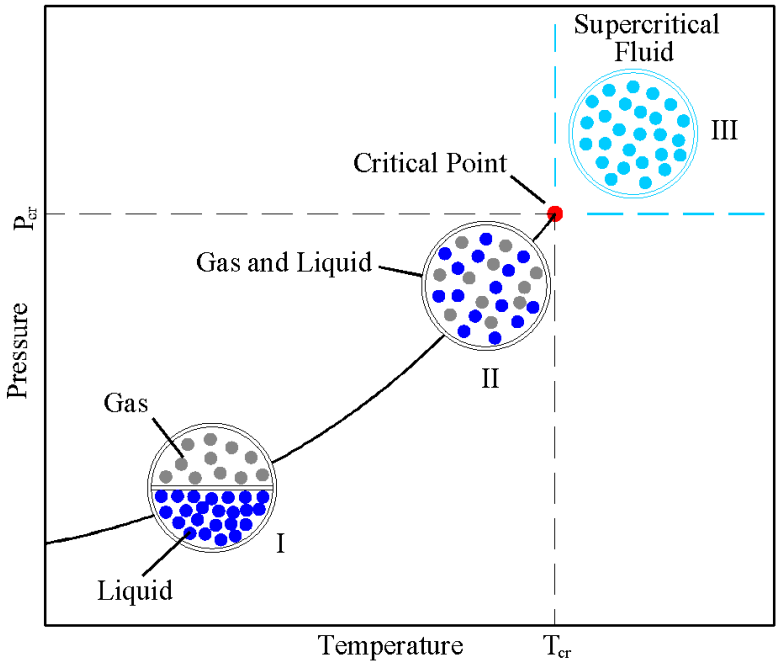

Figure 3.1: Effects of Pressure and Temperature on Fluid.

Other terms related to supercrical fluids are listed below with related Figures 3.2 and 3.3. (Pioro and Duffey, 2007):

Compressed fluid is a fluid at a pressure above the critical pressure but at a temperature below the critical temperature.

Deteriorated Heat Transfer (DHT) is characterized with lower values of the wall heat transfer coefficient compared to those for normal heat transfer; and hence has higher values of wall temperature within some part of a test section or within the entire test section.

Improved Heat Transfer (IHT) is characterized with higher values of the wall heat transfer coefficient compared to those for normal heat transfer; and hence lower values of wall temperature within some part of a test section or within the entire test section. In our opinion, the improved heat-transfer regime or mode includes peaks or "humps" in the heat transfer coefficient near the critical or pseudocritical points.

Near-critical point is actually a narrow region around the critical point, where all thermophysical properties of a pure fluid exhibit rapid variations.

Normal Heat Transfer (NHT) can be characterized in general with wall heat transfer coefficients similar to those of subcritical convective heat transfer far from the critical or pseudocritical regions, when they are calculated according to the conventional single-phase Dittus-Boelter (1930) type correlations: $\boldsymbol{Nu} = 0.0023\ \boldsymbol{Re}^{0.8}\boldsymbol{Pr}^{0.4}$ or by Dittus-Boelter (1930) modified forms like: Bishop *et al*. (1964), Swenson *et al*. (1965), and Mokry *et al*. (2011) correlations.

Pseudocritical line is a line, which consists of pseudocritical points.

Pseudocritical point is a point at a pressure above the critical pressure and at a temperature corresponding to the maximum value of the specific heat at this particular pressure.

Supercritical fluid is a fluid at pressures and temperatures that are higher than the critical pressure and critical temperature.

Superheated steam is a steam at pressures below the critical pressure, but at temperatures above the critical temperature.

Table 3.1 shows the pressure, temperature and density of water at the critical point according to the National Institute of Standards and Technology (NIST) database (NIST, 2010).

Table 3.1: Parameters of Water at the Critical Point (NIST, 2010).

Critical Pressure (MPa)	Critical Temperature (^{o}C)	Critical Density (kg/m^{3})
22.064	373.95	322.0

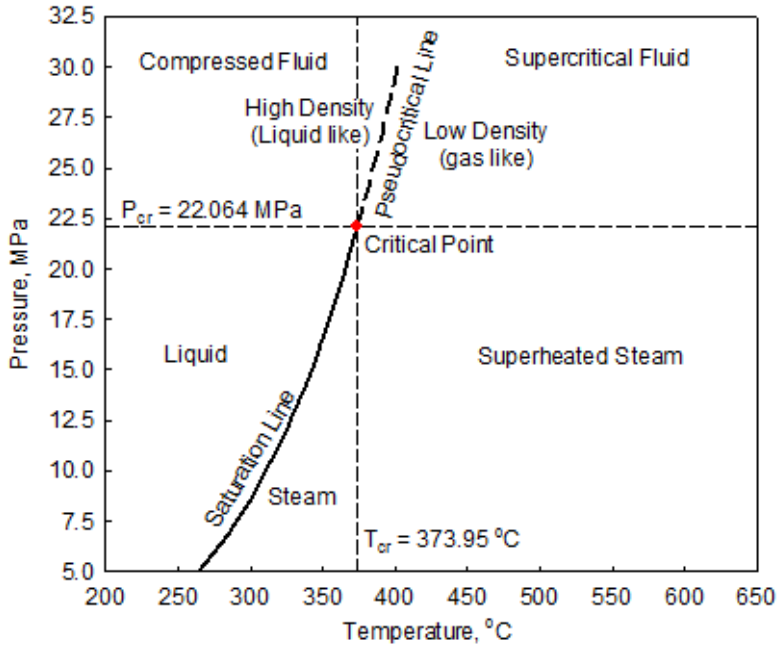

Figure 3.2: Pressure and Temperature Diagram of Water at Critical Region.

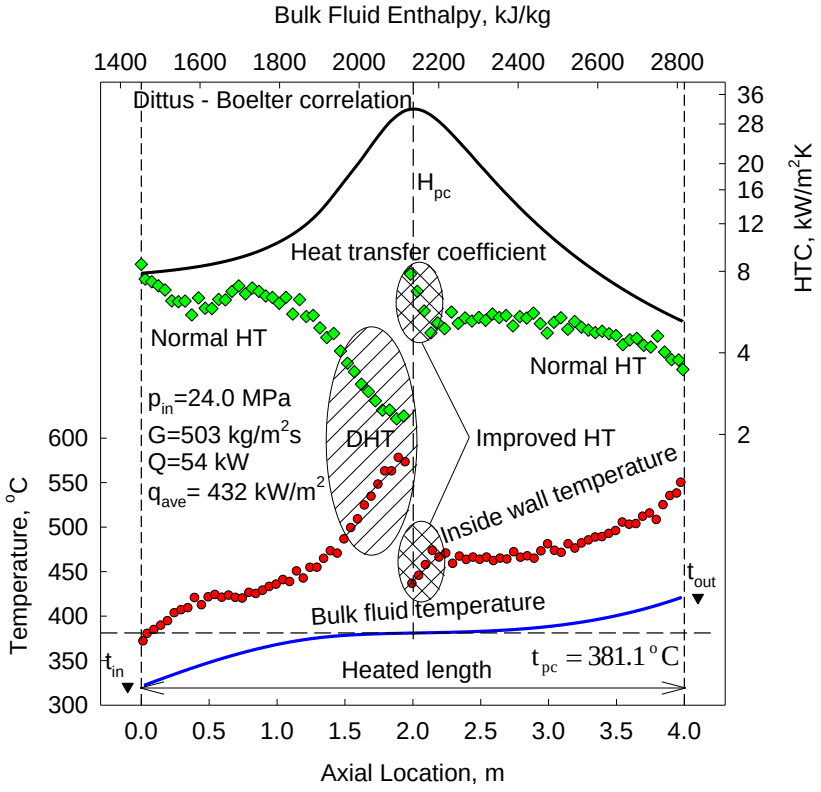

Figure 3.3: Temperature and heat transfer coefficient profiles along heated length of vertical circular tube (Kirillov et al., 2003) (courtesy of S. Mokry) : Water, D = 10 mm and L_h = 4 m.

3.2 Thermophysical Properties of Water in Critical and Pseudocritcal Region

Supercritical fluids have unique properties (Pioro and Duffey, 2007), as they have neither typical liquid, nor vapour properties. Table 3.2 shows the comparison of typical water properties in liquid, gas, compressed fluid, critical point, and supercritical fluid. A Supercritical fluid has liquid like density and gas like viscosity near the critical point. Due to these supercritical fluid capabilities, there is less resistance to flow compared to a liquid, providing more mass transport and at the same time possessing much higher density compared to a gas, therefore providing more heat transport.

Table 3.2: Water Properties Comparison at Liquid, Gas and Supercritical Phase (NIST, 2010).

Phase	Liquid	Gas	Compressed Fluid	Critical Point	Supercritical Fluid
Parameters					
Pressure (MPa)	0.101	0.101	22.064	22.064	22.064
Temperature (^{o}C)	99	101	365	373.95	450
Properties					
Density (kg/m^{3})	959.1	0.59	538.9	287.9	90.3
Viscosity (µPa·s)	284.7	12.3	61.9	39.5	28.2
Thermal Conductivity (W/m·K)	0.68	0.03	0.49	1.37	0.10
Specific Heat (kJ/kg·K)	4.2	2.1	11.6	3885.8	4.4
Enthalpy (kJ/kg)	414.9	2677.7	1770.7	2146.6	3017.8

Like any other fluid the changes in thermophysical properties of water within the critical and pseudocritical region are quite significant. The thermophysical properties of water were generated using the NIST (NIST 2010). Figure 3.4 shows the drastic changes in the

thermophysical properties of water (pressure 25 MPa) in a range of ±25 ^{o}C of the pseudocritical temperature (384.9 ^{o}C). The thermal conductivity decreases from 0.46 to 0.13 W/m·K, the viscosity decreases from 70 to 29 µPa·s and density decreases from 603 to 139 kg/m^3 in this narrow range. The specific heat peaks to 76.4 kJ/kg·K at the pseudocritical point.

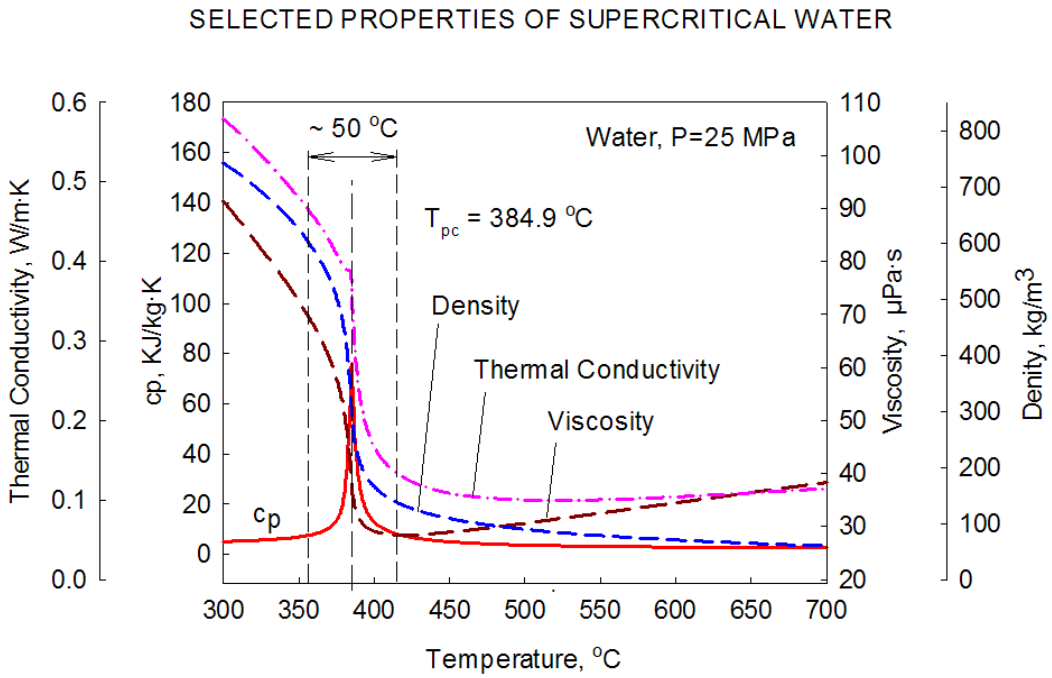

Figure 3.4: Supercritical Water Properties at Pseudocritical Temperature.

Thermophysical properties in Figure 3.5 to 3.9 are obtained from NIST (NIST 2010). Figure 3.5 shows the variations of specific heat with pressure. Specific heat peaks at the critical or pseudocritical point. The peak at the pressure 22.064 MPa is not shown in the graph to capture details for various pressures. The specific heat peak value decreases significantly from 3861.21 kJ/kg·K to 27.03 kJ/kg·K with pressure increase from 22.064 MPa (critical point) to 30 MPa.

Similarly, Figures 3.6 to 3.9 show the density, viscosity, enthalpy, and thermal conductivity of the supercritical fluid in the pseudocritical region. Overall, the thermophysical properties of water at the critical point and at the pseudocritical point undergo significant changes. Within the narrow range of temperature, the density in Figure 3.6 and the viscosity in Figure 3.7 experience a sharp decrease and while the

enthalpy in Figure 3.8 increases sharply in the same region. Specific heat in Figure 3.5 and thermal conductivity in Figure 3.9 peaks at the critical and the pseudo critical points respectively. Figures 3.5 to 3.9 also show that with the increase of pressure, the changes at the pseudo critical points are much smoother. Due to the unique thermophysical properties of supercritical water and significant changes at the critical and the pseudocritical points, it is necessary to investigate, SCW thermophyscial properties influence on the design of the HX. As operating parameters of the HX are likely to be on both sides of the pseudocritical point, heat transfer can be enhanced or diminished due to the changes in fluid properties depending upon the exact fluid conditions.

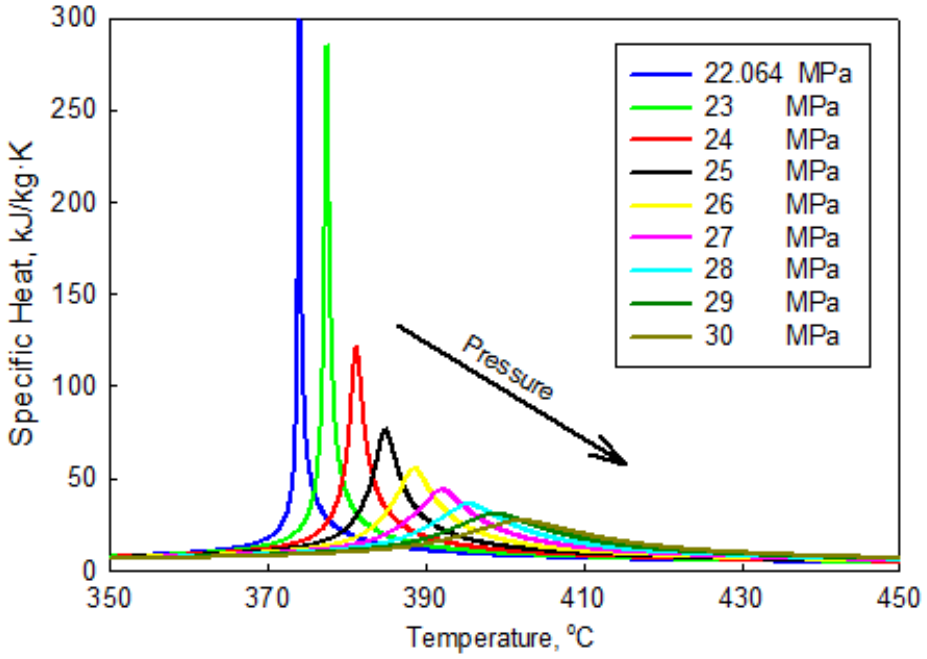

Figure 3.5: Specific Heat Variation with Pressure of Water at Pseudocritical Temperature.

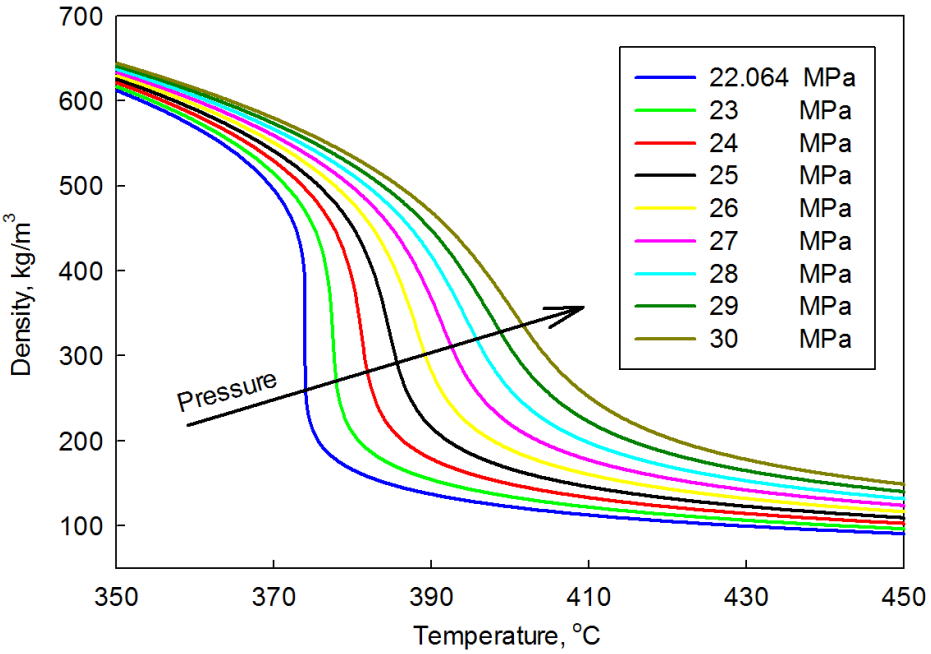

Figure 3.6: Density Variation with Pressure of Water at Pseudocritical Temperature.

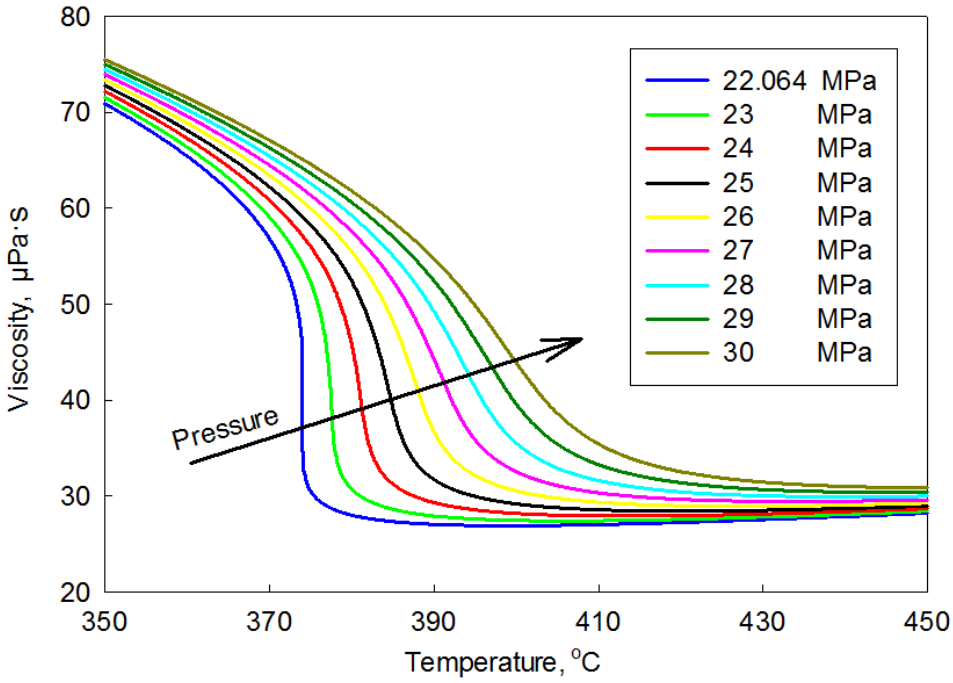

Figure 3.7: Viscosity Variation with Pressure of Water at Pseudocritical Temperature.

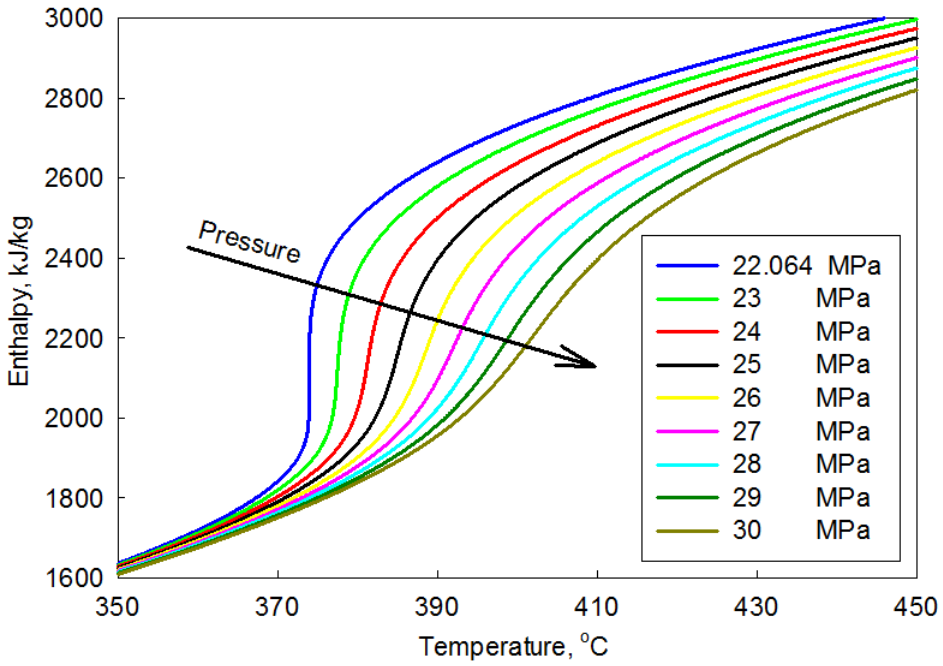

Figure 3.8: Enthalpy Variation with Pressure of Water at Pseudocritical Temperature.

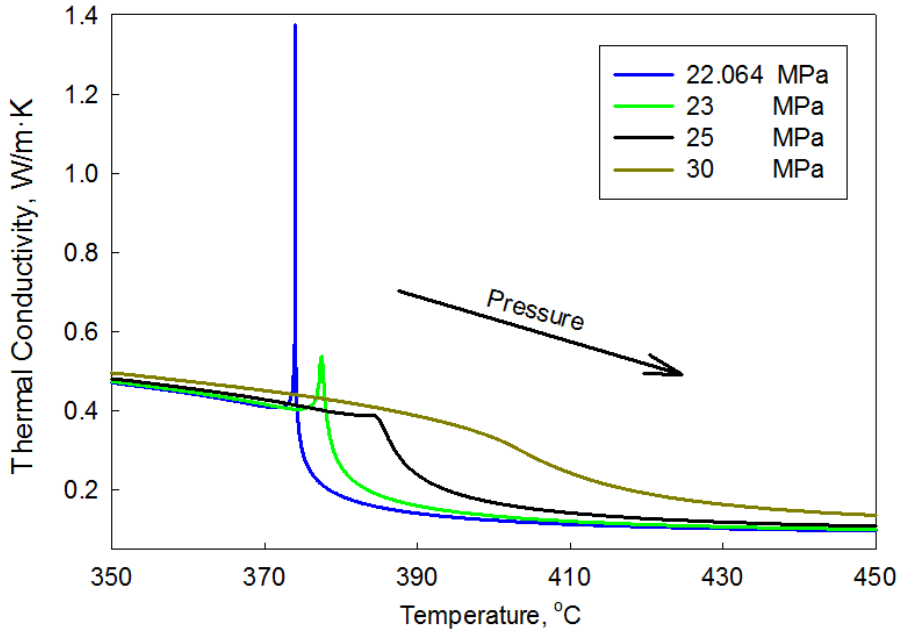

Figure 3.9: Thermal Conductivity Variation with Pressure of Water at Pseudocritical Temperature.

3.3 Heat Transfer Correlations

As noted in section 3.2 the supercritical fluid thermophysical property changes are quite significant near the critical point. There are a number of heat-transfer correlations currently available for forced convection of water at supercritical conditions, and each correlation provides different output given the same operating parameters. The variation among these heat transfer correlations is due to the lack of knowledge of the physical behavior of supercritical fluid and the difficulty in obtaining quality experimental data due to the high pressure and sudden changes in the fluid properties involved. Thus it is important to determine an appropriate SCW correlation that will reasonably predict experimental results for heat transfer with sufficient conservation to obtain a reasonable heat exchanger designs.

As mentioned above, there are a number of correlations for the SCW conditions and some are specified as follows: Dittus-Boelter (1930), Bringer and Smith (1957), Domin (1963), Bishop *et al*. (1964), Swenson *et al*. (1965), Gnielinski (1976), Griem (1996), Jackson (2002), and Mokry *et al*. (2011). Based on the expected operating parameters of the SCW reactors and SCW turbines, four correlations are chosen for further evaluation. They are the correlations of Dittus-Boelter (1930), Bishop *et al*. (1964), Swenson *et al*. (1965), and Mokry *et al*. (2011). The operating parameters for both PT and PV reactors are discussed in detail in Chapter 4. All four correlations are compared with the Harrison and Watson (1976) and Lee and Haller (1974) experimental data. The experimental data matches closely with operating parameters of our reactor concept. Also the experimental data in the Harrison and Watson (1976) are based on the 20 mm diameter pipe and in the Lee and Haller (1974) it is based on the 38 mm diameter pipe. This covers a good range of pipe size to optimize the pipe size for the HX. The range also covers some of the existing SCW fossil fuel boiler pipe sizes, e.g., the pipe size for Russian TYP6 fossil fuel boilers are of 25 mm to 38 mm (Ornatskiy *et al*. 1980). The fossil fuel boiler pipe sizes are the bases as a starting reference. The experimental data parameters for Harrison and Watson (1976) and Lee and Haller (1974) experimental data are shown in Table 3.3.

Table 3.3: Parameter of Harrison and Watson (1976) and Lee and Haller (1974) experimental data.

Parameters	Harrison and Watson (1976)	Lee and Haller (1974)
Pressure (MPa)	22.5	24.1
Bulk-fluid temperature (^{o}C)	355 – 382	315 – 384
Mass flux (kg/m^2·s)	1999	2441
Heat flux (MW/m^2)	1.40	1.58
Diameter (mm)	20	38
Pipe length (m)	6	11

The applicable range for each correlation is shown in Table 3.4 and described below:

Dittus-Boelter (1930)

This form of Dittus-Boelter correlation was proposed by McAdams (1942) and is shown in equation 3.1. Where Nu_b is the Nusset number, Re_b is the Reynolds number, and Pr_b is the Prandtl number of the fluid at bulk temperature.

$$Nu_b = 0.0243\, \boldsymbol{Re_b^{0.8} Pr_b^{0.4}} \tag{3.1}$$

In most of the cases, the Dittus-Boelter (1930) correlation is the basis for the modified supercritical heat-transfer correlations. Equation 3.1 shows good agreement with the experimental data of supercritical water flowing inside circular tubes at a pressure of 31 MPa and low heat fluxes (Schnurr *et al*., 1976). However, it may give unrealistic results near the critical and pseudocritical points, because it is very sensitive to variations in the fluid properties.

Bishop et al. (1964)

The Bishop et al. (1964) correlation is shown in equation 3.2. Where Nu_x is the Nusset number, Re_x is the Reynolds number, and Pr_x is the average Prandtl number of the fluid along the heated length of the pipe. ρ_w is the density of fluid at wall temperature and ρ_b is

the density of fluid at bulk temperature. Correlation uses average specific heat to calculate the Prandtl number and also takes into the account the ratio of fluid density at the wall to the bulk fluid density.

$$\boldsymbol{Nu_x} = 0.0069\, \boldsymbol{Re_x^{0.9}\overline{Pr}_x^{0.66}} \left(\frac{\rho_w}{\rho_b}\right)^{0.43} \tag{3.2}$$

Swenson et al. (1965)

The Swenson el al. (1965) correlation is shown in equation 3.3. Where Nu_w is the Nusset number, Re_w is the Reynolds number, and Pr_w is the average Prandtl number of the fluid at wall temperature. ρ_w is the density of fluid at wall temperature and ρ_b is the density of fluid at bulk temperature. Correlation uses wall temperature to calculate Nusselt, Reynolds, and average Prandtl number. Otherwise it is very similar to Bishop et al. (1964) correlation, keeping into account the average specific heat in Prandtl number and ratio of density of the fluid at the wall temperature to the density at the bulk fluid temperature.

$$\boldsymbol{Nu_w} = 0.00459\, \boldsymbol{Re_w^{0.923}\overline{Pr}_w^{0.613}} \left(\frac{\rho_w}{\rho_b}\right)^{0.231} \tag{3.3}$$

Mokry et al. (2011)

The Mokry et al. (2011) correlation is one of the latest modified versions of the Bishop et al. (1964) correlation shown in equation 3.4. Where Nu_b is the Nusset number, Re_b is the Reynolds number, and Pr_b is the average Prandtl number of the fluid at bulk temperature. ρ_w is the density of fluid at wall temperature and ρ_b is the density of fluid at bulk temperature. It calculates the Prandtl number with the average specific heat and the correlation takes into the account the ratio of the fluid density at the wall to the bulk fluid density.

$$\boldsymbol{Nu_b} = 0.0061\boldsymbol{Re_b^{0.904}\overline{Pr}_b^{0.684}} \left(\frac{\rho_w}{\rho_b}\right)^{0.564} \tag{3.4}$$

Table 3.4: Applicable range of Dittus-Boelter (1930), Bishop et al. (1964), Swenson et al. (1965), and Mokry et al. (2011) for correlations.

Parameters	Dittus-Boelter (1930)	Bishop *et al*. (1964)	Swenson *et al*. (1965)	Mokry *et al*. (2011)
Pressure (MPa)	31	22.8 – 27.6	22.8 – 41.4	22.8 – 29.4
Bulk fluid temperature (^{o}C)	-	282 – 527	75 – 576	320 – 406
Mass flux (kg/m^2·s)	-	651 – 3662	542 – 2150	200 – 1500
Heat flux (MW/m^2)	-	0.31 – 3.46	0.2 – 1.8	70 – 1250

Figure 3.10 shows predicted Heat Transfer Coefficient (HTC) behavior in a 30-mm pipe at a pressure of 25 MPa and temperature range from 300 ^{o}C to 700 ^{o}C using the four correlations mentioned above and NIST (NIST 2010) fluid properties. The Dittus-Boelter (1930) correlation shows higher estimated HTC values within the pseudocritical range (~50^{o}C) compared to other correlations, but it shows similar trends as other correlations outside this range.

The Bishop et al. (1964) and Swenson et al. (1965) correlations show significantly lower HTC values within the pseudocritical range compared to those of the Dittus-Boelter (1930) correlation. In general, the Mokry et al. (2011) correlation shows the most conservative results in terms of HTC values compared to those calculated with other correlations. At bulk-fluid temperatures of 450 ºC and higher, HTC values calculated with all four correlations are quite close to each other.

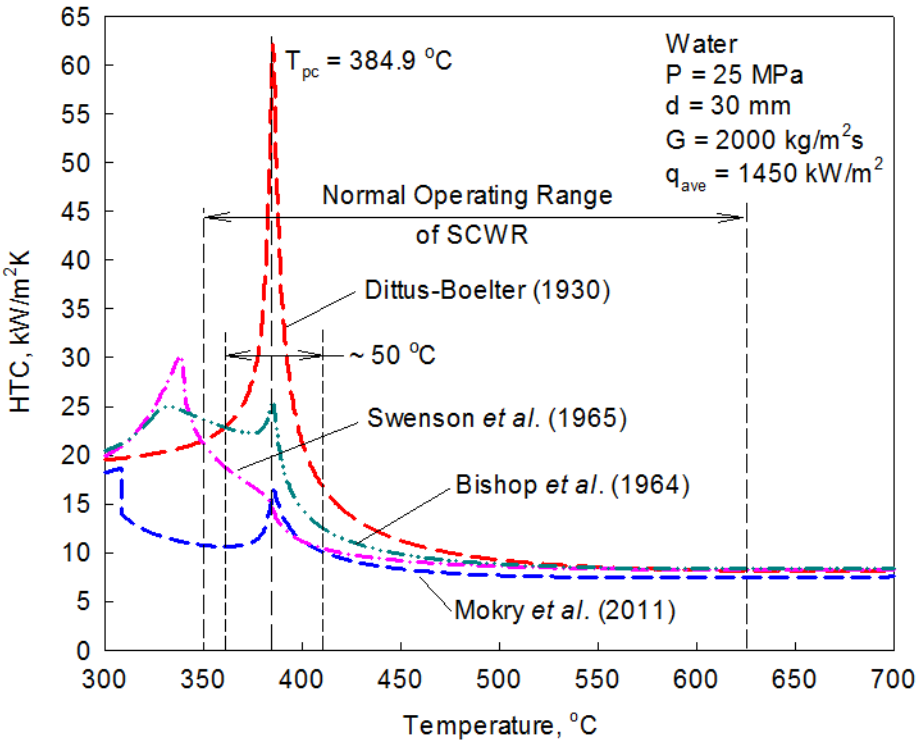

Figure 3.10: HTC vs. Temperature Profiles: *P*=25 MPa, d=30 mm *G*=2000 kg/m^{2}s and *q*=1450 kW/m^2.

An analysis of correlations showed that:

1. Above the pseudocritical point, correlations are well behaved and predict the same trend.
2. All correlations identify a peak or region of enhanced heat transfer.
3. Most of the behaviour discrepancies in correlation trends occur at the temperature just before the pseudocritical point.

Figure 3.11 shows calculated HTC and temperature profiles for along a heated length of a 6m pipe compared to the Harrison and Watson (1976) data. The comparison showed that HTCs calculated with the Dittus-Boelter (1930) correlation are higher than the experimental HTC values by ~12 times, HTC values calculated with the Bishop *et al.* (1964) correlation are higher by ~2.5 times,

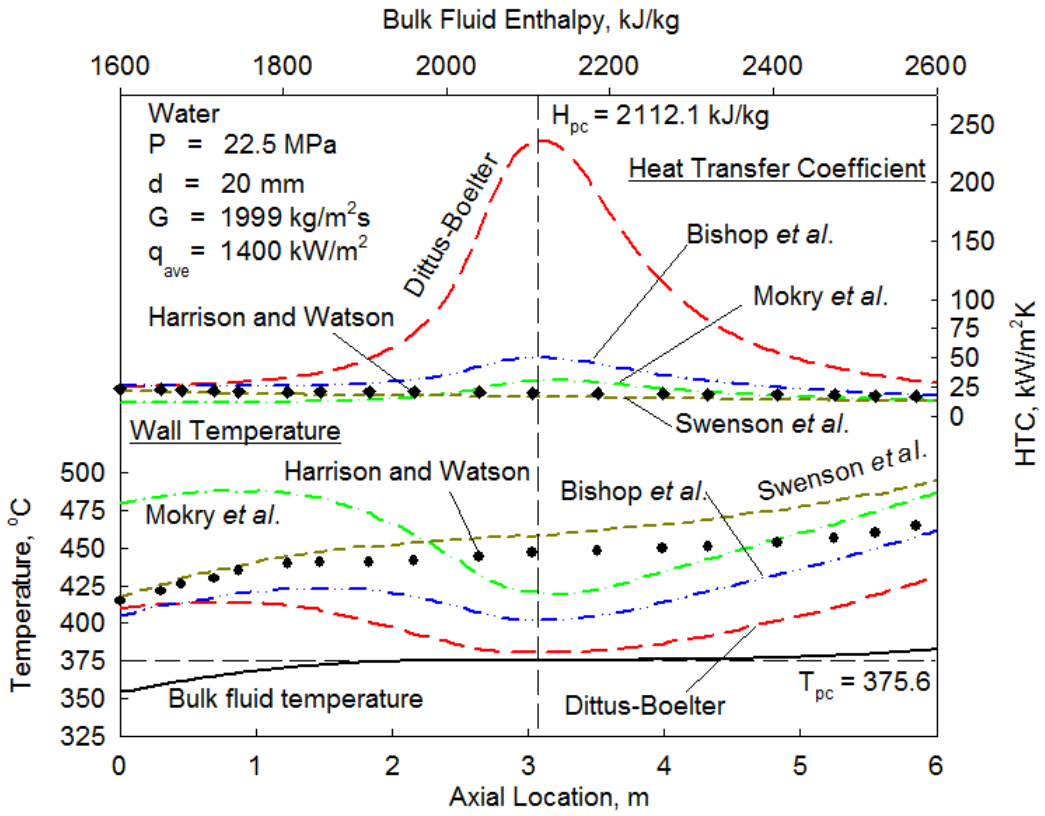

Figure 3.11: HTC and Temperature Profiles along Heated Length of Pipe: *P*=22.5 MPa, d=20 mm, *G*=1999 kg/m^{2}s and *q*=1400 kW/m^2.

HTC values calculated with the Mokry *et al*. (2011) correlation are higher by ~1.5 times, and HTC values calculated with the Swenson *et al*. (1965) correlation are lower by ~1.15 times at the pseudocritical point. The Mokry *et al*. (2011) and Swenson *et al*. (1965) correlation showed much better result, whereas the HTC for both correlations follows closely with the Harrison and Watson (1976) experimental data along the whole heated length.

Figure 3.12 shows a comparison of the HTC and the temperature profiles along the heated length of a pipe for all four correlations, with the Lee and Haller (1974) experimental data. The comparison showed calculated Dittus-Boelter (1930) correlation HTCs are higher than the experimental HTC values by ~3.5 times, Bishop et al. (1964) correlation calculated HTC values are higher by ~1.5 times, Swenson et al. (1965) correlation calculated HTC values are lower by ~1.15 times, and Mokry et al. (2011)

correlation calculated HTC values are lower by 1.05 times from the experimental HTC values at the pseudocritical point. The calculated Mokry et al. (2011) correlation HTC values showed consistency with the Lee and Haller (1974) experimental data.

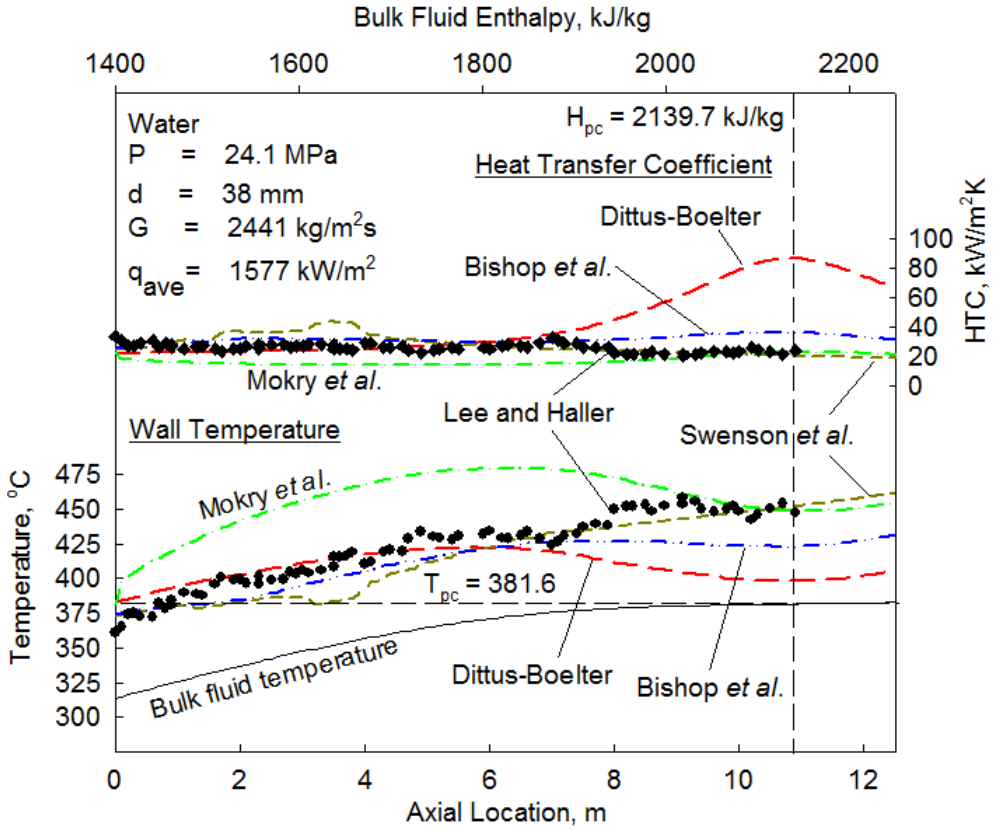

Figure 3.12: HTC and Temperature Profiles along Heated Length of Pipe: *P*=24.1 MPa, d=38 mm, *G*=2441 kg/m^{2}s and *q*=1577 kW/m^2.

The calculated Swenson *et al*. (1965) correlation HTC and wall temperature values showed similar accuracy for both the Harrison and Watson (1976) and Lee and Haller (1974) experimental data along the heated length of the pipe. The Mokry *et al*. (2011) correlation has shown better HTC results with Lee and Haller (1974) data, whereas Swenson *et al*. (1965) has shown better HTC results with Harrison and Watson (1976) data at pseudocritical point. However the Swenson *et al*. (1965) correlation has shown better wall temperature profiles along the length as compared to the Mokry *et al*. (2011) correlation. Overall the results from both the Swenson *et al*. (1965) and Mokry *et al*.

(2011) correlations have shown good consistency with experimental data compared to the Dittus-Boelter (1930) or the Bishop *et al*. (1964) correlation.

Table 3.5 shows the comparison of several correlations (Zahlan *et al*. 2010). In this table the Gospodinov *et al*. (2008) (Gospodinov *et al*. (2008) correlation is similar to Mokry *et al*. (2011) correlation) has the smallest percentage error compared to the others, followed by the Swenson *et al*. (1965) However, the Swenson *et al*. (1965) correlation has shown better results when compared with the Harrison and Watson (1976) and Lee and Haller (1974) experimental data for SCW HX operating parameters. The results from both the Swenson *et al*. (1965) correlation and the Mokry *et al*. (2011) correlation are close, and the percentage of HX operating range in pseudocritical region is much less compared to its overall operating range (350 ^{o}C to 625 ^{o}C). Either correlation can be used for the HX heat transfer calculations. Since the Swenson et al. (1965) correlation has predicted better results for the SCW HX operating parameters, therefore, it is selected for the HX calculations.

Table 3.5: Average Error of Correlation in Three Supercritical Sub-Regions (Zahlan et al., 2010).

Correlation	Liquid-like region		Gas-like region		Close to Critical or PseudoCritical Point	
	Average error, %	RMS error %	Average error, %	RMS error %	Average error, %	RMS error %
Bishop *et al*. (1965)	6.3	24.2	5.2	18.4	20.9	28.9
Swenson *et al*. (1965)	1.5	25.2	-15.9	20.4	5.1	23.0
Krasnochekov *et al*. (1967)	15.2	33.7	-33.9	35.8	25.2	61.6
Watts and Chou (1982), Normal	4.0	25.0	-9.7	20.8	5.5	24.0
Watts and Chou (1982), Deteriorated	5.5	23.1	5.7	22.2	16.5	28.4
Griem (1996)	1.7	23.2	4.1	22.8	2.7	31.1
Jackson (2002)	13.5	30.1	11.5	28.7	22.0	40.6
Mokry, Gospodinov and Pioro (2008)	-3.9	21.3	-8.5	16.5	-2.3	17.0
Kuang et al. (2008)	-6.6	23.7	2.9	19.2	-9.0	24.1
Cheng et al. (2009)	1.3	25.6	2.9	28.8	14.9	90.6
Hadaller and Banerjee (1969)	7.6	30.5	10.7	20.5	-	-
Sieder and Tate (1936)	20.8	37.3	93.7	133.6	-	-
Dittus-Boelter (1930)	32.5	46.7	87.7	131.0	-	-
Gnielinski (1976)	42.5	57.6	106.3	153.3	-	-

CHAPTER 4 - SCWR CONCEPTS, SCW TURBINES, AND SCWR CYCLES

This chapter concentrates on SCWR type concepts, SCW turbines, and SCWR cycles. There are mainly two types of SCWR concepts: PV and PT. The PV SCWR concepts are largely developed in United States, European Union, Japan, Korea, and China, where as the later PT SCWR concepts are largely developed in Canada and Russia. The major parameters of the SC-turbines used in fossil fuel plants are discussed. The chapter also discusses different types of cycle layouts and various SCWR NPP layouts for indirect cycles with an intermediate HX.

4.1 SCWR Concepts

At present, there are a number of Generation-IV nuclear reactor concepts under development worldwide, and the SCWR type is one of them. The main objective of developing SCWRs is to increase the thermal efficiency of current NPPs from 30 – 35% to approximately 45 – 50%, and to decrease capital and operating costs. SCW NPPs are expected to have much higher operating parameters compared to current NPPs (i.e., pressures of about 25 MPa and outlet temperatures up to 625 °C). Figure 4.1 shows the operating parameters of SCWR CANDU and SCWR USA under investigation. The figure also shows the operating parameters of current NPPs, i.e., BWR, CANDU-6, and PWR. Apart from electricity, SCWRs can produce hydrogen, process heat, hydrogen, industrial isotopes as by products. SCWRs high temperature can facilitate an economical production of hydrogen through thermochemical cycles or direct high-temperature electrolysis (Naidin *et al*. 2009). Figure 4.2 shows a PT reactor type concept with capability of sustaining multiple products.

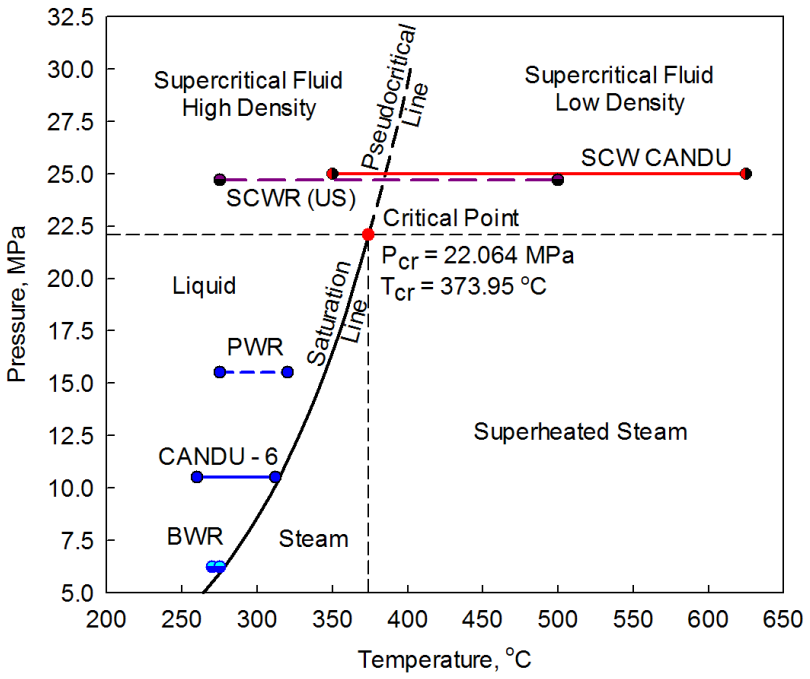

Figure 4.1: Pressure-Temperature Diagram: Operating Parameters of SCWRs, PWRs, CANDU-6 Reactors and BWRs.

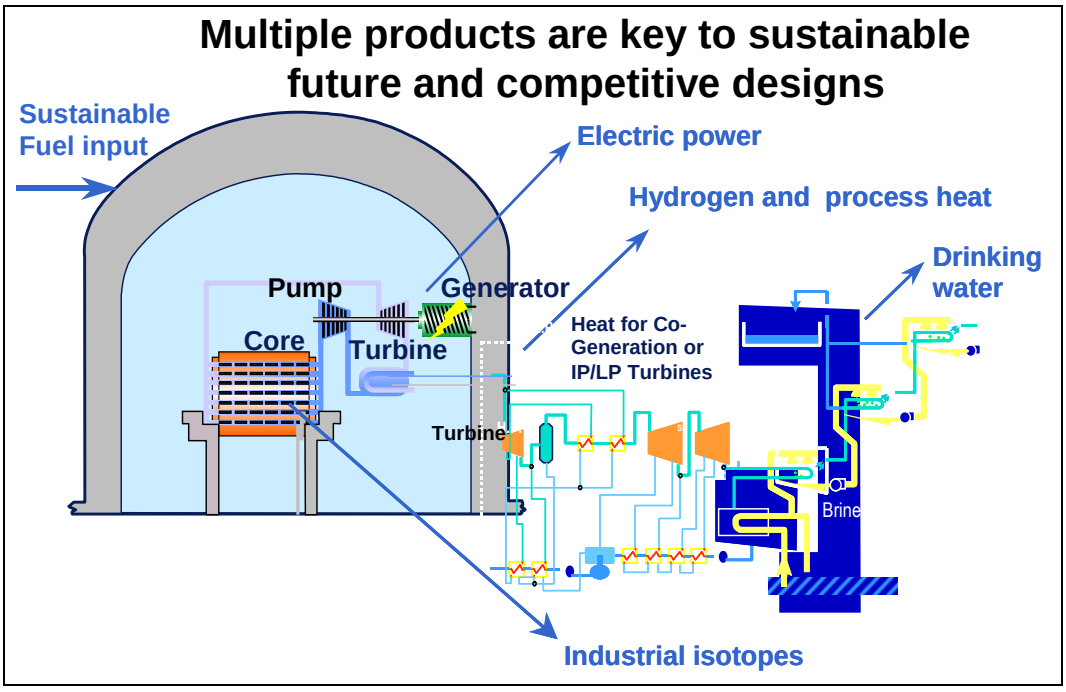

Figure 4.2: Pressure-Tube Supercritical Water CANDU Nuclear Reactor concept (courtesy of Dr R. Duffey (AECL) (Pioro and Duffey, 2007)).

4.2 SCWR Types

The SCWR concepts (Pioro and Duffey, 2007) follow two main types: (a) PV with a wall thickness of about 0.5 m to contain the reactor-core heat source, analogous to conventional LWRs or (b) PTs or fuel channels analogous to conventional HWRs. Figures 4.3 and 4.4 show the PV and PT reactors, respectively, for an indirect cycle with an intermediate HX. Within these two main classes (PV and PT), the PT reactor design gives the flexibility of accommodating a single reheat option. However, the addition of the steam-reheat option will increase the complexity of reactor core design.

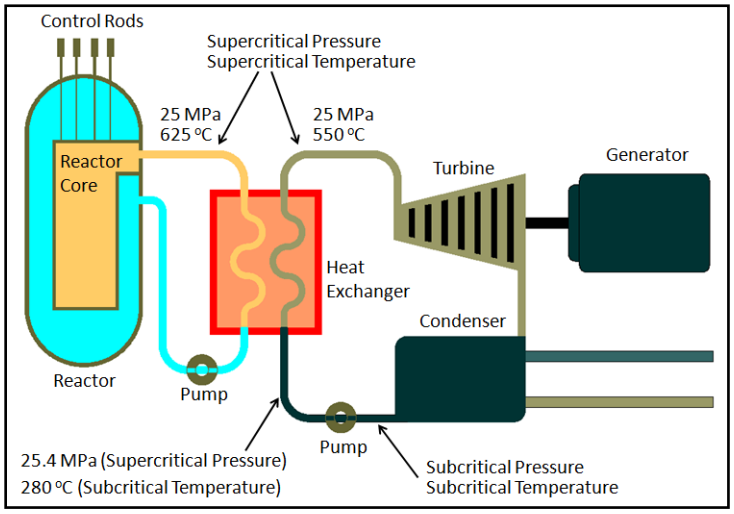

Figure 4.3: Indirect Cycle Pressure Vessel SCW Nuclear Reactor Concept.

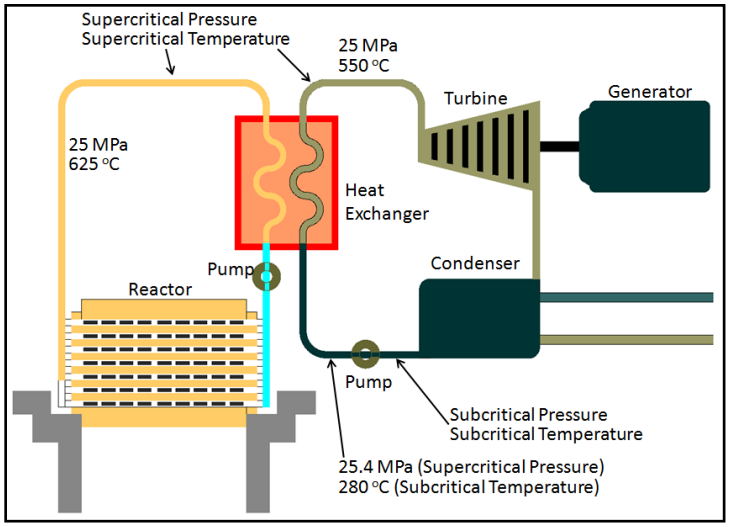

Figure 4.4: Indirect Pressure Tube SCW Nuclear Reactor Concept.

Due to higher pressure and temperature, the current CANDU fuel channel designs cannot be used. There are several SCWR channel designs under investigation, e.g., ceramic insulation design (Peiman *et al*., 2009) and re-entrant flow pressure-channel concept (Samuel *et al*., 2010) are two of them. The ceramic insulation design shown in Figure 4.5 uses a ceramic liner to reduce heat losses to the moderator. The re-entrant design shown in Figure 4.6 consists of two tubes, the inner tube (flow channel) and outer tube (pressure tube). The coolant enters through the outer gap between flow tube and pressure tube from one side and reverses the direction through the inside of the flow channel. The outer gap, also referred to as the annulus gap, preheats the coolant before it enters into the fuel channel and acts as insulator between the moderator and the fuel channel. A thin ceramic over the pressure tube can be used to decrease heat loss.

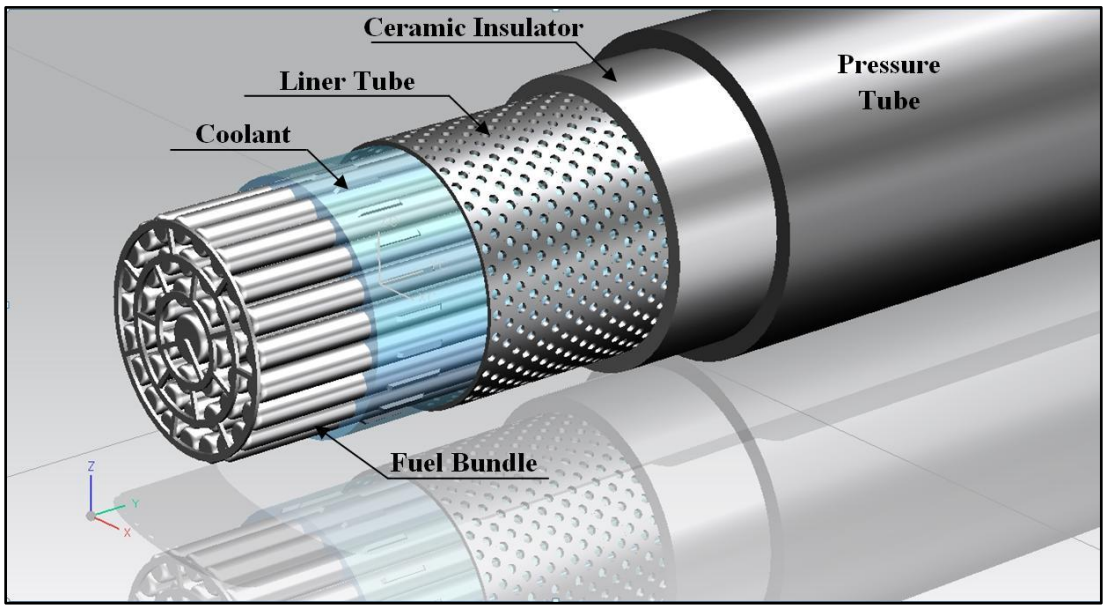

Figure 4.5: SCW PT Channel with Ceramic Insulated Concept (courtesy of W. Peiman).

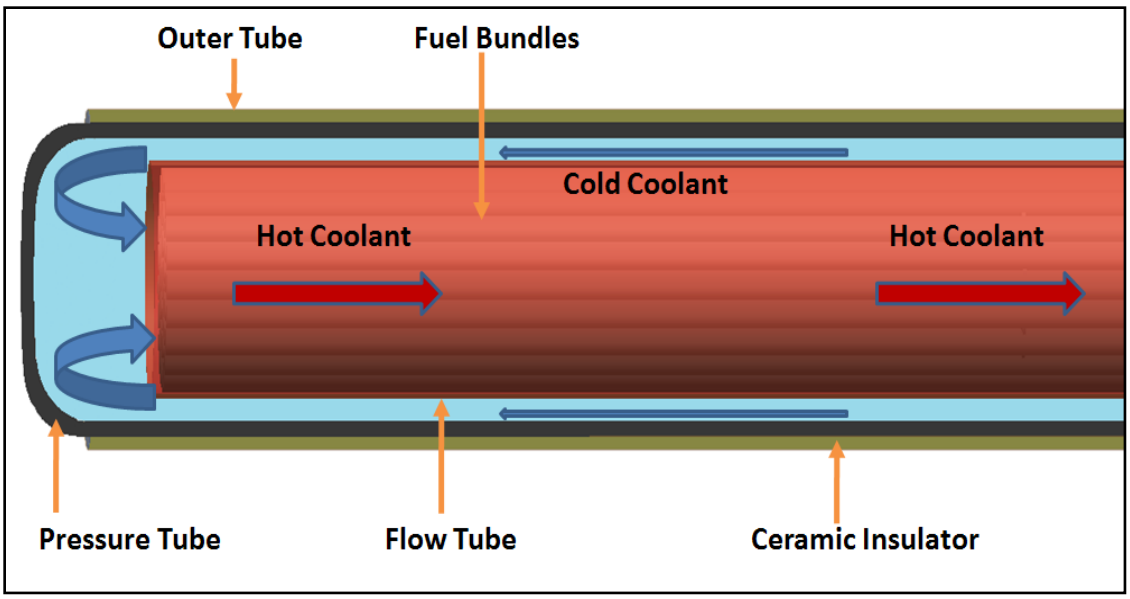

Figure 4.6: SCW PT Re-entrant Flow Channel Reactor Concept (courtesy of J. Samuel).

The major parameters of the PT supercritical reactor type developed by AECL and Kurchatov Institute (Duffey *et al*., 2008a; Pioro and Duffey, 2007), the major parameters of PV supercritical reactor type, developed by University of Tokyo -Japan (Yamaji et al. 2004), Kurchatov Institute - Russia (Filippov *et al*. 2003), and INEEL - USA (Buongiorno and MacDonald 2003) are listed in Table 4.1. Others PT and PV SCWR concepts are listed in Pioro and Duffey (2007). Table 4.1 shows the wide range of operating conditions of different conceptual PT and PV reactors. The thermal power varies from 2540 to 3575 MW, the outlet temperature varies from 500 to 625 ^{o}C, the inlet temperature varies from 270 to 350 ^{o}C, and the mass flow rate from varies 1020 to 1843 kg/s. It will not be possible to cover all the ranges for the SCW HX analysis in this study and the focus is on the SCW CANDU reactors, therefore primary side operating parameters for the HX analysis are based on SCW CANDU reactor.

Table 4.1: Major Parameters of PT and PV Nuclear Reactor Concepts (Pioro and Duffey, 2007).

Parameters	Reactors				
	SCW CANDU	ChUWR	SCLWR-H	PVWR	SCWR
Developer	AECL	Kurchatov Institute	University of Tokyo	Kurchatov Institute	INEEL
Country	Canada	Russia	Japan	Russia	USA
Reactor Type	PT		PV		
Reactor Spectrum	Thermal				
Coolant	Light water				
Moderator	Heavy water		Light water		
Thermal Power, MW_{th}	2540	2730	2740	3500	3575
Electric Power, MW_{el}	1220	1200	1217	1500	1600
Thermal Efficiency, %	48	42	44.4	43	44.8
Pressure, MPa	25	24.5	25	25	25
Inlet Temperature, °C	350	270	280	280	280
Outlet Temperature, °C	625	545	530	550-610	500
Mass Flow Rate, kg/s	1320	1020	1342	1600	1843
Number of Fuel Bundles	300	1693	121	37	145
Number of Fuel Rods in Bundle	43	10	300	-	300

4.3 Supercritical Turbines and Major Parameters

To achieve higher efficiency, better economy, and cleaner electricity generation, SC turbines have been widely deployed in newly built SCW fossil-fuelled power plants (with the exception of combined-cycle power plants). Most of the SC turbines are within the pressure range of 24 to 25.5 MPa and temperature range of 540 to 600 ^{o}C. SC turbine capacity ranges from 300 MW_{el} to 1200 MW_{el} (Pioro and Duffey, 2007). Note turbines for ultra-supercritical plants are being researched and deployed worldwide, particularly in Japan, Korea, and China, for an inlet temperature of 625 ^{o}C and pressures up to 34 MPa. In Denmark the main parameters of ultra-supercritical units are pressures of 29-30 MPa and temperatures of 580/600 ^{o}C (main/reheat) range.

Table 4.2 lists the parameters of selected Russian SC thermal plants turbines and Table 4.3 lists the parameters for selected current and upcoming Hitachi SC thermal plant turbines.

Table 4.2: Major Parameters of Selected Russian SC Thermal Plants Turbines (Ornatskiy *et al*., 1980; Pioro and Duffey, 2007).

Power Rating MW_{el}	P_{main} **MPa**	T_{main} ^{o}**C**	P_{reheat} **MPa**	T_{reheat} ^{o}**C**
300	25	545-585	3.5-3.9	260-265
500	25	545	3.95	545
800	25	545	3.44	545

Table 4.3: Major Parameters of Selected Current and Upcoming Hitachi SC Plant Turbines (Pioro and Duffey, 2007).

First Year of Operation	Power Rating MW_{el}	P MPa	T_{main} ^{o}C	T_{reheat} ^{o}C
2011	495	24.1	566	566
2010	809	25.4	579	579
	790	26.8	600	600
2009	1000	25.0	600	620
	1000	25.5	566	566
	677	25.5	566	566
	600	24.1	600	620
2008	1000	24.9	600	600
	887	24.1	566	593
	887	24.1	566	593
	677	25.5	566	566
2007	1000	24.9	600	600
	870	25.3	566	593
2006	600	24.1	566	566
	600	24.1	566	566

Table 4.4 lists the major parameters of some of the modern SC steam boilers for fossil fuel plants in China, Denmark, Germany, and Japan. The plants are deployed with a single reheat cycle to increase the efficiency. The parameters of the SC steam boilers give enough information to determine, the operating parameters of the turbines in these plants.

Table 4.4: Major Parameters of Modern SC Steam boilers (Pioro and Duffey, 2007).

Country	P_{main} MPa	T_{main} ^{o}C	P_{reheat} MPa	T_{reheat} ^{o}C
China	25	538	-	566
Denmark	30	580	7.5	600
Germany	26.8	547	5.2	562
Japan	24.1	538	-	566
	25	600	-	610
	31.1	566	-	566

Based on the above information it can be concluded that: the main/primary inlet parameter for the most of the SC turbines, pressure varies from 24.1 to 26.8 MPa and temperature varies from 545 to 600^{o}C; and the reheat/secondary pressure varies from 3.44 to 7.5 MPa and temperature varies from 545 to 620 ^{o}C. Conventionally the inlet temperature for the main/primary and reheat/secondary are the same or very close to each other.

Due to the maturity and the high efficiency of reheat steam-cycles for fossil–fueled plants, it would make sense to use the same technology in SCWR, at least for the first design. Also, with the current and the ongoing development of SC-turbines, technology required for SCWR parameters will be well proven by the time Generation-IV SCWRs are ready for the market. Based on the parameters of current and upcoming SC turbines, it is logical to design the secondary side of the first HX (main cycle) to be a SCW type for a pressure range of ~24 – 27 MPa and a temperature range of ~545 – 600 ^{o}C, and for the secondary side, the second HX (reheat cycle) to be a SCW to SHS type for a pressure range of ~3 – 7.5 MPa and a temperature range of ~545 – 620 ^{o}C.

4.4 SCWR Nuclear Power Plant Cycles

The SCWR NPP can be categorized by three cycle types: direct cycle, indirect cycle, and dual cycle. These cycles can be further classified into reheat or no-reheat cycles. The efficiency of these three cycles is based on the Rankine cycle (Cengel *et al*. 2008) and

analyzed as steady-flow process. Therefore the conservation of energy for pump, reactor/ HX, turbine and condenser can be expressed as follows:

$$\dot{W}_{pump,in} = H_{out} - H_{in} \quad (4.1)$$

$$\dot{Q}_{Reactor\ or\ HX,in} = H_{out} - H_{in} \quad (4.2)$$

$$\dot{W}_{Turbine,out} = H_{in} - H_{out} \quad (4.3)$$

$$\dot{Q}_{Condenser,Out} = H_{in} - H_{out} \quad (4.4)$$

$$\dot{W}_{net} = \dot{Q}_{in} - \dot{Q}_{out} = \dot{W}_{Turbine,out} - \dot{W}_{pump,in} \quad (4.5)$$

$$\eta_{th} = \frac{\dot{W}_{net}}{\dot{Q}_{in}} = 1 - \frac{\dot{Q}_{Out}}{\dot{Q}_{in}} \quad (4.6)$$

Direct Cycle

In a direct cycle, the SCW from a nuclear reactor is fed directly into a SC turbine (Duffey *et al*., 2008b). Current BWR NPPs are based on this concept. This cycle has the highest thermal efficiency, but it has some safety concerns related to radioactive exposure/contamination of equipment in a turbine building. The thermal efficiency of this cycle can be 45.6%.

Indirect Cycle

The indirect cycle has intermediate heat exchangers. Similar to the current CANDU and PWR NPPs, these intermediate heat exchangers separate the primary loop from the secondary loop. This way the primary loop can be completely enclosed in the reactor building. The nuclear activity stay within the reactor building, and there is a reduced possibility for radioactive contamination of equipment in the turbine building. The thermal efficiency of this cycle can be 45.1%.

Dual Cycle

The dual cycle is a combination of the direct cycle and the indirect cycle. The SCW from the reactor is sent to the High Pressure (HP) and Intermediate Pressure (IP) turbines, which can be located in the enclosure of the reactor. The steam exhausting the IP turbine

is sent to SGs utilizing a system very similar to those of current CANDU and PWR plants. Since the extra heat-transfer process reduces the steam temperature, the cycle efficiency will be somewhat lower than that in the direct cycle, while providing a secondary barrier to radioactivity, thus capturing the added safety advantages of the indirect cycle. The thermal efficiency of this cycle can be 45.4%.

Reheat and No-Reheat Cycle

In the reheat cycle the steam exhausted from the HP turbine is sent back to a HX or reactor (PT) for reheating. Then the reheated steam flows through the IP and LP turbines. All of the SC turbines used in fossil-fueled plants are designed for the reheat-steam cycle.

The no-reheat cycle offers a simplified SCW NPP layout, contributing to lower capital costs. However, the efficiency of this cycle is lower than that of the reheat cycle. After safety, the thermal efficiency is the main focus in SCW type NPP's. Therefore, the no-reheat cycle is not considered in this paper. Usually the no-reheat cycle has 2-3% less efficiency as compared to reheat cycle (Pioro *et al*., 2008).

4.5 SCWR NPP Layouts – Indirect Cycle for PT and PV Reactors

There are four different indirect cycle layouts developed in this study for PT and PV reactors.

Indirect Single-Reheat Cycle for PT and PV Reactors

A SCW NPP indirect single-reheat-cycle arrangement is shown in Figure 4.7. The corresponding T-S diagram is illustrated in Figure 4.8 and the thermodynamic boundaries of HX1 and HX2 for this layout are shown in Table 4.5. The SCW from the reactor at a pressure of 25 MPa and temperature of 625 °C transfers the heat through a heat exchanger (HX1) to the secondary loop. The supercritical "steam" from the secondary loop is expanded inside a single-flow HP turbine from the supercritical pressure of 25 MPa and temperature 600 °C (Point 3) to an intermediate pressure of 8 MPa and temperature of 400 °C (Point 4). The SHS at a pressure of 25 MPa and a temperature of

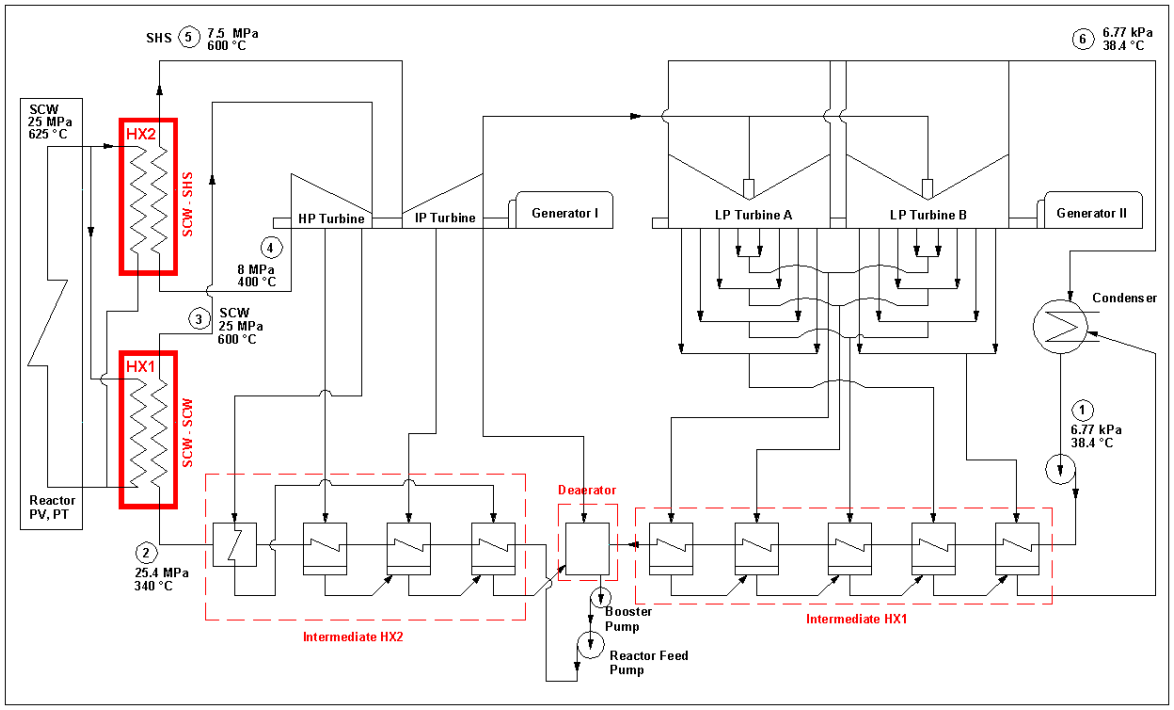

Figure 4.7: SCWR NPP Indirect Single Reheat Cycle for PT and PV Reactors.

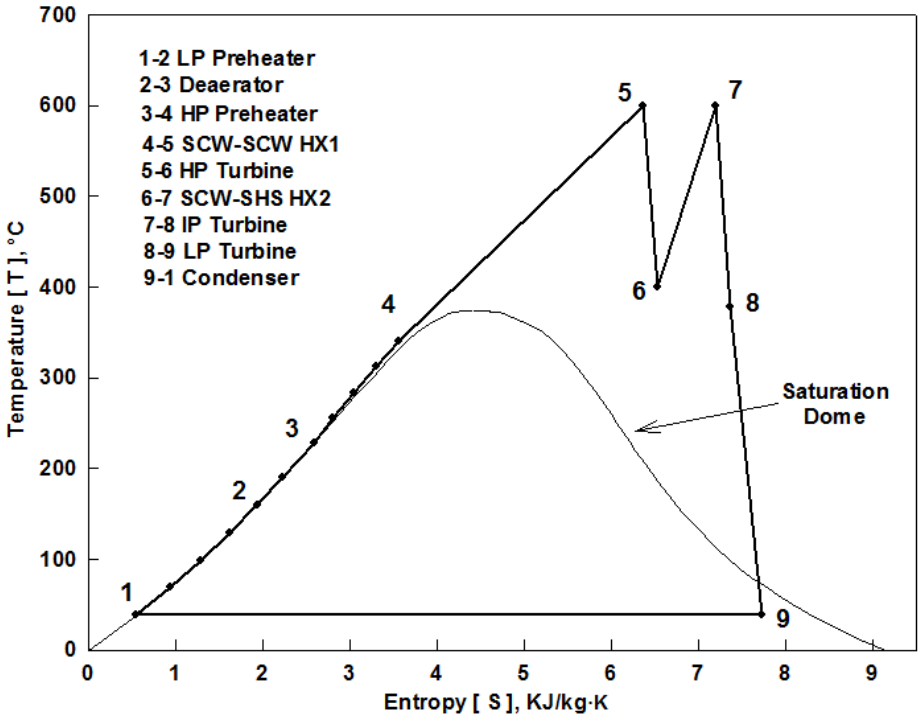

Figure 4.8: T-S diagram of SCWR NPP Indirect Single Reheat Cycle for PT and PV Reactors.

625 ^{o}C raises the steam temperature in the secondary loop to superheated conditions. Then the SHS, at a subcritical pressure of 7.5 MPa and temperature 600 °C (Point 5), is expanded in the IP turbine and transferred through a cross-over pipe and expanded in the LP turbine to a pressure of 6.77 kPa and temperature of 38.4 °C (Point 6).

Table 4.5: HX1 and HX2 Parameters of SCWR NPP Indirect Single Reheat Cycle for PT and PV Reactors.

Parameters	Primary Loop (Hot Side)	Secondary Loop (Cold Side)
HX1 (SCW – SCW)		
Pressure (MPa)	25	25.4
Inlet Temperature (^{o}C)	625	340
Outlet Temperature (^{o}C)	350	600
Mass Flow Rate (kg/s)	1083	1087
HX2 (SCW – SHS)		
Pressure (MPa)	25	8
Inlet Temperature (^{o}C)	625	400
Outlet Temperature (^{o}C)	410	600
Mass Flow Rate (kg/s)	485	860

Indirect Single-Reheat Cycle for PT Reactors only

A SCW NPP indirect single-reheat cycle for PT reactors is shown in Figure 4.9. The corresponding T-S diagram is illustrated in Figure 4.10 and the thermodynamic boundaries of HX1 and HX2 for the layout are shown in Table 4.6. The SCW from the reactor, at a pressure of 25 MPa and temperature of 625 °C, transfers the heat through a HX1 to the secondary loop. The supercritical "steam" from the secondary loop is expanded inside a single-flow HP turbine from the supercritical pressure of 25 MPa and temperature 600 °C (Point 3) to an intermediate pressure of 8 MPa and a temperature of 400 °C (Point 4). The SHS steam from the HP turbine is sent to the second HX2, where SHS from the reactor at a pressure of 9 MPa and a temperature of 625 °C raises the steam temperature in the secondary loop to superheated conditions through HX2. Then the SHS

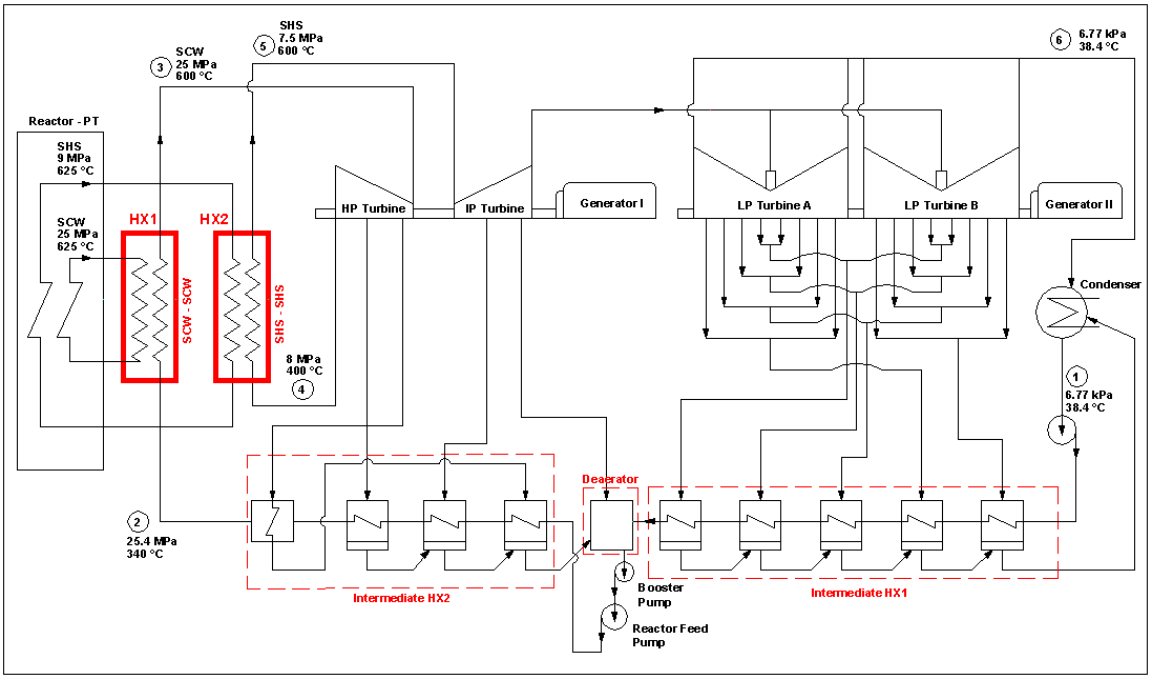

Figure 4.9: SCWR NPP Indirect Single Reheat Cycle for PT Reactor

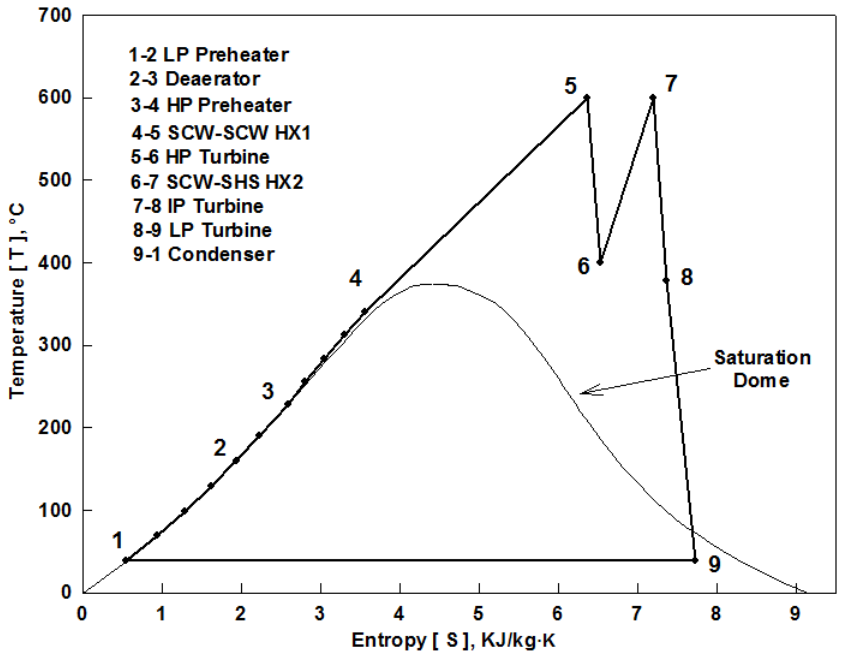

Figure 4.10: T-S diagram of SCWR NPP Indirect Single Reheat Cycle for PT Reactor

at a subcritical pressure of 7.5 MPa and temperature 600 ^{o}C (Point 5) is expanded in the IP turbine and transferred through a cross-over pipe and expanded in the LP turbine to a pressure of 6.77 kPa and temperature of 38.4 °C (Point 6).

Table 4.6: HX1 and HX2 Parameters of SCWR NPP Indirect Single Reheat Cycle for PT Reactor Only.

Parameters	Primary Loop (Hot Side)	Secondary Loop (Cold Side)
HX1 (SCW – SCW)		
Pressure (MPa)	25	25.4
Inlet Temperature (^{o}C)	625	340
Outlet Temperature (^{o}C)	350	600
Mass Flow Rate (kg/s)	1083	1087
HX2 (SHS – SHS)		
Pressure (MPa)	9	8
Inlet Temperature (^{o}C)	625	400
Outlet Temperature (^{o}C)	410	600
Mass Flow Rate (kg/s)	780	860

No Reheat Indirect Cycle for PT and PV Reactors

A SCWR NPP no-reheat indirect cycle arrangement for PT and PV reactors is shown in Figure 4.11. The corresponding T-S diagram is illustrated in Figure 4.12 and the thermodynamic boundaries of HX1 for this layout are shown in Table 4.7. In this arrangement the SCW from a reactor at a pressure of 25 MPa and temperature of 625 °C transfers the heat through a HX1 to the secondary loop. The supercritical "steam" from the secondary loop is expanded inside an HP turbine from the supercritical pressure of 25 MPa and temperature 600 °C (Point 3) to an intermediate pressure of 10 MPa and temperature of 440 °C (Point 4). The subcritical steam from the HP turbine is transferred through a cross-over pipe and expanded in the IP/LP turbines to a pressure of 6.77 kPa and temperature of 38.4 °C (Point 5).

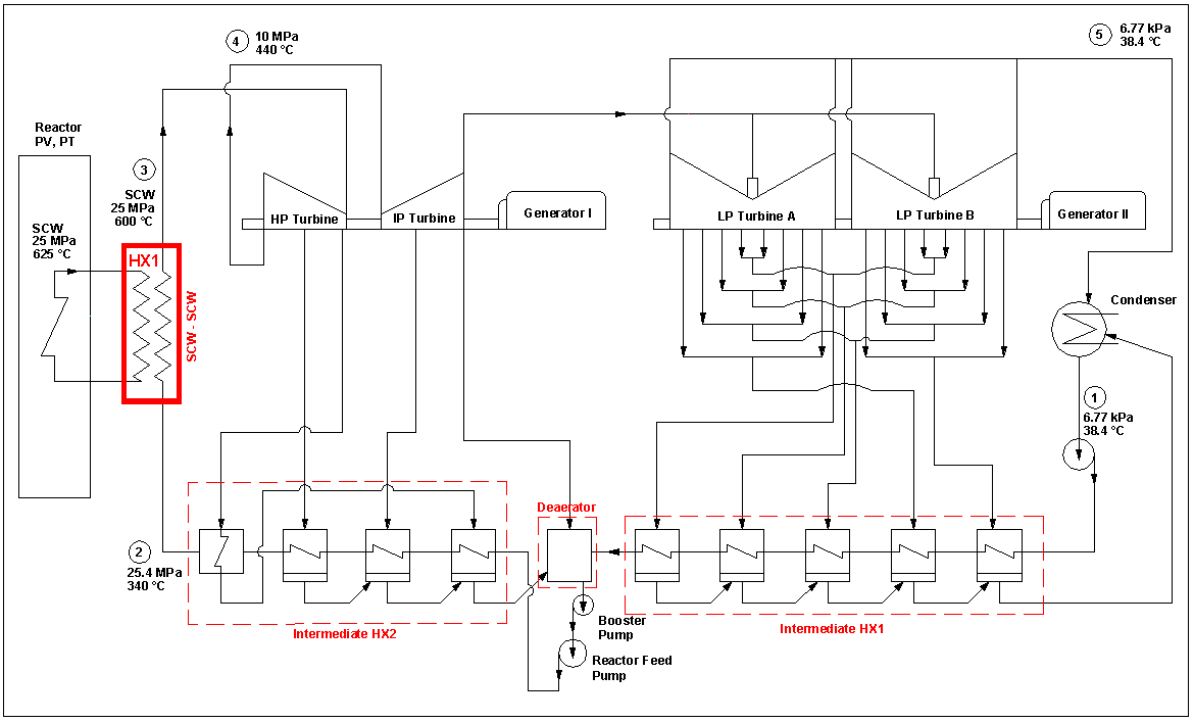

Figure 4.11: SCWR NPP Indirect Cycle for PT and PV Reactors.

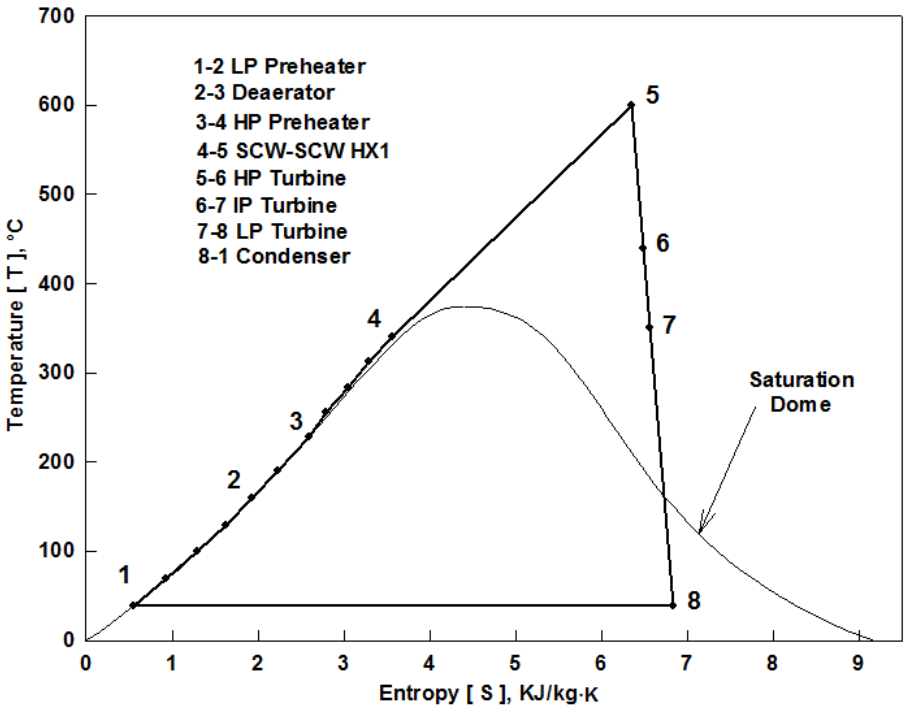

Figure 4.12: T-S diagram of SCWR NPP Indirect Cycle for PT and PV Reactors.

Table 4.7: HX1 Parameters of SCWR NPP Indirect Cycle for PT and PV Reactors.

Parameters	Primary Loop (Hot Side)	Secondary Loop (Cold Side)
HX1 (SCW – SCW)		
Pressure (MPa)	25	25.4
Inlet Temperature (^{o}C)	625	340
Outlet Temperature (^{o}C)	350	600
Mass Flow Rate (kg/s)	1307	1312

Indirect Dual Cycle for PT and PV Reactors

A SCWR NPP indirect dual-cycle arrangement for PT and PV reactors is shown in Figure 4.13. The corresponding T-S diagram is illustrated in Figure 4.14 and the thermodynamic boundaries of HX1 and HX2 for this layout are shown in Table 4.8. The SCW from the reactor at a pressure of 25 MPa and temperature of 625 °C transfers the heat through a HX1 to the secondary loop. The supercritical "steam" from the secondary loop is split into two flows: the first portion is expanded inside a single-flow HP turbine from the supercritical pressure of 25 MPa and temperature 600 °C (Point 3) to an intermediate pressure of 5.5 MPa and temperature of 340 °C (Point 4). The second portion of the supercritical "steam" (Point 3) from the HX1 at the pressure of 25 MPa and temperature of 600 °C goes to the second HX2, where it raises the subcritical steam temperature (Point 5) to 550 °C at a pressure of 12.3 MPa (Point 6). Then SHS at a subcritical pressure of 12.3 MPa and temperature of 550 °C (Point 6) is expanded in the IP turbine and transferred through a cross-over pipe and expanded in the LP turbine to a pressure of 6.77 kPa and temperature of 38.4 °C (Point 7).

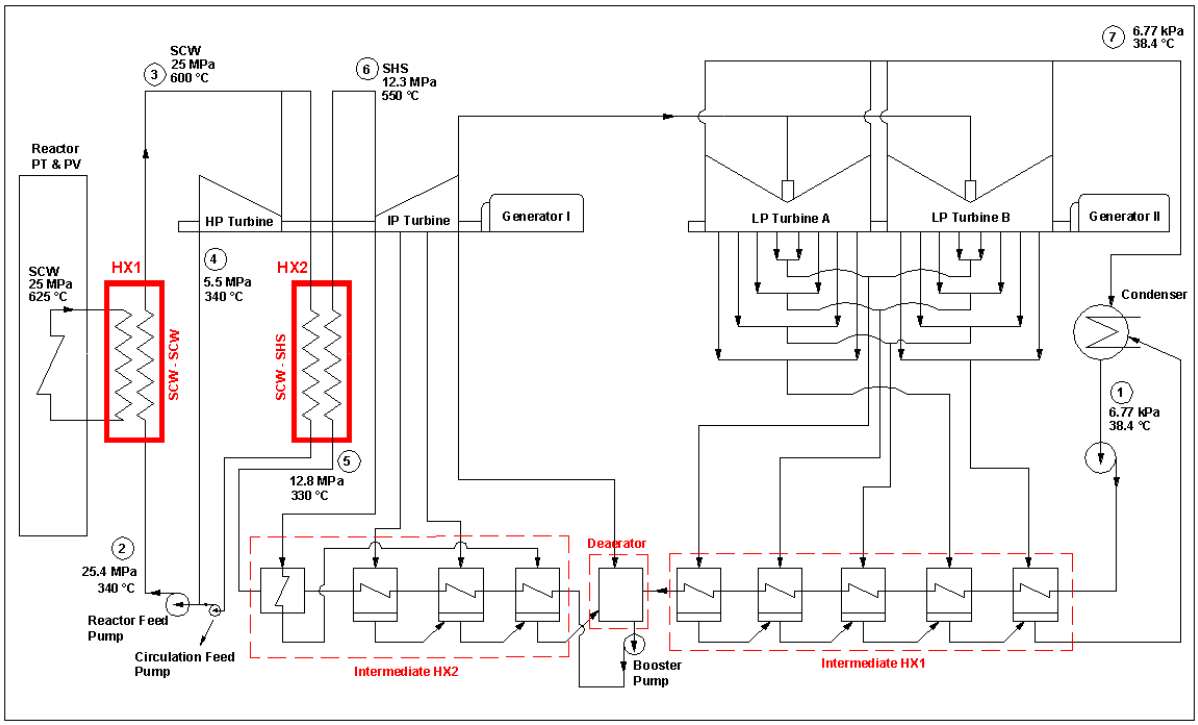

Figure 4.13: SCWR NPP Indirect Duel Cycle for PT and PV Reactors.

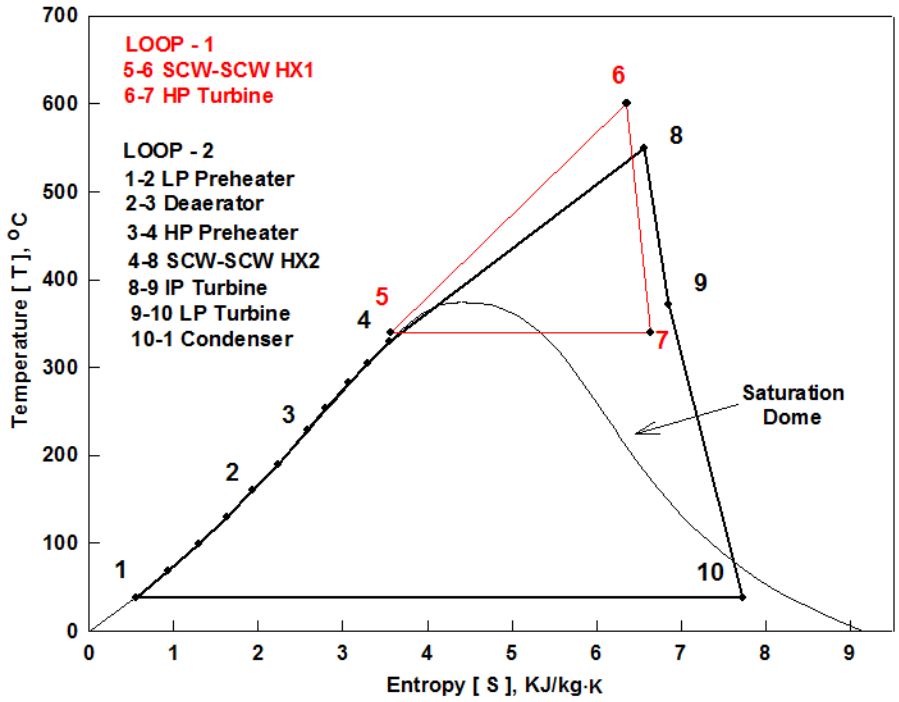

Figure 4.14: T-S diagram of SCWR NPP Indirect Duel Cycle for PT and PV Reactors.

Table 4.8: HX1 and HX2 Parameters of SCWR NPP Indirect Duel Cycle for PT and PV Reactors.

Parameters	Primary Loop (Hot Side)	Secondary Loop (Cold Side)
HX1 (SCW – SCW)		
Pressure (MPa)	25	25.4
Inlet Temperature (^{o}C)	625	340
Outlet Temperature (^{o}C)	350	600
Mass Flow Rate (kg/s)	1307	1312
HX2 (SCW – SHS)		
Pressure (MPa)	25	12.8
Inlet Temperature (^{o}C)	600	330
Outlet Temperature (^{o}C)	340	550
Mass Flow Rate (kg/s)	512	1230

As such, an intermediate HX is useful for several different SCW-based thermodynamic configurations. Both shell and tube type HX and a double pipe type HX were considered for the HX. Preliminary study identified the double pipe HX as the best choice for the design at this time. Details are provided in Appendix A. To complete the plant design, the HX must be analyzed for various parameters against the expected boundary conditions of the plant layout. This will allow for plant optimization studies in the future. A double-pipe configuration HX is simulated for a reference set of conditions that will be useful for each concept proposed.

Table 4.9 summarizes the thermodynamic boundaries conditions for the HX1 and HX2 that will be used in this work. In this study it was not possible to cover operating parameters of all the SCWR's in table 4.1. Hence selection of the primary side boundary condition is mainly based on a SCW CANDU reactor. Secondary side boundary conditions of the HX's are based on the SC turbine and indirect SCW-based thermodynamic configuration analysis. The heat flux 2000 kg/m^{2}·s is based on the

Ornatskiy et al. (1980) experience with SCW thermal power plants. The study will determine the effect of variation on the secondary side parameters on HX surface area and change in fluid property behavior along the length of HX pipe. It will give the general behavior pattern of fluid properties on both the primary and secondary side based on different ratios of temperature, pressure, mass flow rate, and pipe size. This can be useful for other SCWR parameters and applications.

Table 4.9: Summary of thermodynamic boundaries of HX1 and HX2.

Parameters	**Primary Loop (Hot Side)**	**Secondary Loop (Cold Side)**
HX1 (SCW – SCW)		
Pressure (MPa)	24.5 - 25	24 – 28
Inlet Temperature (^{o}C)	625	340
Outlet Temperature (^{o}C)	350	550 - 600
Mass Flow Rate (kg/s)	1320	1200 - 1350
HX2 (SCW – SHS)		
Pressure (MPa)	24.5 - 25	4 – 12
Inlet Temperature (^{o}C)	625	340
Outlet Temperature (^{o}C)	350	550 - 600
Mass Flow Rate (kg/s)	500	800 - 1150

CHAPTER 5 - NUMERICAL MODEL OF DOUBLE-PIPE HEAT EXCHANGER

5.1 Methodology

Various analyses were performed by varying pressure, pipe size, temperature, and mass flow rate on both hot and cold side of the HX. The thermodynamic boundary conditions for the analysis were based on the study in chapter 4.

Pipes wall thickness of the HX is sized for the design pressure with a safety factor of +25% on operating pressure. The explicit finite temperature difference method was used to perform heat transfer analysis on a double pipe HX. The length of the HX pipe is divided into several nodes. The initial wall temperature was assumed below the entrance hot side bulk fluid temperature for each node. For a given node the thermophysical properties of a fluids were calculated at the entrance of the hot side and thermophyscial properties for cold side were calculated at the exit. Based on the initial temperature and pressure, the thermophysical properties of the water were obtained from NIST REFPROP (NIST, 2010). The initial assumed wall temperature set the iterative calculations for a given node. The iterations were performed until the calculated wall temperature and assumed wall temperature values converge to a desired value, followed by the thermal resistance and HTC calculations of the hot fluid, tube, and cold fluid. The inlet cold bulk fluid temperature was assumed below the exit cold bulk fluid temperature. Based on the assumed inlet cold bulk fluid temperature, the second set of iterations was performed to converge the assumed and calculated values of the cold inlet bulk fluid temperature and thermal energy balance between the hot and cold fluid. The thermal energy gain by cold fluid should be equal to the loss of the hot fluid of the HX.

5.2 Assumptions

During development of the code for the HX, the following assumptions were considered: there was negligible heat loss to the environment; fully developed conditions for water on both hot and cold side along the length of HX pipe, the existence of entrance region is

negligible as compared to overall length of the HX pipe. For a 25 mm pipe diameter, the entrance region is ~0.75 m (Incropera *et al.*, 2006), which is significantly small as compared to ~150 m average length of the HX pipe; there was negligible fouling factor considered along the length of the HX pipe. Fouling is an accumulation of undesirable material on heat exchanger surface, it adds an additional thermal resistance to heat flow from hot to cold side, also the thermal conductivity of the fouling deposits is usually lower than that for the metal used for HX pipe. In general fouling results in a reduction in thermal performance of the HX.

5.3 Node Analysis

The length of the HX pipe is divided into several equal nodes. The node layout and cross-section of the double pipe HX is shown in Figure 5.1. For a given node the hot fluid properties are calculated at the entrance of the hot side into a node, where as cold fluid properties are calculated at the exit from the node. Figure 5.2 shows the heat transfer from the hot side to the cold side of counter-flow fluids and the reference positions where properties are calculated. The properties of a given node will be calculated at position n-1 and n, and will be valid at all points within that node. The fluid temperature of the node can be determined using the NIST REFPROP code (NIST, 2010).

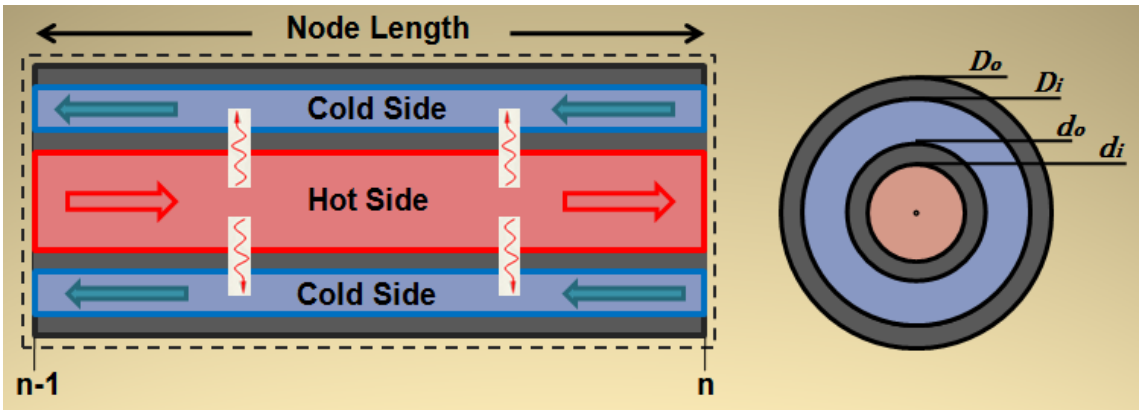

Figure 5.1: Diagram of a single node for a double-pipe heat exchanger.

5.4 Correlation

Based on the analysis shown in chapter 3, the Swenson *et al*. (1965) correlation was used in the code. The equation is shown in equation 5.1. Where Nu_w was the Nusset number, Re_w was the Reynolds number, Pr_w was Prandtl number, and ρ_w/ρ_b was the density.

$$\mathbf{Nu_w} = 0.00459\ \mathbf{Re_w^{0.923}\overline{Pr}_w^{0.613}}\left(\frac{\rho_w}{\rho_b}\right)^{0.231} \tag{5.1}$$

5.5 Heat Transfer Calculations

To determine the Nusset number, the Reynolds number and Prandtl number for the Swenson correlation, the mass flow rate in each pipe is calculated from mass flux and cross-section area of the pipe. The mass flow rate is calculated using equation 5.2. Where $\dot{m}_{pipe}$ was the mass flow rate of a pipe, G was the mass flux, and A_c is cross-section area of the pipe.

$$\dot{m}_{pipe} = GA_c \tag{5.2}$$

For each node an initial wall temperature ($T_{w,n-1}$) was assumed, below the hot side bulk fluid temperature ($T_{b,h,n-1}$) at the entrance of the node. The initial assumed wall temperature set the iterative calculations for that node. Using this temperature the wall fluid properties were obtained from the NIST REFPROP (NIST, 2010) to calculate the Reynold number, average specific heat and the average Prandtl number.

The Reynold number for hot side was calculated using equation 5.3 and for cold side equation 5.4. Where $Re_{w,h}$ and $Re_{w,c}$ were Reynolds number for the hot and cold side respectively; G_h and G_c were mass flux for the hot and cold side respectively; d_i and D_{hy} were inside diameter of the inner pipe and hydraulic diameter of the annulus pipe respectively; $\mu_{w,h}$ and $\mu_{w,c}$ were viscosity at wall temperature respectively;

$$Re_{w,h} = \frac{G_h d_i}{\mu_{w,h}} \tag{5.3}$$

$$Re_{w,c} = \frac{G_c D_{hy}}{\mu_{w,c}} \tag{5.4}$$

The average specific heat was calculated using equation 5.5. Where $\bar{C}_p$ was the average specific heat; H_w and H_b were the enthalpy of fluid at wall and bulk temperature respectively; T_w and T_b were the wall and bulk fluid temperatures respectively.

$$\overline{Cp} = \left(\frac{H_w - H_b}{T_w - T_b}\right) \tag{5.5}$$

The average Prandtl number was calculated using equation 5.6. Where Pr_w was the Prandtl number; k_w was thermal conductivity of the fluid at wall temperature.

$$\overline{Pr_w} = \frac{\mu_w \overline{Cp}}{k_w} \tag{5.6}$$

The Heat Transfer Coefficient (HTC) for the hot side was calculated using equation 5.7.

$$HTC_h = \frac{Nu_{h,w} k_h}{d_i} \tag{5.7}$$

The HTC for the cold side (annulus pipe) was calculated using equation 5.8.

$$HTC_c = \frac{Nu_{c,w} k_c}{D_{hy}} \tag{5.8}$$

The hydraulic diameter was calculated using equation 5.9.

$$D_{hy} = D_i - d_o \tag{5.9}$$

The thermal resistance for the hot fluid is calculated using equation 5.10. Where R_h was the resistance of the hot fluid.

$$R_h = \frac{d_o}{HTC_h \, d_i} \tag{5.10}$$

The thermal resistance for the pipe is calculated using equation 5.11. Where R_{pipe} was the resistance of the pipe thickness.

$$R_{pipe} = \frac{\mathrm{d_o} \ln\left(\frac{d_o}{d_i}\right)}{2k} \tag{5.11}$$

The thermal conductivity of stainless steel (SS-304) was calculated using equation 5.12. (Appendix - B)

$$k_{ss-304} = 2 \times 10^{-8} T_w^3 - 4 \times 10^{-5} T_w^2 + 3.98 \times 10^{-2} T_w + 5.728 \quad (5.12)$$

The thermal resistance for the cold fluid was calculated using equation 5.13. Where R_c was the resistance of the cold fluid.

$$R_c = \frac{1}{HTC_c} \quad (5.13)$$

The total resistance of the hot fluid, tube material, and cold fluid was calculated using equation 5.14.

$$R = \frac{d_o}{HTC_h . d_i} + \frac{\mathrm{d_o}.\ln\left(\frac{d_o}{d_i}\right)}{2k} + \frac{1}{HTC_c} \quad (5.14)$$

The wall temperature was then calculated using equation 5.15 (Shah *et al*., 2003). The iterations were performed until the calculated wall temperature and assumed wall temperature difference was equal or less than 0.01 ^{o}C.

$$T_{w,n-1} = \frac{\left(\frac{T_{b,h,n-1}}{R_{h,n}}\right) + \left(\frac{T_{b,c,n-1}}{R_{c,n}}\right)}{\left(\frac{1}{R_{h,n}}\right) + \left(\frac{1}{R_{c,n}}\right)} \quad (5.15)$$

For thermal energy balance, the second set of iterations was used to solve for the operating fluid temperatures in each node. The equation 5.16 and 5.17 were used for the energy balance, developed for computer-based HX numerical analysis (Ribando *et al*., 1997).

$$\dot{m}_h Cp_{h,n}\left(T_{h,n-1} - T_{h,n}\right) - U_n A_n \left[\frac{T_{h,n-1} + T_{h,n}}{2} - \frac{T_{c,n} + T_{c,n-1}}{2}\right] = 0 \quad (5.16)$$

$$\dot{m}_c Cp_{c,n}\left(T_{c,n} - T_{c,n-1}\right) - U_n A_n \left[\frac{T_{c,n} + T_{c,n-1}}{2} - \frac{T_{h,n-1} + T_{h,n}}{2}\right] = 0 \quad (5.17)$$

The thermal energy gain by cold fluid should be equal to the loss of the hot fluid in given node. Similar to the wall temperature calculations, the cold side inlet temperature ($T_{c,n}$) was assumed, less than the outlet cold side temperature ($T_{c,n-1}$). The assumed cold inlet value was used in the equation 5.18. The calculated value of hot side outlet temperature from equation 5.18 was then used in equation 5.19 to calculate new value of cold side inlet temperature.

$$T_{h,n} = \frac{(\dot{m}_h Cp_{h,n} - 0.5U_n A_n)T_{h,n-1} + 0.5U_n . A_n (T_{c,n-1} + T_{c,n})}{\dot{m}_h Cp_{h,n} - 0.5U_n A_n} \quad (5.18)$$

$$T_{c,n} = \frac{(\dot{m}_c Cp_{c,n} - 0.5U_n A_n)T_{c,n-1} + 0.5U_n A_n (T_{h,n-1} + T_{h,n})}{\dot{m}_c Cp_{c,n} - 0.5U_n A_n} \quad (5.19)$$

Once the temperature of hot and cold side were found from equation 5.18 and 5.19, the thermal energy change for both hot and cold side was be found by equation 5.20 and 5.21.

$$Q_h = \dot{m}_h Cp_{h,n}(T_{h,n-1} - T_{h,n}) \quad (5.20)$$

$$Q_c = \dot{m}_c Cp_{c,n}(T_{c,n} - T_{c,n-1}) \quad (5.21)$$

The iterations were performed until the difference between the thermal energy on both hot and cold side is equal or less than 0.01 J.

The above heat transfer calculations were repeated for each node until the cold outlet temperature reach 340 ^{o}C (desired value) or the thermal power reach 2540 MW, corresponds to SCW CANDU reactor (Grande el al. 2011). The heat transfer calculation and MATLAB code for the HX was independently verified by UOIT Nuclear Design Laboratory Team member Jeffrey Samuel.

CHAPTER 6 - ANALYSIS

The heat transfer analysis is performed to study the effect of various parameters such as pressure, temperature, mass flow rate, and pipe size on the heat transfer surface area of the HX. The analysis is divided into two main parts: the first part is from SCW to SCW HX, and the second part is from SCW to SHS HX. Several trial and error test cases were performed by varying pressure, temperature, mass flow rate, and pipe size to develop test conditions for the analysis.

6.1 SCW to SCW Heat Transfer Analysis

The SCW to SCW heat transfer analysis is performed on HX1 and the Figures 6.1 to 6.10 shows the results. Where horizontal dashed lines (T_{pc}) shows the pseudocritical temperature and vertical dashed lines (L_{pc}) shows the location of the pseudocritical point along the length of pipe for the hot and cold side. The parameters on both hot and cold side are at supercritical fluid conditions.

6.1.1 Effect of Pressure

Heat-transfer analysis was performed by varying pressure on the hot and cold side to determine the effect on the heat transfer surface area and fluid properties along the length of the pipe of the HX. Based on these test cases it is noted that, when the pressure on hot side is high compared to the cold side, the operating parameters like mass flow rate and temperature are more forgiving compared to when the pressure on hot side is lower than the cold side. When the pressure on hot side is higher, the mass flow rate was 1320 kg/s and outlet temperature is 600 ^{o}C on cold side for analysis. Whereas when the pressure on the cold side is higher, the mass flow rate is lowered to 1200 kg/s and outlet temperature is lowered to 550 ^{o}C for analysis.

Table 6.1 shows the inputs and results obtained from the code, when the pressure on the hot side is high as compared to cold side. Figure 6.1 shows the temperature profile and variations in fluid properties of the hot and cold sides along the length of the double-pipe HX for a variation in the hot side pressure from 25.5 to 30 MPa. The results show that

the heat transfer is enhanced or deteriorated due to the change in fluid properties depending on the exact fluid conditions. In Figure 6.1a, the heat transfer rate drop is much quicker in the beginning, as compared to Figure 6.1b, when the pressure on hot side is raised to 26 MPa. Whereas in Figure 6.1c-d the heat transfer rate shows opposite trend, it rises in the beginning and drops as it enters into the pseudocritical region. In Figure 6.1 the viscosity drops in the beginning and rises as it enters into pseudocritical region. Since the Reynolds number is inversely proportional to viscosity. The heat transfer rate rises in the beginning, but its effect is more visible in Figure 6.1c-d due to delay in the pseudocritical region, whereas in Figure 6.1 the effect of viscosity is dominated by the rise of specific heat as compared to Figure 6.1c-d.

In Figure 6.1a, the heat transfer in the pseudocritical range is small starting at approximately 300 m to 400 m along the length of the HX. After 400 m, heat transfer starts again from the hot to cold sides at a very low rate. The length of the psudocritical region is large when the pressure on both hot and cold side is same and reduces with the increase of pressure on the hot side. In Figure 6.1d when the pressure on the hot side is much higher (30 MPa) than that in the cold side (it is 25.5 MPa), the length of the pseudocritical region is much smaller. For SCW the peak of specific heat reduces and shifts towards higher temperature with the increase of pressure. Comparing the Figures 6.1a and 6.1d; the specific heat peak in Figure 6.1a is same for both hot and cold side and location of specific heat peak along the length of the pipe is further apart due to their thermophysical behaviour, whereas in Figure 6.1d the with the increase of pressure on hot side specific heat peak reduces and moves towards higher temperature, reducing the location difference ΔL_{pc} between pseudocritical points to 0.6 m. Also due to decrease in the specific heat peak on hot side, the temperature change in pseudocritical region for hot side in Figure 6.1d is more significant as compared to the temperature change in Figure 6.1a. As there is a shorter pseudocritical region in Figure 6.1d the heat transfer rate has a much sharper relationship as compared to that in Figure 6.1a. In pseudocritical region the most of the heat is used up due to a higher specific heat capacity of the fluid, resulting in reduced or negligible temperature change between the hot and cold sides.

Table 6.1: Parameters and results for pressure variation on hot side.

Input Parameters						
Hot Side						
Pressure (MPa)	25.5	26	27	28	29	30
Inlet Temperature (^oC)	625	625	625	625	625	625
Total mass flow rate (kg/s)	1320	1320	1320	1320	1320	1320
Mass flux ($kg/m^2 \cdot s$)	2000	2000	2000	2000	2000	2000
Outer diameter of pipe (mm)	25.4	25.4	25.4	25.4	25.4	25.4
Cold Side						
Pressure (MPa)	25.5	25.5	25.5	25.5	25.5	25.5
Outlet Temperature (^oC)	600	600	600	600	600	600
Total mass flow rate (kg/s)	1320	1320	1320	1320	1320	1320
Code Output						
Total Q (MW)	2540	2540	2540	2540	2540	2540
Q/Pipe (MW)	1.563	1.557	1.542	1.528	1.514	1.500
No. of Pipes	1625	1632	1647	1662	1677	1693
Heat Transfer Area/Pipe (m^2)	43.49	29.78	21.94	18.84	17.19	16.25
Total Heat Transfer Area (m^2)	70651	48593	36137	31327	28848	27524
Length of Pipe (m)	545.1	373.2	275	236.2	215.5	203.7
Total Length of Pipe (m)	885400	608968	452876	392589	361523	344929
Hot Side						
Outlet Temperature (^oC)	352.2	351.8	351.1	350.3	349.4	348.4
Mass flow rate/Pipe (kg/s)	0.812	0.808	0.801	0.794	0.786	0.779
Inner diameter of pipe (mm)	22.7	22.7	22.6	22.5	22.4	22.3
Cold Side						
Inlet Temperature (^oC)	341.2	341.1	341.2	341.1	341.1	341
Mass flow rate/Pipe (kg/s)	0.812	0.808	0.801	0.794	0.786	0.779
Mass flux ($kg/m^2 \cdot s$)	2000	2000	2000	2000	2000	2000
Outer diameter of pipe (mm)	38.1	38	38	37.9	37.8	37.7
Inner diameter of pipe (mm)	34.1	34.1	34	33.9	33.9	33.8

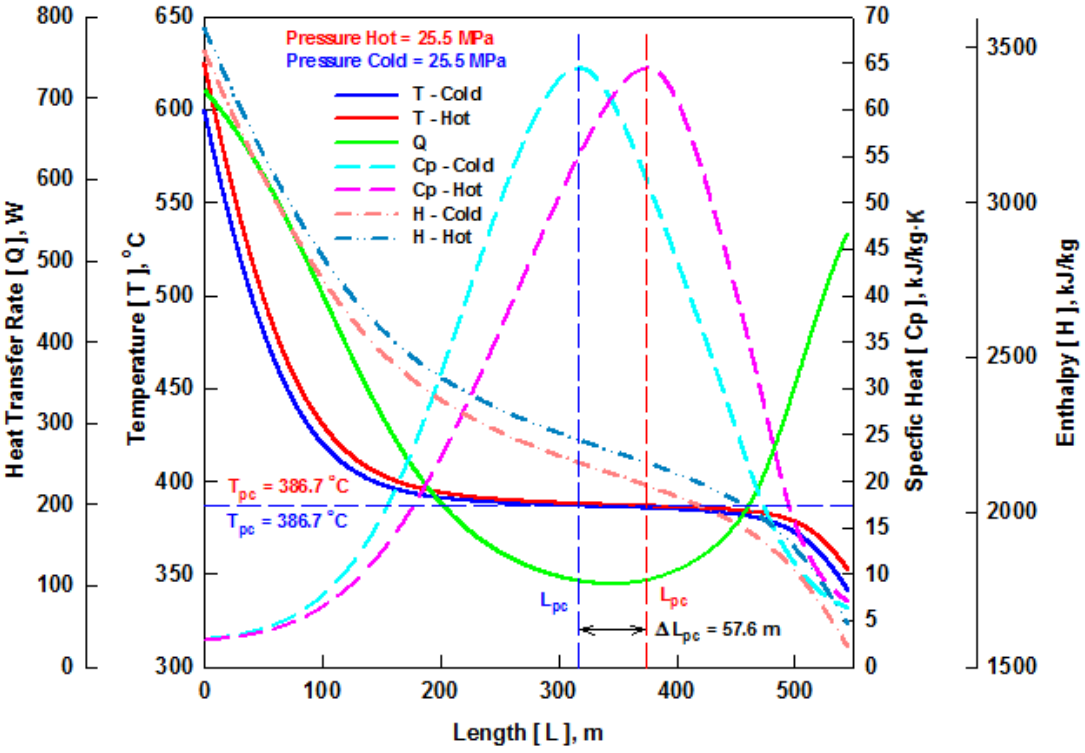
Pressure Hot = 25.5 MPa
Pressure Cold = 25.5 MPa
T - Cold
T - Hot
Q
Cp - Cold
Cp - Hot
H - Cold
H - Hot
Heat Transfer Rate [Q], W
Temperature [T], °C
Specific Heat [Cp], kJ/kg·K
Enthalpy [H], kJ/kg
Length [L], m
T_pc = 386.7 °C
T_pc = 386.7 °C
L_pc
L_pc
ΔL_pc = 57.6 m

(a)

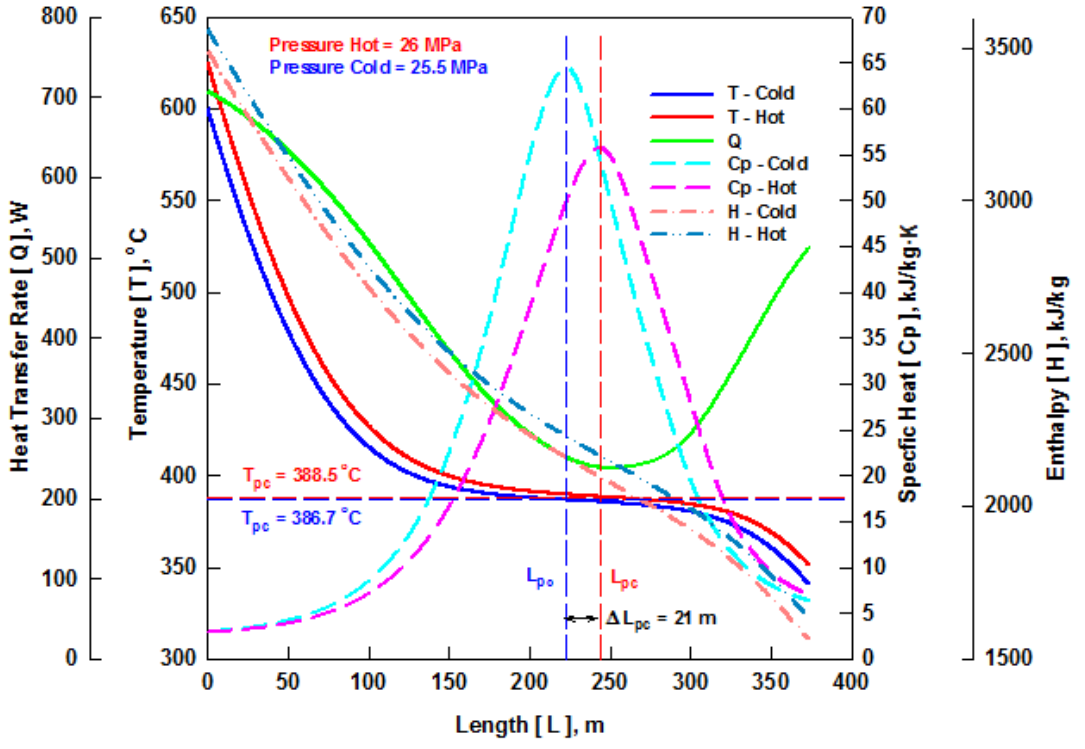
Pressure Hot = 26 MPa
Pressure Cold = 25.5 MPa
T - Cold
T - Hot
Q
Cp - Cold
Cp - Hot
H - Cold
H - Hot
Heat Transfer Rate [Q], W
Temperature [T], °C
Specific Heat [Cp], kJ/kg·K
Enthalpy [H], kJ/kg
Length [L], m
T_pc = 388.5 °C
T_pc = 386.7 °C
L_pc
L_pc
ΔL_pc = 21 m

(b)

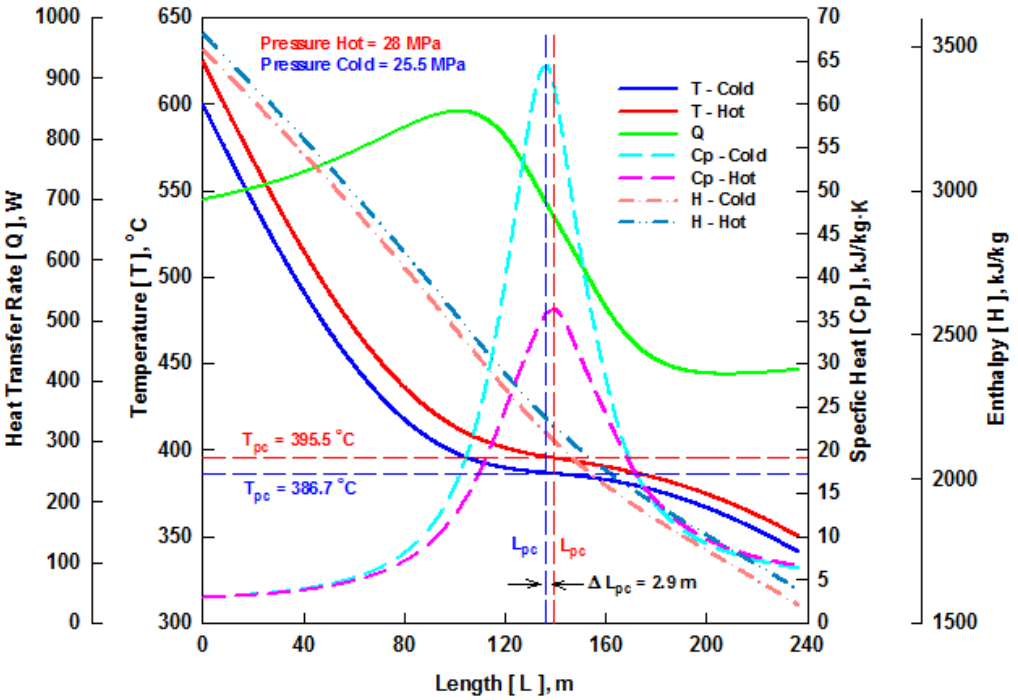

(c)

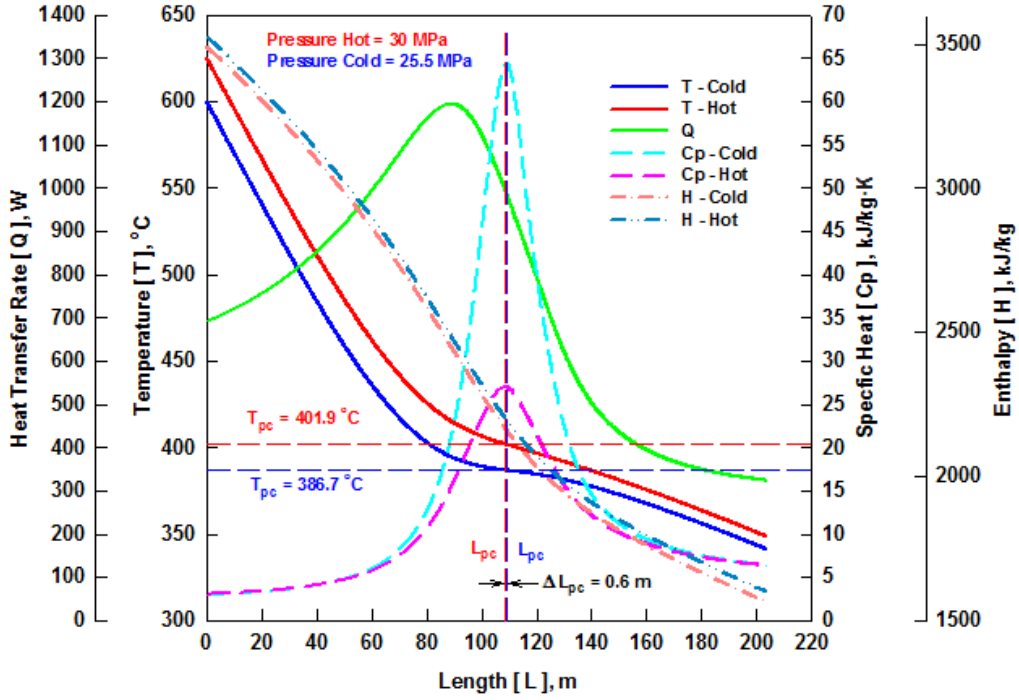

(d)

Figure 6.1: Effect of pressure (hot) on temperature profile and fluid properties along length of double-pipe HX: P_{hot} = (a) 25.5 MPa, (b) 26 MPa, (c) 28 MPa, and (d) 30 MPa.

Figure 6.2 shows the effect of change in hot side pressure on heat transfer area of the HX and location difference pseudocritical points on hot and cold side. The heat-transfer-surface area decreases approximately by 2.6 times with pressure difference of 4.5 MPa on hot side. The graph also shows the location difference ΔL_{pc} along the length of the pipe for the hot and the cold side. Psudocritical point location difference ΔL_{pc} decreases along the length of the pipe with the increase of pressure on the hot side.

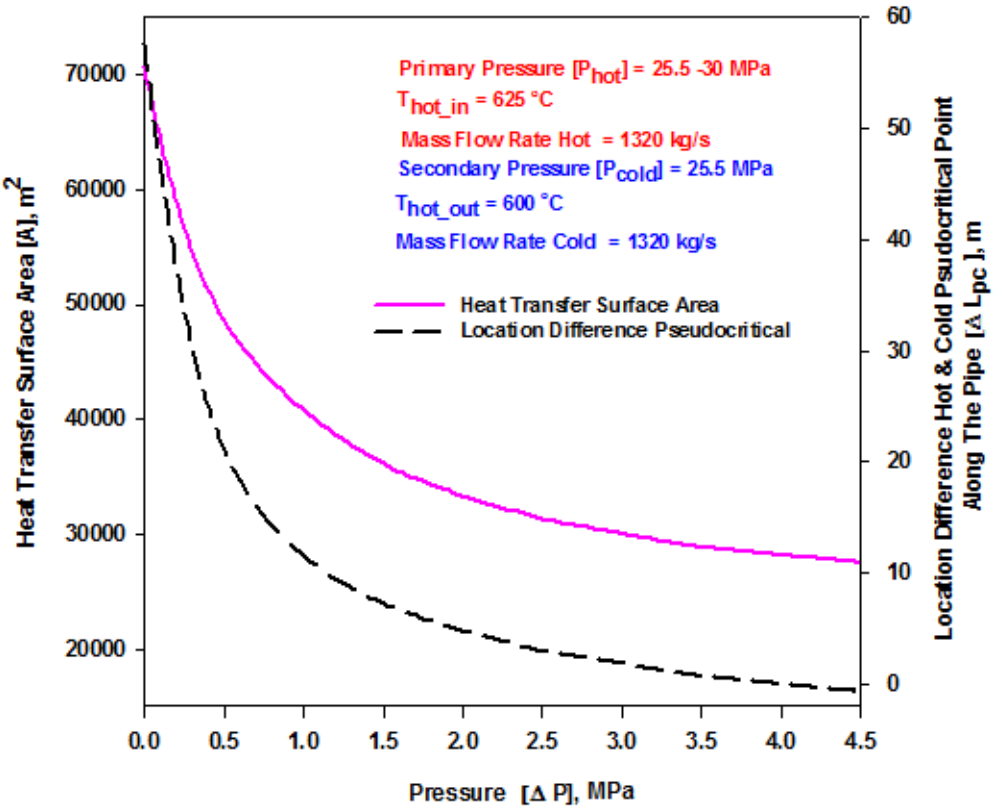

Figure 6.2: Effect of pressure (hot) on heat-transfer-surface area of HX and location variation of pseudocritical point along the length of the pipe.

Although it seems higher pressure difference on the hot side reduces the heat transfer surface area of the HX, higher pressure might add complexity to the core design. Also the higher pressure difference on hot side and cold side may not be good idea for the overall plant efficiency. Higher pressure difference of 0.5 to 1.5 MPa on hot side seems a more optimal configuration for the heat transfer surface area of a HX and the plant efficiency, and should be investigated further in future analysis.

Table 6.2 shows the operating parameters selected for analysis and results obtained when the pressure on the cold side is higher compared to the hot side. Figure 6.3 shows the temperature profile and variations in fluid properties of the hot and cold sides along the length of the double-pipe HX for a variation in the cold side pressure from 24 to 28 MPa, pressure on the hot side is kept constant at 25 MPa. The results show that the heat transfer is enhanced or deteriorated due to the change in fluid properties depending on the exact fluid conditions. In Figure 6.3a, the pseudocritical region is much smaller as compared to the psudocritical region in Figure 6.3d. In Figure 6.3d the heat transfer was small starting at approximately 150 m length and continues up to roughly 650 m along the length of the HX.

In Figure 6.3a, the heat transfer rate rises in the beginning and drops as it enters into the pseudocritical region. The entrance heat transfer rate rise effect diminishes as the pressure on the cold side is raised, in Figure 6.3d the heat transfer rate drop is much quicker as compared to Figure 6.3a. The viscosity drops in the beginning and rise as it enters into pseudocritical region, since the Reynolds number is inversely proportional to viscosity. The heat transfer rate rise in the beginning, but its effect was more visible in Figure 6.3a, due to delay in the pseudocritical region. In Figure 6.3b-c the effect of viscosity is dominated by the rise of specific heat in the entrance region.

In Figure 6.3a when the pressure on the cold side was below the hot side, the length of the pseudocritical region is much smaller as compared to Figure 6.3b-d. For SCW the peak of specific heat reduces and shifts towards higher temperature with the increase of pressure. Comparing the extreme cases Figure 6.3a and 6.3d; the specific heat peak on cold side is smaller in Figure 6.3d compared to Figure 6.3a, but still the pseudocritical region is much larger in 6.3d. Because with increase of the pressure on the cold side in Figure 6.3d the specific heat peak for both hot and cold side along the length of the pipe were moving away from each other due to their thermophysical property behavior. In Figure 6.3a when the pressure on the cold side is smaller ΔL_{pc} location difference between hot and cold side is 29.8 m as compared to Figure 6.1d when the pressure was much higher ΔL_{pc} location difference between the hot and the cold side was 645 m.

Table 6.2: Parameters and results for pressure variation on cold side.

Input Parameters					
Hot Side					
Pressure (MPa)	25	25	25	25	25
Inlet Temperature (^oC)	625	625	625	625	625
Total mass flow rate (kg/s)	1320	1320	1320	1320	1320
Mass flux ($kg/m^2 \cdot s$)	2000	2000	2000	2000	2000
Outer diameter of pipe (mm)	25.4	25.4	25.4	25.4	25.4
Cold Side					
Pressure (MPa)	24	25	26	27	28
Outlet Temperature (^oC)	550	550	550	550	550
Total mass flow rate (kg/s)	1200	1200	1200	1200	1200
Code Output					
Total Q (MW)	2146	2136	2127	2115	2103
Q/Pipe (MW)	1.327	1.321	1.315	1.308	1.300
No. of Pipes	1617	1617	1617	1617	1617
Heat Transfer Area/Pipe (m^2)	7.38	8.61	10.7	15.16	58.78
Total Heat Transfer Area (m^2)	11947	13921	17314	24526	95050
Length of Pipe (m)	92.6	107.9	134.2	190.1	736.7
Total Length of Pipe (m)	149723	174461	216985	307369	1191156
Hot Side					
Outlet Temperature (^oC)	380.1	380.4	380.7	381	381.3
Mass flow rate/Pipe (kg/s)	0.816	0.816	0.816	0.816	0.816
Inner diameter of pipe (mm)	22.8	22.8	22.8	22.8	22.8
Cold Side					
Inlet Temperature (^oC)	340	340	340	340	340
Mass flow rate/Pipe (kg/s)	0.742	0.742	0.742	0.742	0.742
Mass flux ($kg/m^2 \cdot s$)	1818	1818	1818	1818	1818
Outer diameter of pipe (mm)	37.9	38	38.2	38.4	38.6
Inner diameter of pipe (mm)	34.1	34.1	34.1	34.1	34.1

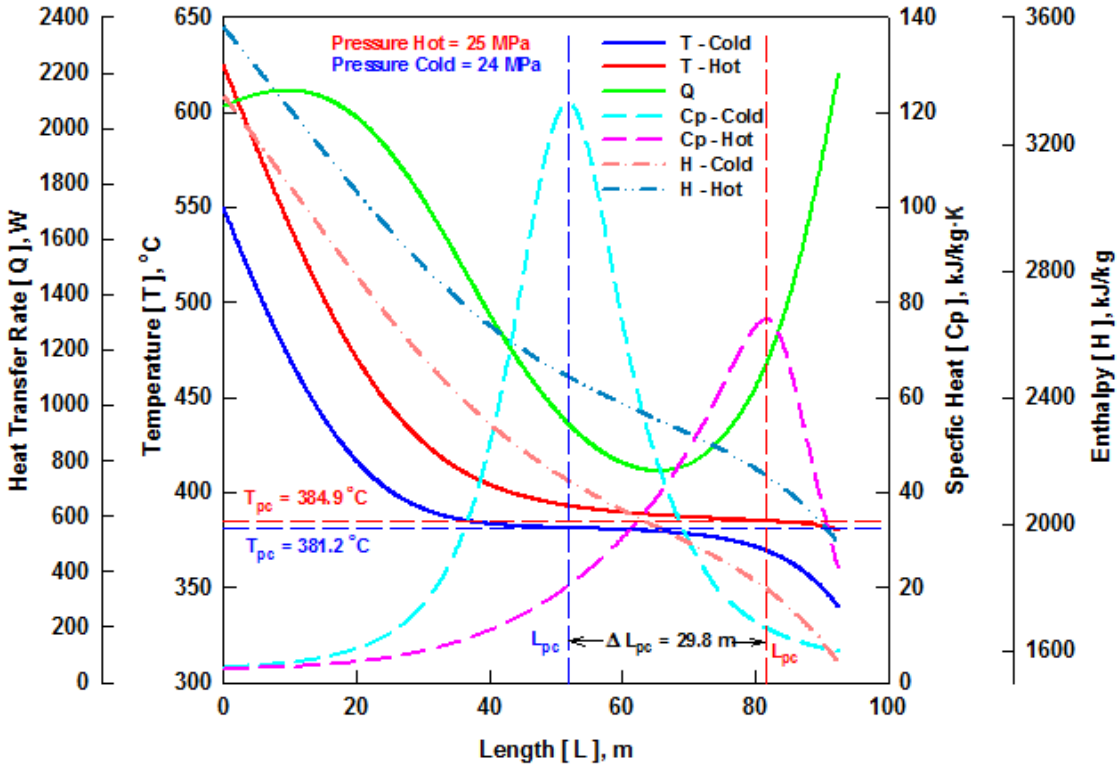
Pressure Hot = 25 MPa
Pressure Cold = 24 MPa
T - Cold
T - Hot
Q
Cp - Cold
Cp - Hot
H - Cold
H - Hot
Heat Transfer Rate [Q], W
Temperature [T], °C
Specific Heat [Cp], kJ/kg·K
Enthalpy [H], kJ/kg
Length [L], m
T_pc = 384.9 °C
T_pc = 381.2 °C
L_pc
Δ L_pc = 29.8 m
L_pc

(a)

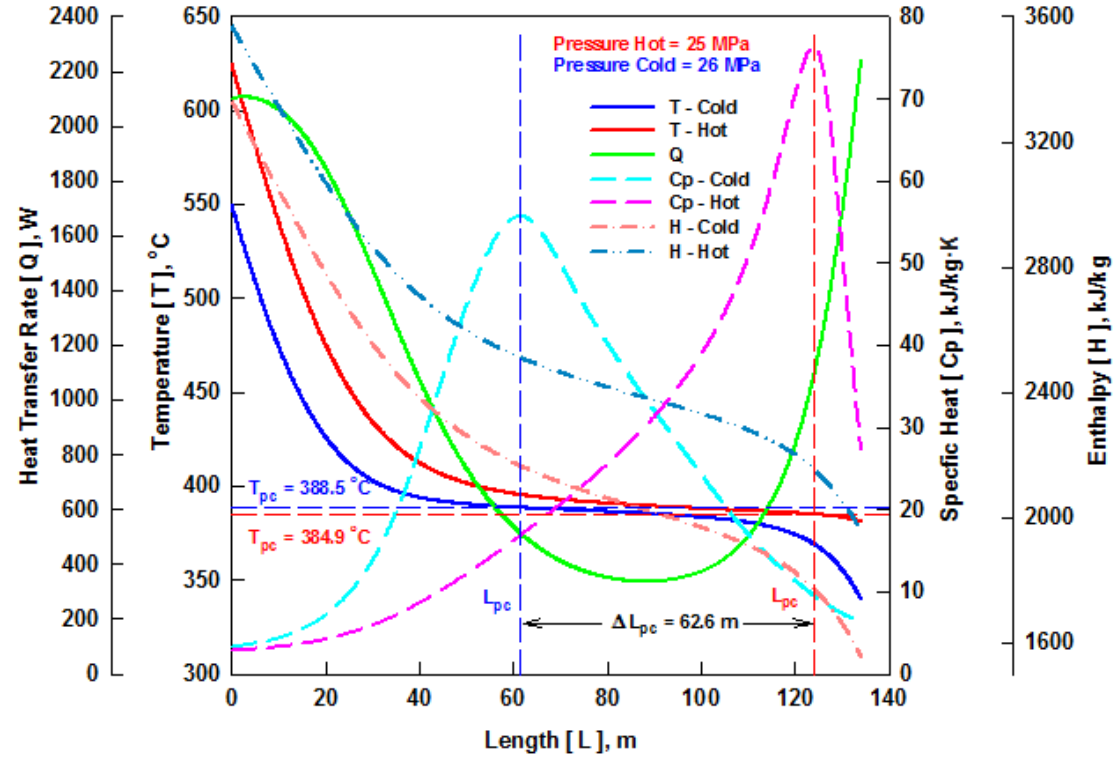
Pressure Hot = 25 MPa
Pressure Cold = 26 MPa
T - Cold
T - Hot
Q
Cp - Cold
Cp - Hot
H - Cold
H - Hot
Heat Transfer Rate [Q], W
Temperature [T], °C
Specific Heat [Cp], kJ/kg·K
Enthalpy [H], kJ/kg
Length [L], m
T_pc = 388.5 °C
T_pc = 384.9 °C
L_pc
Δ L_pc = 62.6 m
L_pc

(b)

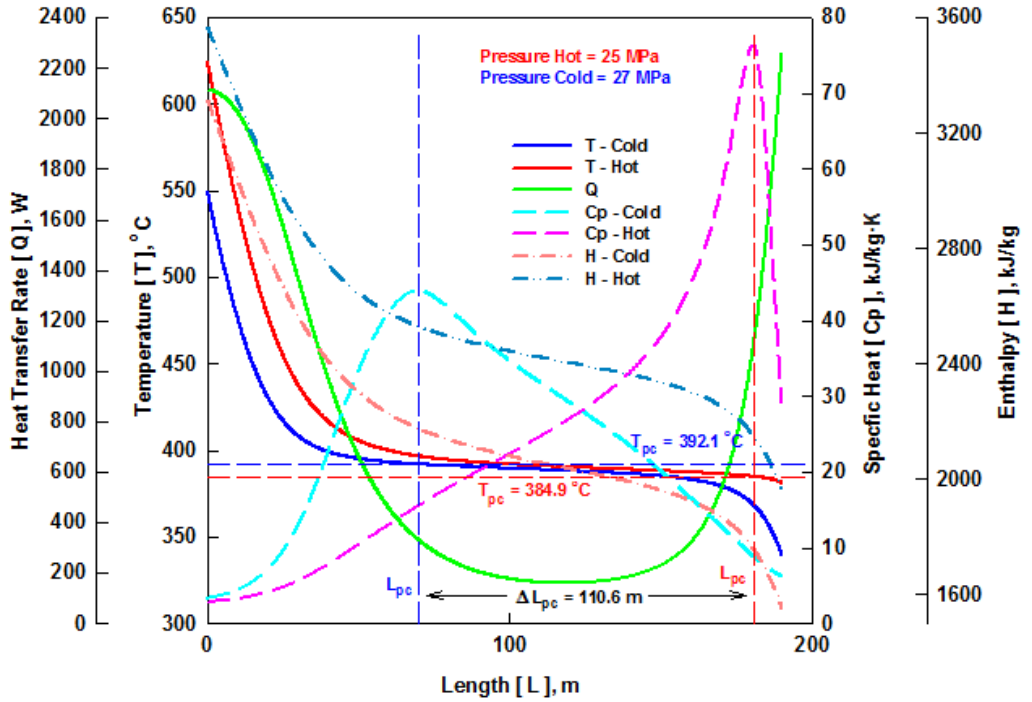

(c)

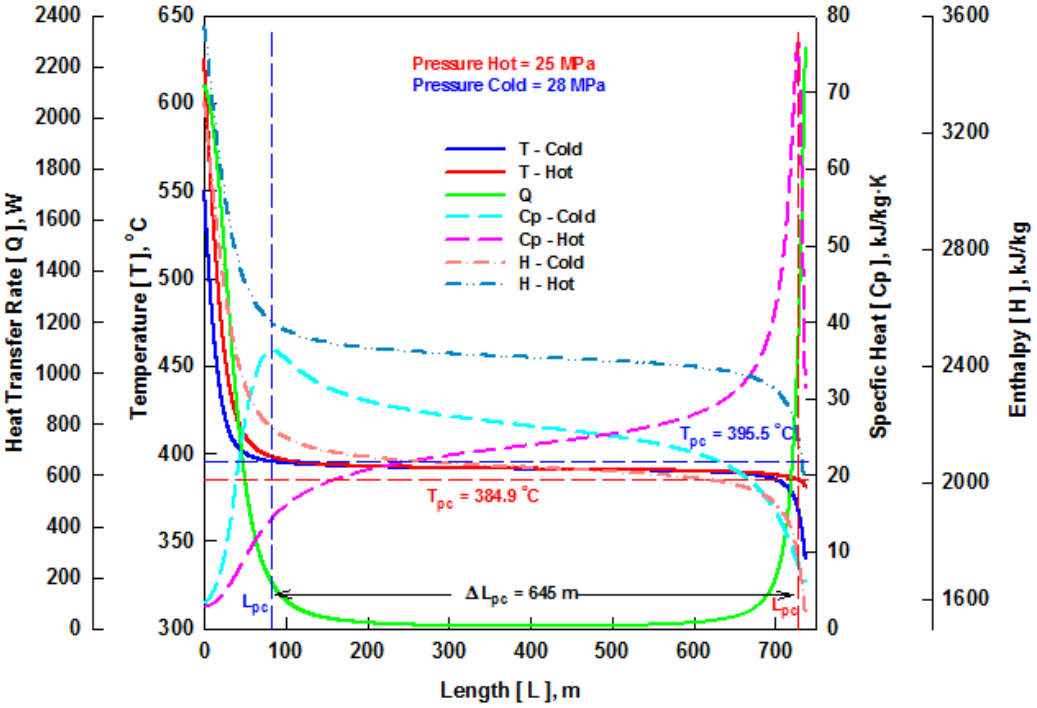

(d)

Figure 6.3: Effect of pressure (cold) on temperature profile and fluid properties along length of double-pipe HX: P_{cold} = (a) 24 MPa, (b) 26 MPa, (c) 27 MPa, and (d) 28 MPa.

Figure 6.4 shows the effect of change in cold side pressure. The heat-transfer-surface area increases by ~7 times with a pressure difference of 3 MPa (higher on the cold side). The graph also shows the location difference pseudocritical point along the length of the pipe for the hot and the cold side. Pseudocritical point location difference increases along the length of the pipe, with the increase of the pressure on the cold side. The pseudocritical point location difference is 62.6 m when the pressure on cold side is 26 MPa and the pseudocritical point location difference increases to 645 m, when the pressure is increased to 28 MPa on the cold side along the length of the HX.

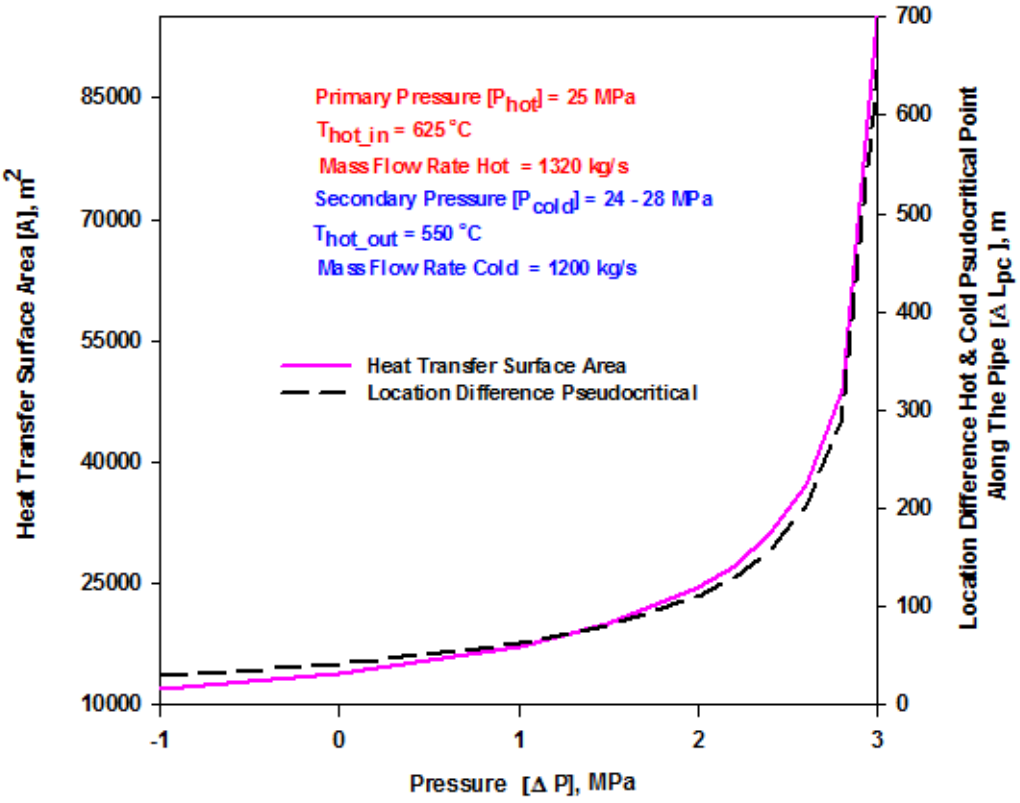

Figure 6.4: Effect of pressure (cold) on heat-transfer-surface area of HX and location variation of pseudocritical point along the length of the pipe.

It was noted that higher pressure difference on cold side tends to increase the heat transfer surface area of the HX. Also, higher pressure on cold side compared to hot side is less forgiving to the operating parameters like mass flow rate, temperature, and pipe size. The higher pressure difference of 0.5 to 2 MPa on cold side seems an optimal configuration for the heat transfer surface area of the HX and plant efficiency.

6.1.2 Effect of Temperature

Heat-transfer analysis was performed by varying the temperature on the cold side. Table 6.3 shows the operating parameters selected for analysis and results obtained. The inlet temperature on the hot side is kept constant at 625 ^{o}C and outlet temperature on the cold side is varied from 550 ^{o}C to 600 ^{o}C. The pressure on the hot and cold side is kept constant at 25 MPa and 25.5 MPa respectively. Figure 6.5 shows a temperature profile and variations in fluid properties of the hot and cold sides along the length of the double-pipe HX with variation in the outlet temperature on hot side. The heat transfer in the pseudocritical region decreases due to the higher specific heat capacity of the water. The effect of the pseudocritical region is higher as the temperature difference between the hot (in) and cold (out) side starts decreasing. Since the pressure on both hot and cold side is constant for this temperature analysis, the peak value of the specific heat is same in Figure 6.5. As the temperature difference between hot (in) and cold (out) side decreases, the location difference ΔL_{pc} between pseudocritical points along the length of the HX pipe increases. In Figure 6.5a the location difference ΔL_{pc} was 60.6 m and increases to 186.2 m in Figure 6.5d with the temperature increase from 550 ^{o}C to 600 ^{o}C on cold (out) side.

The heat transfer rate is directly proportional to temperature difference between hot and cold side. When temperature difference between hot (in) and cold (out) side is higher, the heat transfer rate is higher as shown in Figure 6.5. Due to higher heat transfer rate and temperature difference in Figure 6.5a the temperature on cold side approaches pseudocritical region much earlier as compared to hot side. By the time pseudocritical region on hot side dominates, effect of pseudocrtical region on cold side diminishes and leads to much faster temperature drop on cold side as compared to hot side. Whereas in Figure 6.5d the temperature difference between hot (in) and cold (out) side is less, leading to lower heat transfer rate and slower temperature change on hot and cold side. Due to slower heat transfer rate and smaller temperature difference the overlap of hot and cold side pseudocritical region is much higher in Figure 6.5d as compared to Figure 6.5a.

In Figure 6.5 the heat transfer rate drop is small at the entrance region, where as in Figure 6.5c-d the heat transfer rate shows opposite trend, it rises in the beginning and drops as it enters into the pseudocritical region. This is due to the viscosity drops at the entrance region and rises as it enters into pseudocritical region. The effect of viscosity is more visible in Figure 6.5c-d due to delay in the pseudocritical region, whereas in Figure 6.5a the effect of viscosity is dominated by the rise of specific heat. In pseudocritical region the most of the heat is used up due to a higher specific heat capacity of the fluid, resulting in reduced or negligible temperature change between the hot and cold sides.

Table 6.3: Parameters and results for temperature variation on cold side.

Input Parameters						
Hot Side						
Pressure (MPa)	25	25	25	25	25	25
Inlet Temperature (^oC)	625	625	625	625	625	625
Total mass flow rate (kg/s)	1320	1320	1320	1320	1320	1320
Mass flux ($kg/m^2 \cdot s$)	2000	2000	2000	2000	2000	2000
Outer diameter of pipe (mm)	25.4	25.4	25.4	25.4	25.4	25.4
Cold Side						
Pressure (MPa)	25.5	25.5	25.5	25.5	25.5	25.5
Outlet Temperature (^oC)	550	560	570	580	590	600
Total mass flow rate (kg/s)	1250	1250	1250	1250	1250	1250
Code Output						
Total Q (MW)	2219	2259	2300	2340	2377	2416
Q/Pipe (MW)	1.372	1.397	1.422	1.447	1.471	1.494
No. of Pipes	1617	1617	1617	1617	1617	1617
Heat Transfer Area/Pipe (m^2)	11.76	13.97	16.96	21.29	28.27	42.14
Total Heat Transfer Area (m^2)	19030	22591	27429	34435	45712	68136
Length of Pipe (m)	147.5	175.1	212.6	266.9	354.3	528.1
Total Length of Pipe (m)	238489	283115	343748	431545	572860	853874
Hot Side						
Outlet Temperature (^oC)	377.3	375.3	372.9	370.3	367.5	364.4
Mass flow rate/Pipe (kg/s)	0.816	0.816	0.816	0.816	0.816	0.816
Inner diameter of pipe (mm)	22.8	22.8	22.8	22.8	22.8	22.8
Cold Side						
Inlet Temperature (^oC)	340	340	340	340	340	340
Mass flow rate/Pipe (kg/s)	0.773	0.773	0.773	0.773	0.773	0.773
Mass flux ($kg/m^2 \cdot s$)	1894	1894	1894	1894	1894	1894
Outer diameter of pipe (mm)	38.1	38.1	38.1	38.1	38.1	38.1
Inner diameter of pipe (mm)	34.1	34.1	34.1	34.1	34.1	34.1

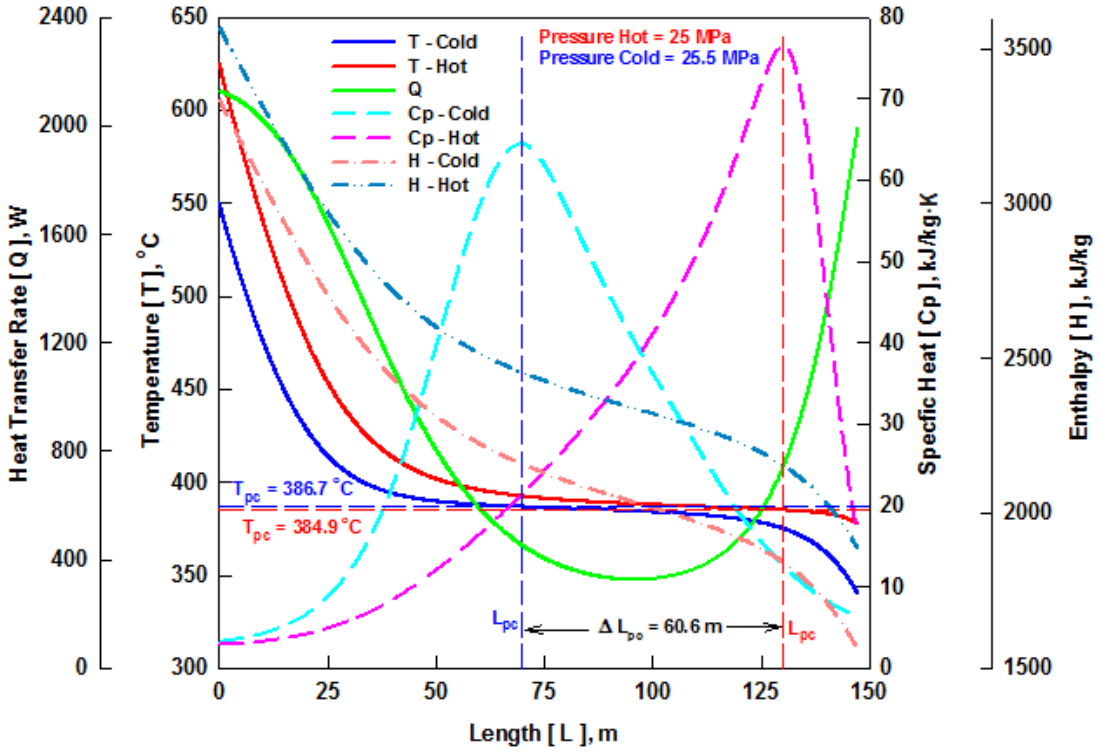
T - Cold
T - Hot
Q
Cp - Cold
Cp - Hot
H - Cold
H - Hot
Pressure Hot = 25 MPa
Pressure Cold = 25.5 MPa
Heat Transfer Rate [Q], W
Temperature [T], °C
Specific Heat [Cp], kJ/kg·K
Enthalpy [H], kJ/kg
Length [L], m
T_{pc} = 386.7 °C
T_{pc} = 384.9 °C
L_{pc}
ΔL_{pc} = 60.6 m
L_{pc}

(a)

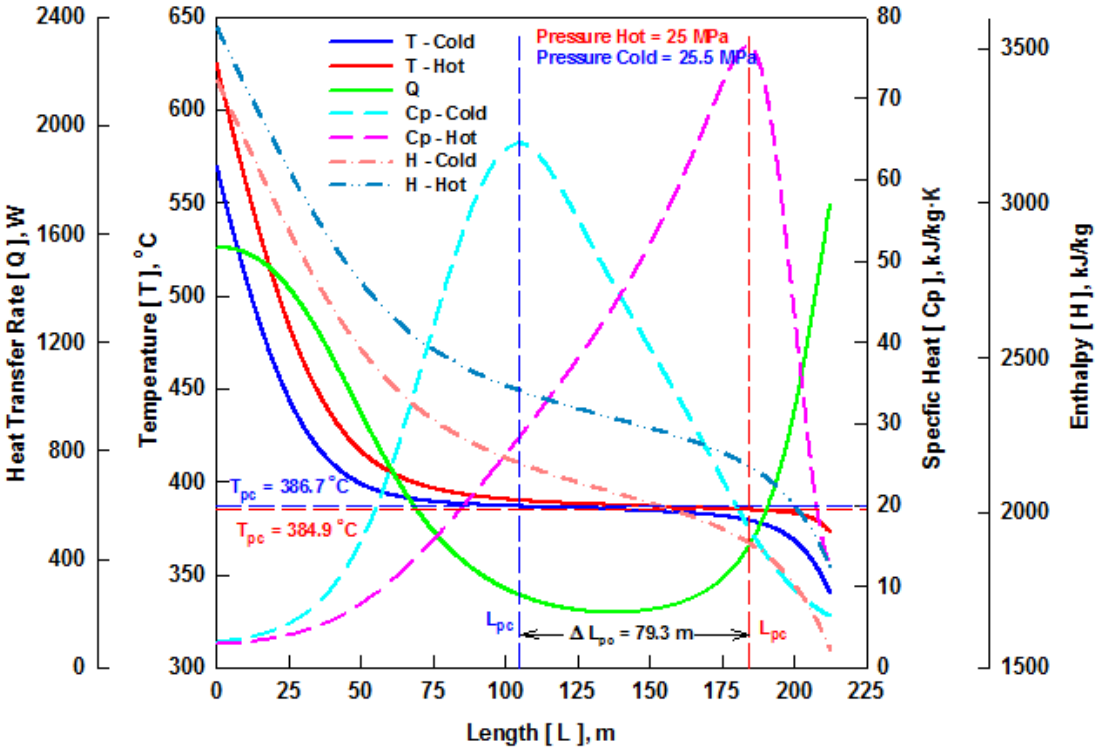
T - Cold
T - Hot
Q
Cp - Cold
Cp - Hot
H - Cold
H - Hot
Pressure Hot = 25 MPa
Pressure Cold = 25.5 MPa
Heat Transfer Rate [Q], W
Temperature [T], °C
Specific Heat [Cp], kJ/kg·K
Enthalpy [H], kJ/kg
Length [L], m
T_{pc} = 386.7 °C
T_{pc} = 384.9 °C
L_{pc}
ΔL_{pc} = 79.3 m
L_{pc}

(b)

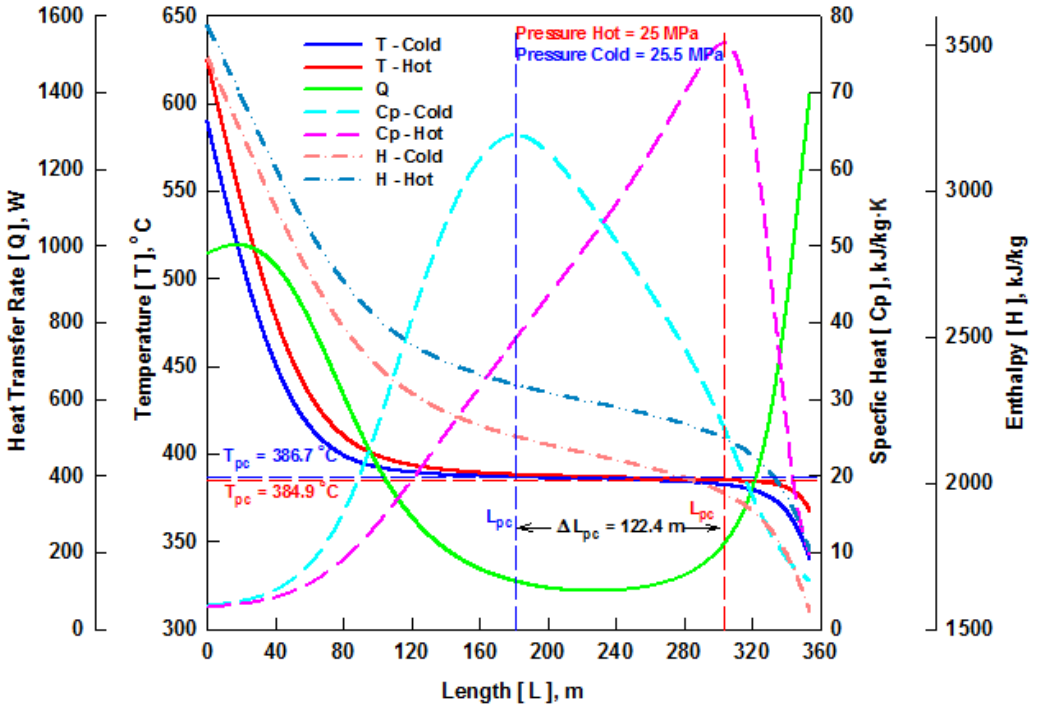

(c)

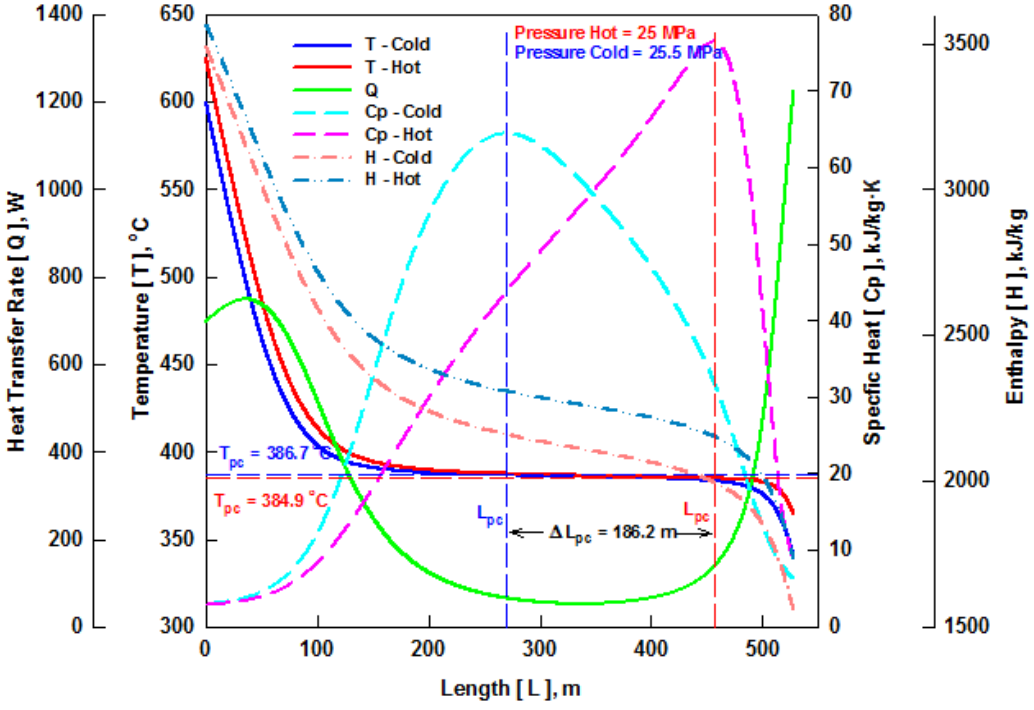

(d)

Figure 6.5: Effect of temperature difference between hot and cold side on temperature profile and fluid properties along length of double-pipe HX: T_{cold_out} = (a) 550 °C, (b) 570 °C, (c) 590 °C, and (d) 600 °C.

Figure 6.6 shows the variation in the heat-transfer-surface area with the change in the outlet temperature of the HX on the cold side. The Figure 6.6 also shows the location difference ΔL_{pc} between pseudocritical point along the pipe length of the HX for hot and cold side with change in temperature difference. The heat-transfer-surface area increases by approximately 3.4 times with a cold side outlet-temperature change from 550 to 600 °C. The higher temperature of 600 ^{o}C on the cold side will increase the thermal efficiency of the plant compared to the lower temperature of 550 ^{o}C. The cost of increase in heat transfer surface area of the HX may not be justifiable vs the increase in thermal efficiency at 600 ^{o}C. It may be optimal to have 580 ^{o}C on cold side. At 580 ^{o}C the heat transfer surface area of HX is almost half compared to 600 ^{o}C on cold side.

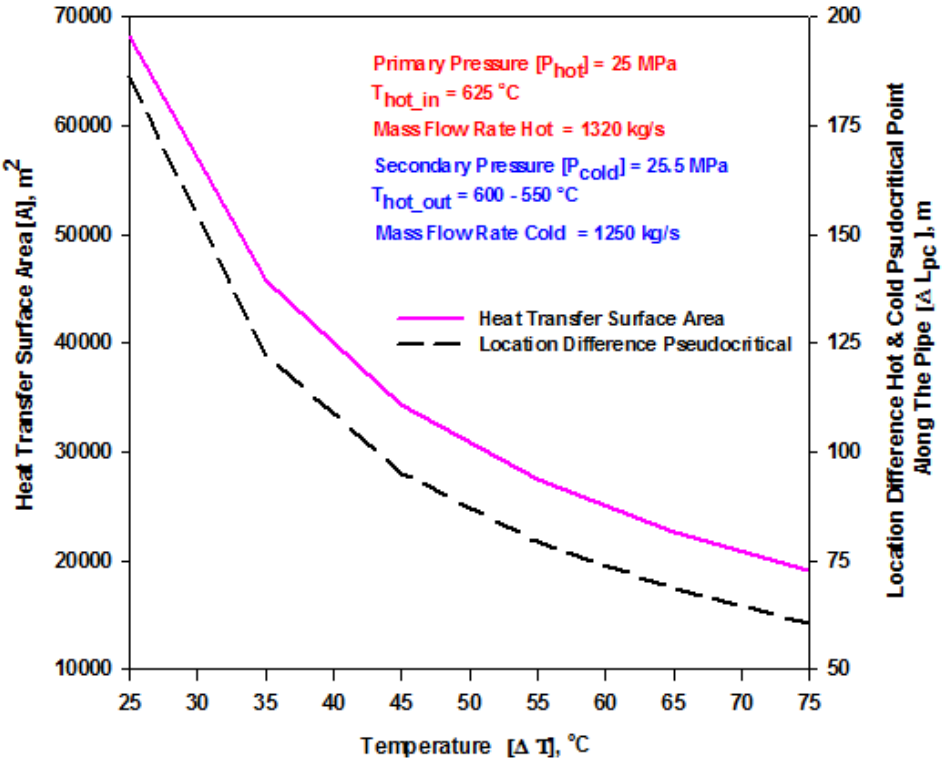

Figure 6.6: Effect of temperature difference on heat transfer surface area of HX and location difference pseudocritical point on hot and cold sides.

6.1.3 Effect of Pipe Variation

Heat-transfer analysis was performed by varying the inner pipe diameter of the double-pipe HX. Table 6.4 shows the operating parameters selected for analysis and results obtained. The pressure and inlet temperature for the hot side is 25 MPa and 625 ^{o}C and for cold side pressure and outlet temperature is 25.5 MPa and 600 ^{o}C are kept constant for the analysis. The mass flux and total mass flow rate for hot side is 2000 kg/m^{2}·s and 1320 kg/s, and for cold side 1894 kg/m^{2}·s and 1250 kg/s respectively kept constant for the analysis. The number of pipes in a HX changes from 2112 to 719 as the pipe diameter changed from 22.23 mm to 38.1 mm. The cross-section area of the inner and outer pipe is kept same. Figure 6.7 shows the temperature profile and variations in fluid properties of the hot and cold sides along the length of the double-pipe HX with variations in the pipe diameter. The results show that the heat transfer is enhanced or deteriorated due to the change in fluid properties depending on the exact fluid conditions. The heat transfer rate in the pseudocritical region decreases significantly due to a higher specific heat capacity of the fluid, resulting in reduced or negligible temperature change between the hot and cold sides.

The thermophysical properties and temperature trends are very similar in Figure 6.7a-d. In Figure 6.7a-d, the heat transfer rate shows rising trend in the beginning and drops as it enters into the pseudocritical region. The rise in the heat transfer rate is due to the viscosity drops in the beginning and rises as it enters into pseudocritical region. In Figure 6.7a location difference $\triangle L_{pc}$ between pseudocritical points was 147.4 m and increases to 385.6 in Figure 6.7d as the pipe diameter increases from 22.23 mm to 38.1 mm. The HTC is inversely proportional to the pipe diameter, in Figure 6.7a when pipe diameter is small the temperature drop on hot and cold side is much sharp due to higher HTC as compared to Figure 6.7d when pipe diameter bigger.

Table 6.4 Parameters and results for pipe diameter variation.

Input Parameters						
Hot Side						
Pressure (MPa)	25	25	25	25	25	25
Inlet Temperature (^oC)	625	625	625	625	625	625
Total mass flow rate (kg/s)	1320	1320	1320	1320	1320	1320
Mass flux ($kg/m^2 \cdot s$)	2000	2000	2000	2000	2000	2000
Outer diameter of pipe (mm)	22.23	25.4	28.58	31.75	34.93	38.1
Cold Side						
Pressure (MPa)	25.5	25.5	25.5	25.5	25.5	25.5
Outlet Temperature (^oC)	600	600	600	600	600	600
Total mass flow rate (kg/s)	1250	1250	1250	1250	1250	1250
Code Output						
Total Q (MW)	2416	2416	2416	2416	2416	2416
Q/Pipe (MW)	1.144	1.494	1.891	2.335	2.825	3.362
No. of Pipes	2112	1617	1278	1035	855	719
Heat Transfer Area/Pipe (m^2)	29.68	42.14	57.57	76.27	98.56	124.73
Total Heat Transfer Area (m^2)	62697	68136	73547	78930	84290	89635
Length of Pipe (m)	425.2	528.1	641.3	764.7	898.3	1042.1
Total Length of Pipe (m)	897956	853874	819283	791314	768234	748867
Hot Side						
Outlet Temperature (^oC)	364.4	364.4	364.4	364.4	364.4	364.4
Mass flow rate/Pipe (kg/s)	0.625	0.816	1.033	1.275	1.543	1.836
Inner diameter of pipe (mm)	20	22.8	25.7	28.5	31.4	34.2
Cold Side						
Inlet Temperature (^oC)	340	340	340	340	340	340
Mass flow rate/Pipe (kg/s)	0.591	0.773	0.978	1.207	1.461	1.739
Mass flux ($kg/m^2 \cdot s$)	1894	1894	1894	1894	1894	1894
Outer diameter of pipe (mm)	33.4	38.1	42.9	47.6	52.4	57.2
Inner diameter of pipe (mm)	29.9	34.1	38.4	42.7	46.9	51.2

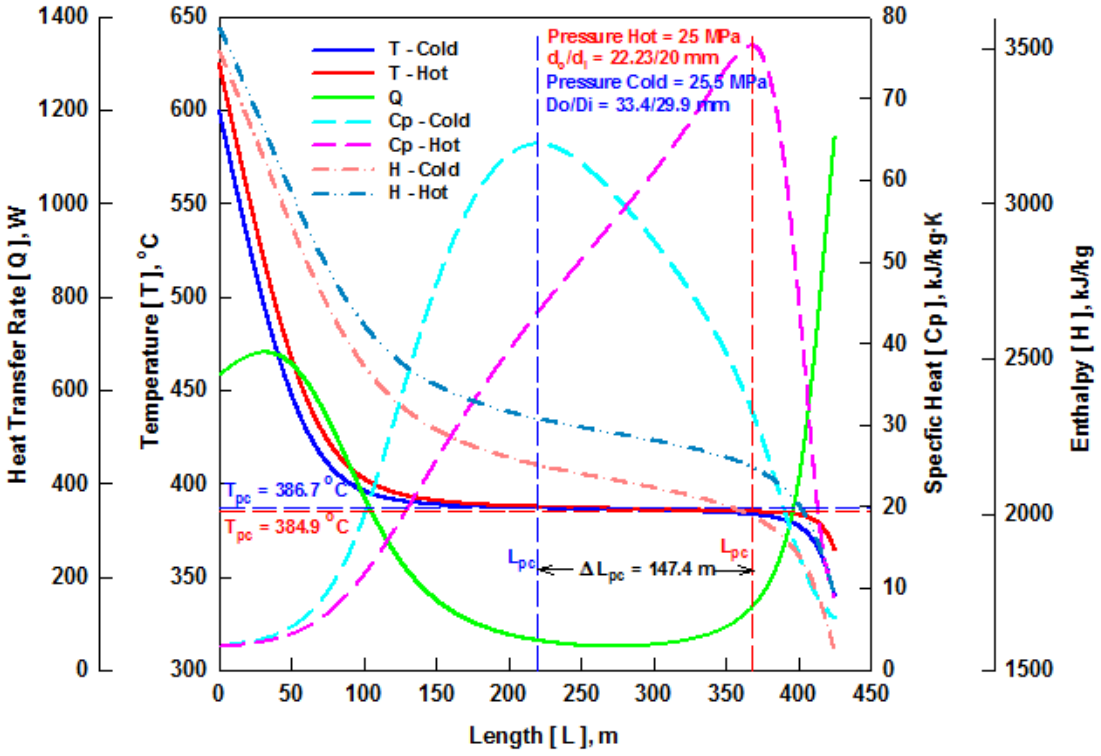
T - Cold
T - Hot
Q
Cp - Cold
Cp - Hot
H - Cold
H - Hot
Pressure Hot = 25 MPa
d_o/d_i = 22.23/20 mm
Pressure Cold = 25.5 MPa
Do/Di = 33.4/29.9 mm
T_{pc} = 386.7 °C
T_{pc} = 384.9 °C
L_{pc}
ΔL_{pc} = 147.4 m
L_{pc}
Heat Transfer Rate [Q], W
Temperature [T], °C
Specific Heat [Cp], kJ/kg·K
Enthalpy [H], kJ/kg
Length [L], m

(a)

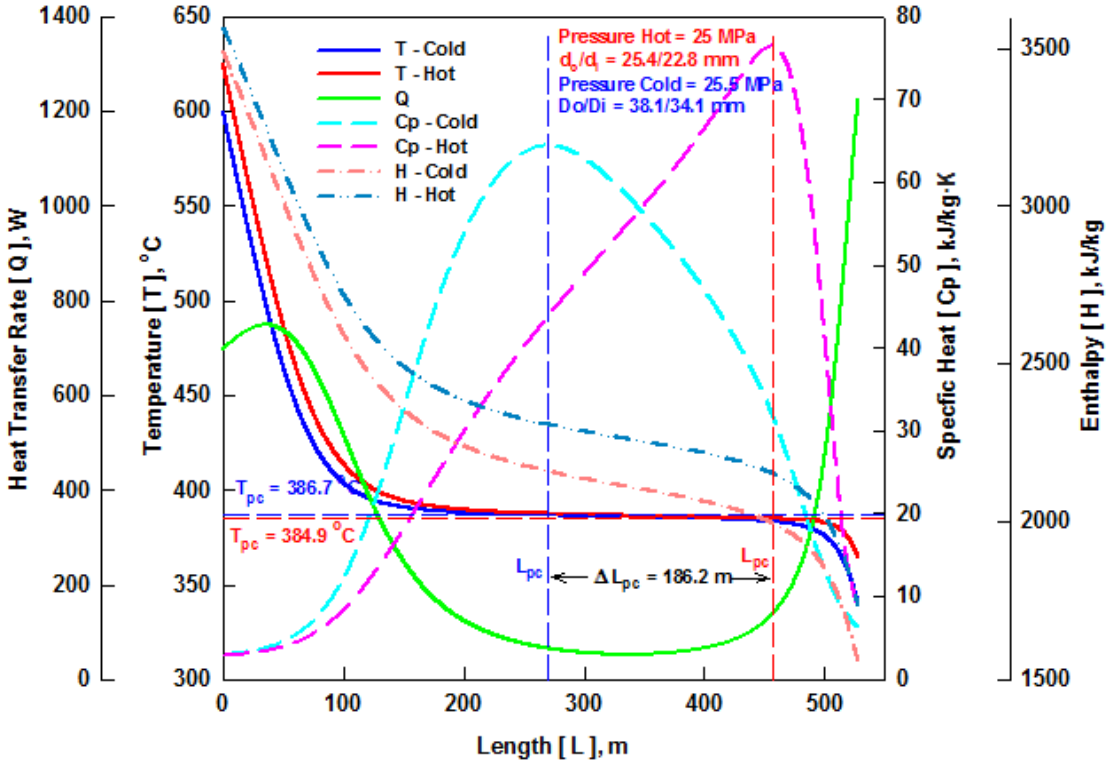
T - Cold
T - Hot
Q
Cp - Cold
Cp - Hot
H - Cold
H - Hot
Pressure Hot = 25 MPa
d_o/d_i = 25.4/22.8 mm
Pressure Cold = 25.5 MPa
Do/Di = 38.1/34.1 mm
T_{pc} = 386.7
T_{pc} = 384.9 °C
L_{pc}
ΔL_{pc} = 186.2 m
L_{pc}
Heat Transfer Rate [Q], W
Temperature [T], °C
Specific Heat [Cp], kJ/kg·K
Enthalpy [H], kJ/kg
Length [L], m

(b)

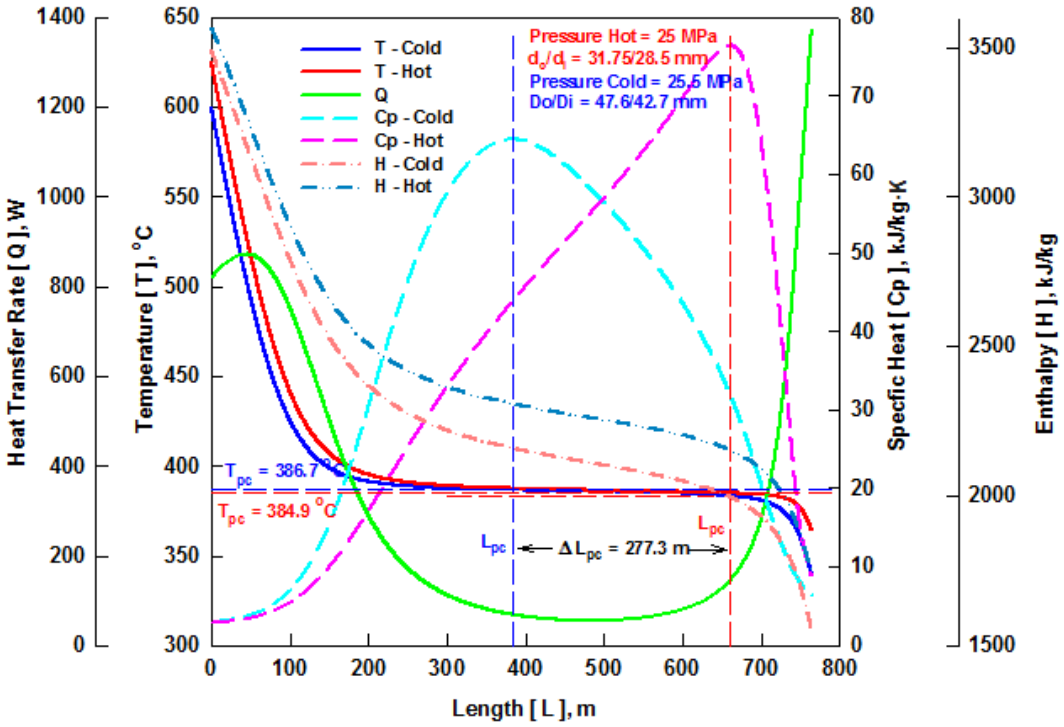

(c)

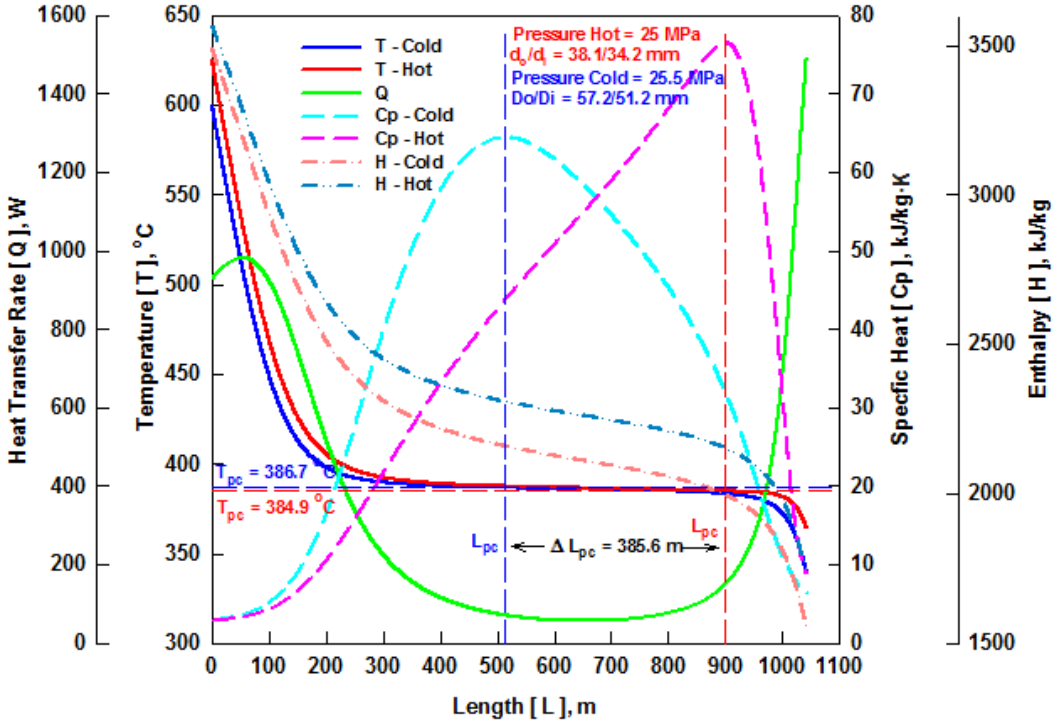

(d)

Figure 6.7: Effect of inner pipe diameter on temperature profile and fluid properties along length of double-pipe HX: d_o = (a) 22.23 mm, (b) 25.4 mm, (c) 31.75 mm, and (d) 38.1 mm

Figure 6.8 shows the effect of the inner-pipe diameter on the heat-transfer-surface area and location difference of the hot and cold side psudocritcal point along the length of the pipe. The heat transfer surface area and location difference of psudocitical point increases linearly with the increase of the pipe diameter. The heat-transfer-surface area increases by ~1.4 times with the increase of pipe diameter from 22.23 mm to 38.1 mm. The change in heat transfer area is not much, compared to variations in other factors like pressure and temperature shown in previous sections. Apart from heat transfer surface area, other factors such as fouling, friction, velocity, and power losses may also influence the selection of the optimal pipe diameter for the HX.

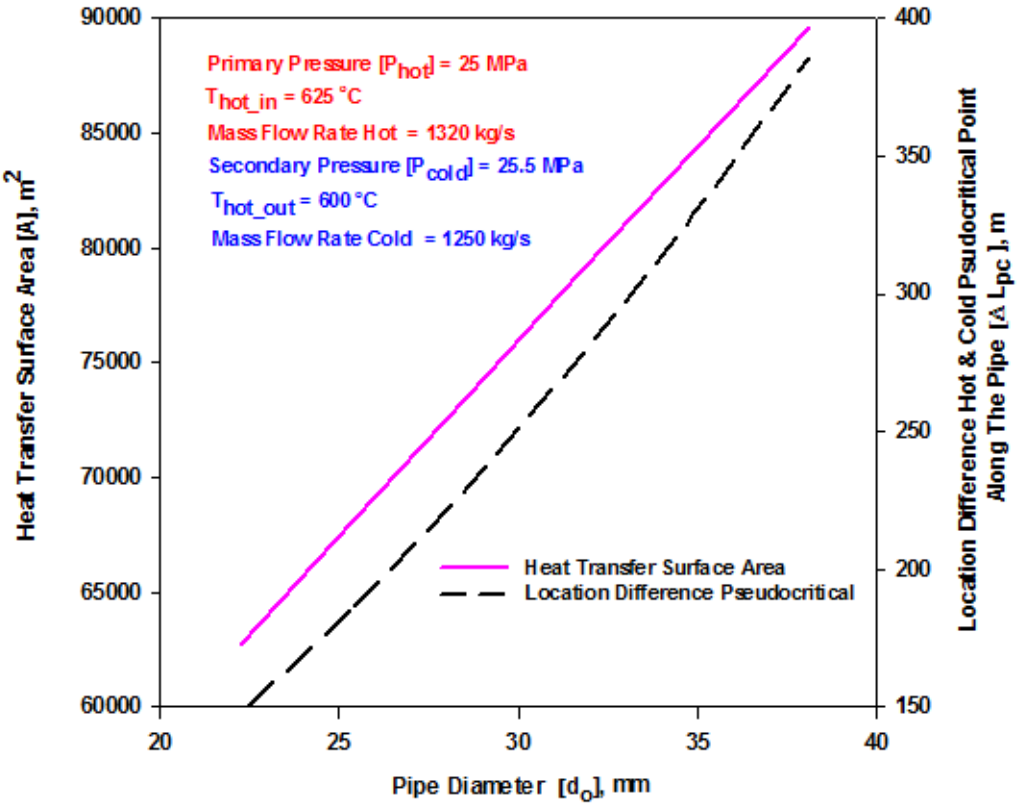

Figure 6.8: Effect of inner pipe diameter on heat-transfer-surface area of HX and location variation of pseudocritical point along the length of the pipe.

6.1.4 Effect of Mass Flow Rate Variation

The mass flow rate on the hot side is kept constant and mass flow rate on cold side is changed from 1200 kg/s to 1250 kg/s. Table 6.5 shows the operating parameters selected for analysis and results obtained. Figure 6.9 shows the effect of mass flow rate on the pseudocritical region and heat transfer pipe length of the HX. The results show that the heat transfer is enhanced or deteriorated due to the change in fluid properties depending on the exact fluid conditions. The heat transfer rate decreases in the pseudocritical region due to the higher specific heat capacity of the water. The heat transfer length of the pipe and pseudocritical region is longer when the mass flow rate difference on the hot and cold side are less as shown in Figure 6.9d. The length of the pipe is 528.1 m and the location difference ΔL_{pc} between pseudocritical points is 186.2 m. In Figure 6.9a, when the mass flow rate difference is larger on hot and cold side, the length of the pipe is 299.2 m and the location difference ΔL_{pc} between pseudocritical points is 95.8 m.

In Figure 6.9a due to lower mass flow rate on cold side, the temperature on cold side approaches pseudocritical region much earlier as compared to hot side. By the time the pseudocritical region on hot side dominates, effect pseudocritical region on cold side diminishes and leads to much faster temperature drop on the cold side as compared to hot side. Whereas in Figure 6.9d the pseudocritical point on cold side shifts further along length of the pipe due to higher mass flow rate on the cold side, leading to large overlap of pseudocritical region of the hot and cold side. The enthalpy trend in Figure 6.9a-d depends on the temperature profile along the length of the pipe and pressure selected for the analysis on the hot and cold side. The heat transfer rate shows rising trend in the beginning because of drop in viscosity and lesser influence of specific heat, as the temperature approaches pseudocritical region the heat transfer rate declines due to rise in specific heat.

Table 6.5: Parameters and results for mass flow rate variation on cold side.

Input Parameters						
Hot Side						
Pressure (MPa)	25	25	25	25	25	25
Inlet Temperature (^oC)	625	625	625	625	625	625
Total mass flow rate (kg/s)	1320	1320	1320	1320	1320	1320
Mass flux ($kg/m^2 \cdot s$)	2000	2000	2000	2000	2000	2000
Outer diameter of pipe (mm)	25.4	25.4	25.4	25.4	25.4	25.4
Cold Side						
Pressure (MPa)	25.5	25.5	25.5	25.5	25.5	25.5
Outlet Temperature (^oC)	600	600	600	600	600	600
Total mass flow rate (kg/s)	1200	1210	1220	1230	1240	1250
Code Output						
Total Q (MW)	2320	2340	2357	2377	2396	2416
Q/Pipe (MW)	1.435	1.447	1.457	1.470	1.482	1.494
No. of Pipes	1617	1617	1617	1617	1617	1617
Heat Transfer Area/Pipe (m^2)	23.87	26.02	28.63	31.91	36.19	42.14
Total Heat Transfer Area (m^2)	38603	42086	46305	51608	58524	68136
Length of Pipe (m)	299.2	326.2	358.9	400	453.6	528.1
Total Length of Pipe (m)	483770	527426	580298	646752	733417	853874
Hot Side						
Outlet Temperature (^oC)	371.7	370.3	369.1	367.5	366.1	364.4
Mass flow rate/Pipe (kg/s)	0.816	0.816	0.816	0.816	0.816	0.816
Inner diameter of pipe (mm)	22.8	22.8	22.8	22.8	22.8	22.8
Cold Side						
Inlet Temperature (^oC)	340	340	340	340	340	340
Mass flow rate/Pipe (kg/s)	0.742	0.748	0.754	0.760	0.766	0.773
Mass flux ($kg/m^2 \cdot s$)	1818	1833	1848	1863	1878	1894
Outer diameter of pipe (mm)	38.1	38.1	38.1	38.1	38.1	38.1
Inner diameter of pipe (mm)	34.1	34.1	34.1	34.1	34.1	34.1

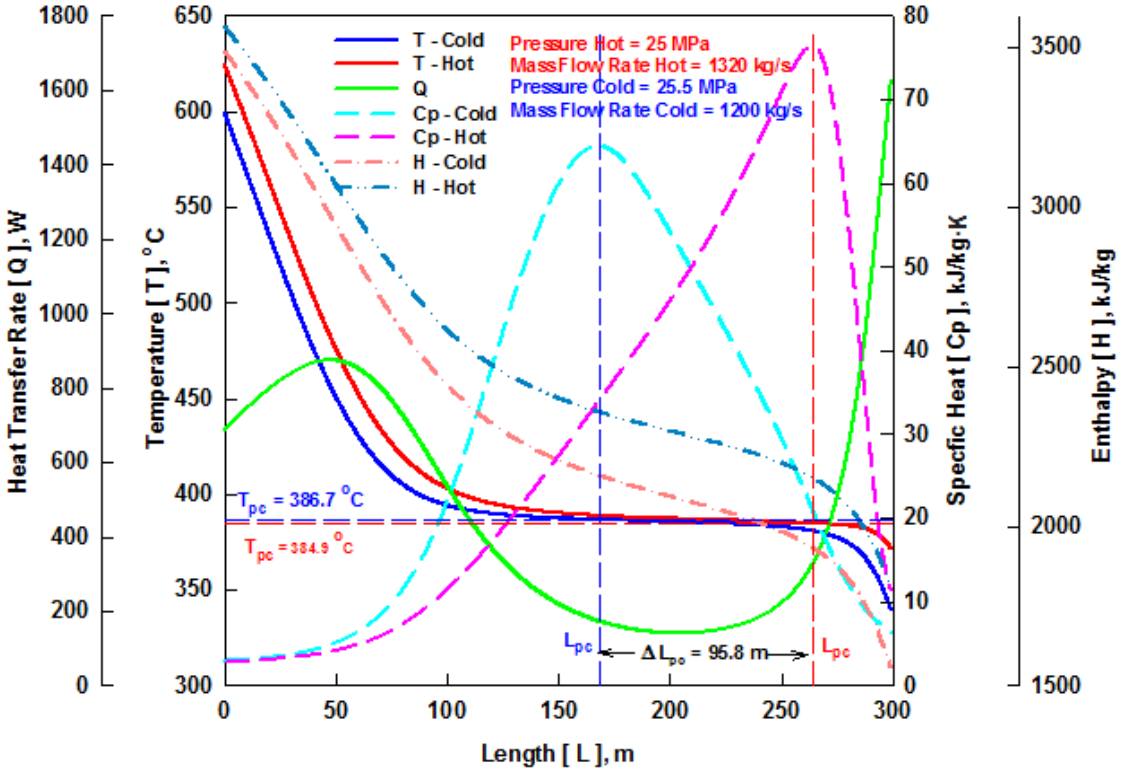
T - Cold
T - Hot
Q
Cp - Cold
Cp - Hot
H - Cold
H - Hot
Pressure Hot = 25 MPa
Mass Flow Rate Hot = 1320 kg/s
Pressure Cold = 25.5 MPa
Mass Flow Rate Cold = 1200 kg/s
Tpc = 386.7 °C
Tpc = 384.9 °C
Lpc
ΔLpc = 95.8 m
Lpc
Heat Transfer Rate [Q], W
Temperature [T], °C
Specific Heat [Cp], kJ/kg·K
Enthalpy [H], kJ/kg
Length [L], m

(a)

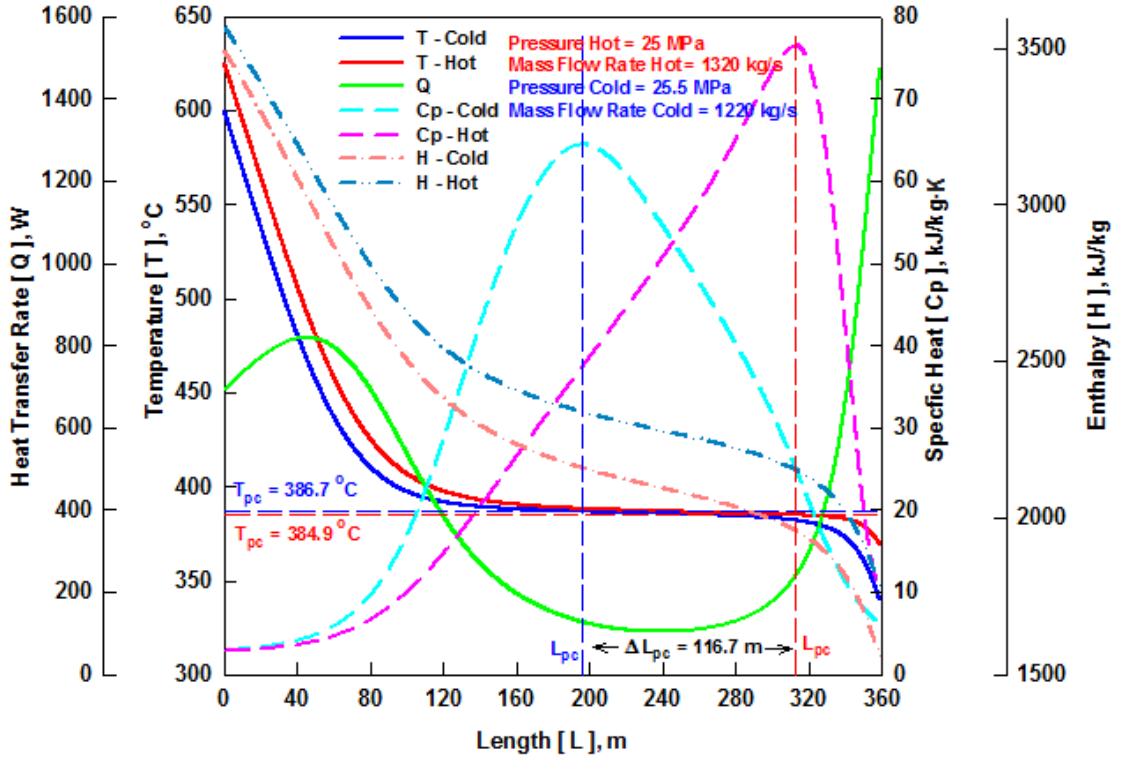
T - Cold
T - Hot
Q
Cp - Cold
Cp - Hot
H - Cold
H - Hot
Pressure Hot = 25 MPa
Mass Flow Rate Hot = 1320 kg/s
Pressure Cold = 25.5 MPa
Mass Flow Rate Cold = 1220 kg/s
Tpc = 386.7 °C
Tpc = 384.9 °C
Lpc
ΔLpc = 116.7 m
Lpc
Heat Transfer Rate [Q], W
Temperature [T], °C
Specific Heat [Cp], kJ/kg·K
Enthalpy [H], kJ/kg
Length [L], m

(b)

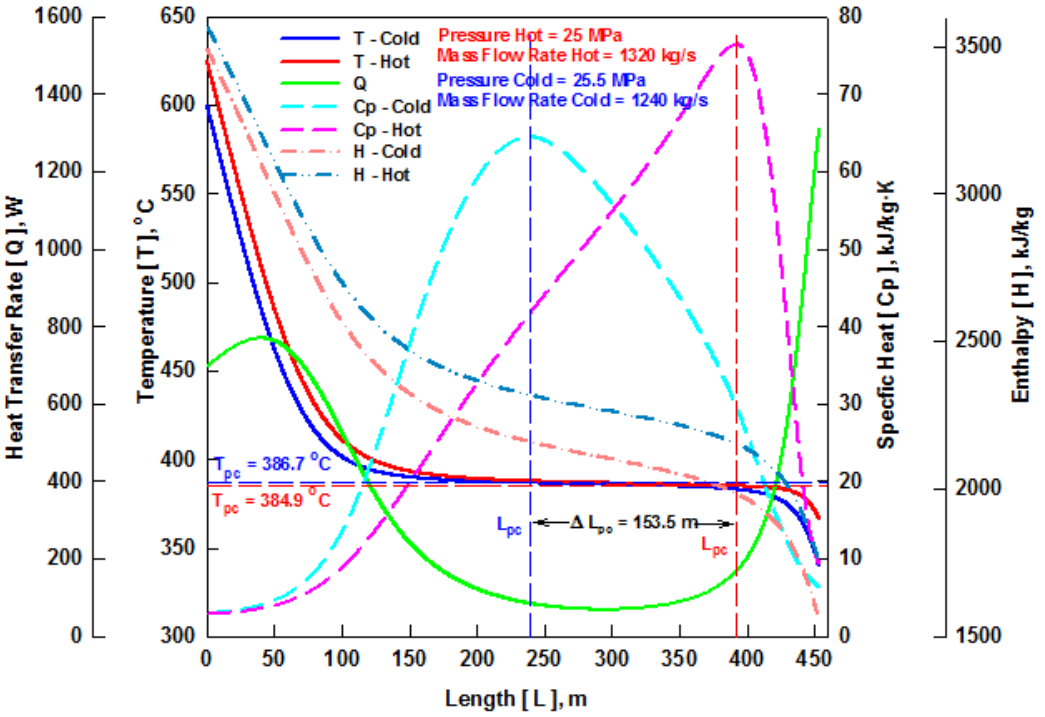

(c)

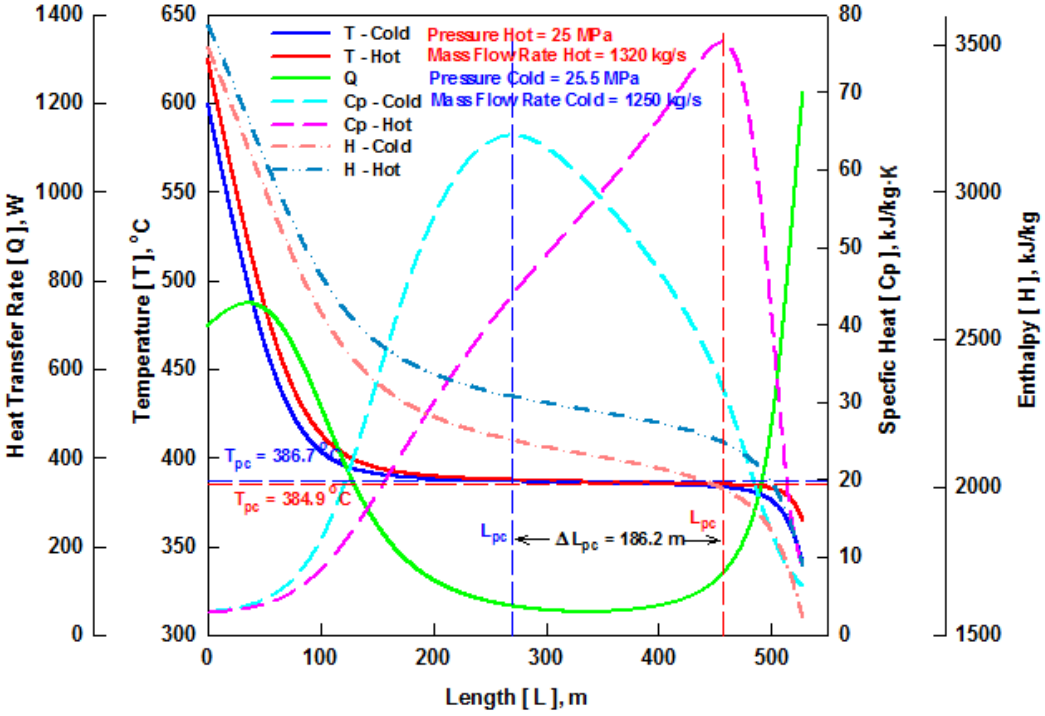

(d)

Figure 6.9: Effect of mass flow rate (cold) on temperature profile and fluid properties along length of double-pipe HX: $\dot{m}_c$ (a) 1200 kg/s, (b) 1220 kg/s, (c) 1240 kg/s, and (d) 1250 kg/s.

Figure 6.10 shows the variation in the heat-transfer-surface area with the change in the mass flow rate on the cold side and location difference of hot and cold side psudocritcal point along the length of the pipe. The heat-transfer-surface area decreases by approximately 1.8 times with a mass flow rate difference from 70 to 120 kg/s on the hot and cold side. The location difference between pseudocritical points shows similar behaviour, when the mass flow rate difference is increased from 70 to 120 kg/s on the hot and cold side. Although the higher mass flow rate on cold side tends to increase the heat transfer surface area of the HX, at same time it will increase the overall efficiency of the plant cycle.

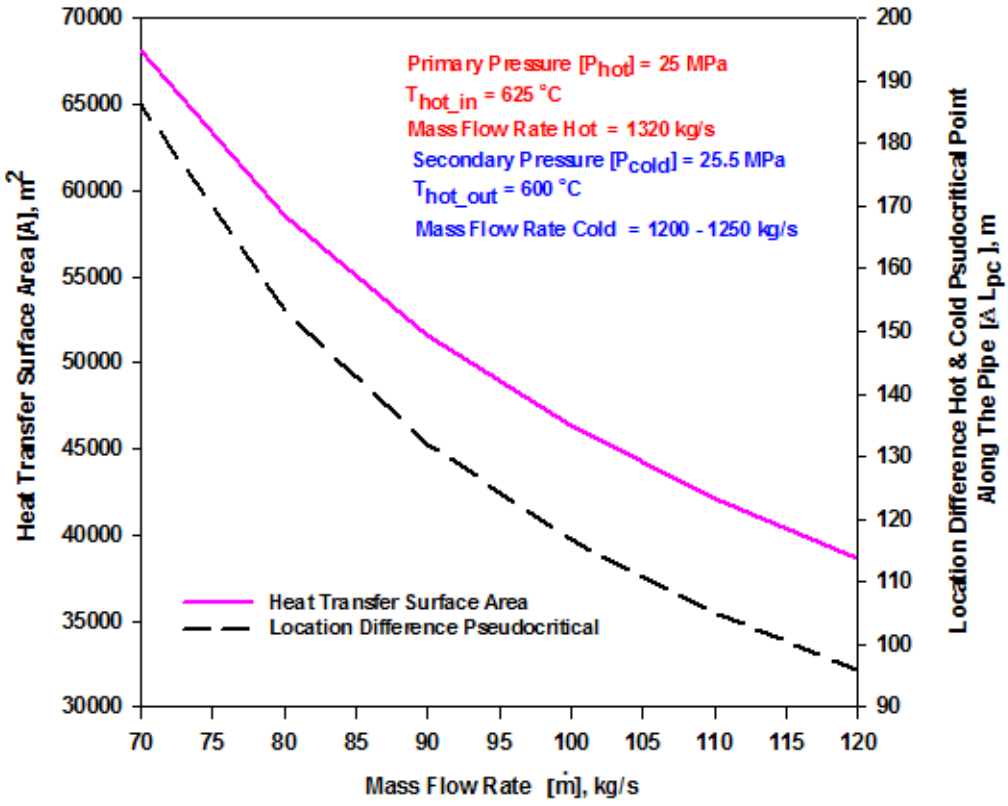

Figure 6.10: Effect of mass flow rate (cold side) on heat-transfer-surface area of HX and location difference of psudocritical point along the length of the pipe.

6.2 SCW to SHS Heat Transfer Analysis

SCW to SHS heat transfer analysis is performed on HX2. The SCW water on the hot side, from the reactor at a pressure 25 MPa and a temperature of 625 ^{o}C transfers the heat through HX2 to the cold (secondary) side.

6.2.1 Effect of Pressure

The pressure on the hot side is kept constant at 25 MPa and the cold side pressure is varied between 4 to 12 MPa. Other variables such as inlet temperature, outlet temperature, mass flow rate, and pipe size were kept constant. Table 6.6 shows the operating parameters and results, when pressure on the cold side is varied from 4 to 12 MPa on cold side. Figure 6.11 shows the temperature profiles and variations in fluid properties of the hot and cold sides along the length of the double-pipe HX for a variation in the cold side pressure. The specific heat on the hot side rises considerably as it approaches the pseudocritical region, whereas on the cold side, the specific heat stays flat and rise by small amount compared to the hot side when it approaches the pseudocritical region. In Figure 6.11a, when the pressure on the cold side is 4 MPa the temperature difference on the hot and cold side stays constant. In Figure 6.11d when the pressure on the cold side is 12 MPa the temperature difference on hot and cold side closes in, due to combined effect of higher overall HTC and higher specific heat on cold side. With the increase of the pressure on cold side the specific heat on the cold side increases, leading to smaller temperature drop on the cold side. In Figure 6.11 the temperature difference increases as the hot side temperature approaches closer to the pseudocritical region. The temperature drop on the hot side is not much as compared to cold side in pseudocritical region due to higher specific heat capacity of the fluid on hot side. Whereas the overall HTC increases due to significant change in thermophysical properties on hot side leading to much fast temperature drop on cold side in pseudocritical region.

Table 6.6: Parameters and results for pressure variation on cold side.

Input Parameters					
No. of Pipes	5000	5000	5000	5000	5000
Hot Side					
Pressure (MPa)	25	25	25	25	25
Inlet Temperature (^oC)	625	625	625	625	625
Total mass flow rate (kg/s)	500	500	500	500	500
Outer diameter of pipe (mm)	25.4	25.4	25.4	25.4	25.4
Cold Side					
Pressure (MPa)	4	6	8	10	12
Outlet Temperature (^oC)	580	580	580	580	580
Total mass flow rate (kg/s)	860	860	860	860	860
Code Output					
Total Q (MW)	482.5	514.9	551.9	599.4	659.8
Q/Pipe (MW)	0.097	0.103	0.110	0.120	0.132
Heat Transfer Area/Pipe (m^2)	3.99	4.7	5.81	7.89	14.16
Total Heat Transfer Area (m^2)	19989	23539	29085	39499	70819
Length of Pipe (m)	50.1	59	72.9	99	177.5
Total Length of Pipe (m)	250500	295000	364500	495000	887500
Hot Side					
Outlet Temperature (^oC)	401.6	396.8	392.7	388.9	386.2
Mass flow rate/Pipe (kg/s)	0.1	0.1	0.1	0.1	0.1
Mass flux ($kg/m^2 \cdot s$)	237.4	237.4	237.4	237.4	237.4
Inner diameter of pipe (mm)	22.8	22.8	22.8	22.8	22.8
Cold Side					
Inlet Temperature (^oC)	340	340	340	340	340
Mass flow rate/Pipe (kg/s)	0.172	0.172	0.172	0.172	0.172
Mass flux ($kg/m^2 \cdot s$)	408.4	408.4	408.4	408.4	408.4
Outer diameter of pipe (mm)	34.7	35	35.3	35.6	35.9
Inner diameter of pipe (mm)	34.1	34.1	34.1	34.1	34.1

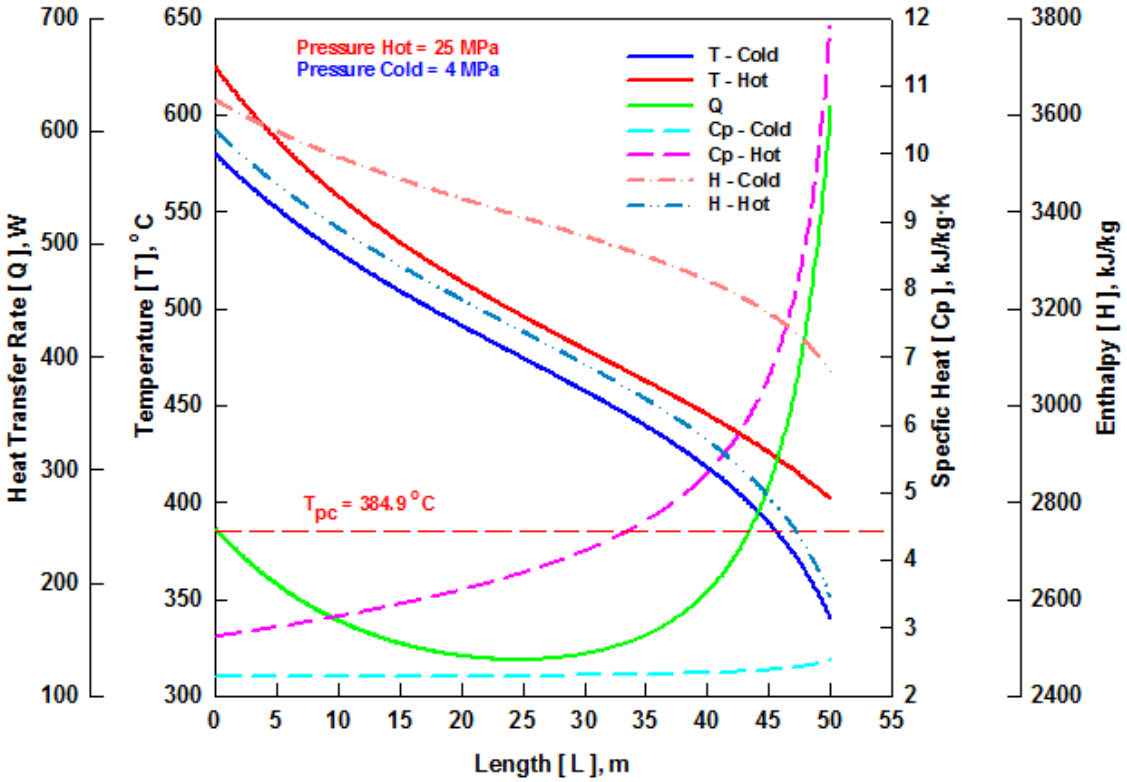
Pressure Hot = 25 MPa
Pressure Cold = 4 MPa
T - Cold
T - Hot
Q
Cp - Cold
Cp - Hot
H - Cold
H - Hot
T_{pc} = 384.9 °C
Heat Transfer Rate [Q], W
Temperature [T], °C
Specific Heat [Cp], kJ/kg·K
Enthalpy [H], kJ/kg
Length [L], m

(a)

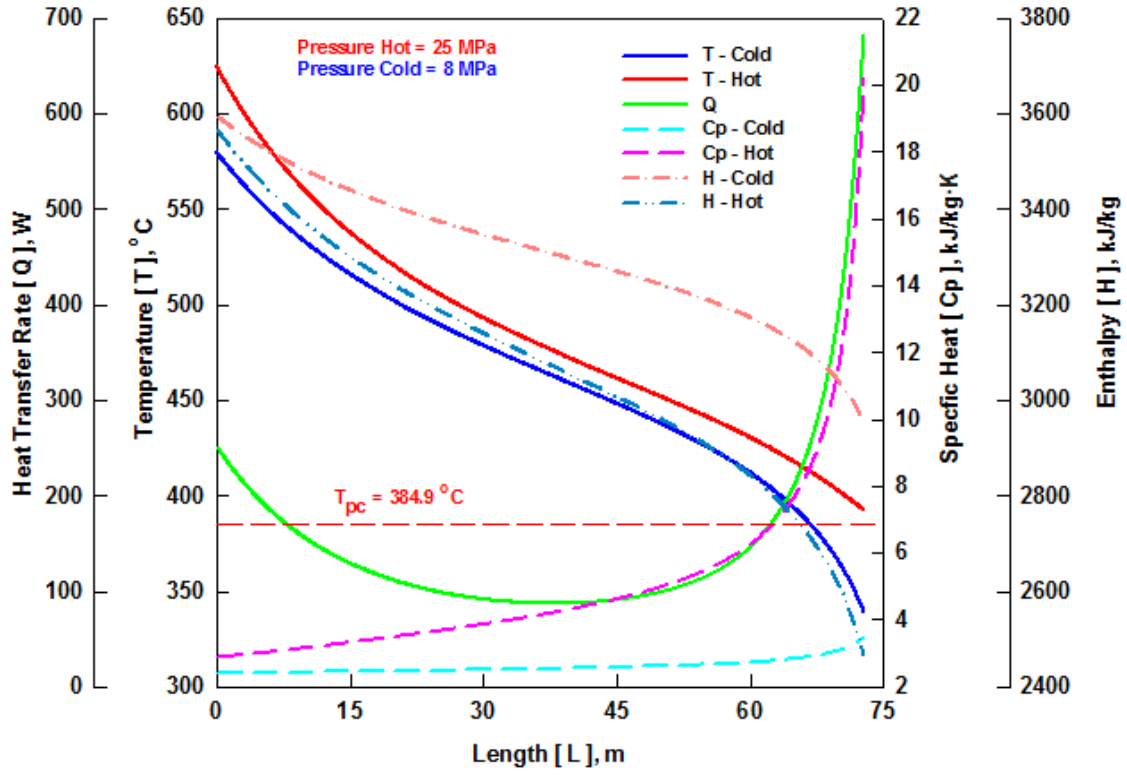
Pressure Hot = 25 MPa
Pressure Cold = 8 MPa
T - Cold
T - Hot
Q
Cp - Cold
Cp - Hot
H - Cold
H - Hot
T_{pc} = 384.9 °C
Heat Transfer Rate [Q], W
Temperature [T], °C
Specific Heat [Cp], kJ/kg·K
Enthalpy [H], kJ/kg
Length [L], m

(b)

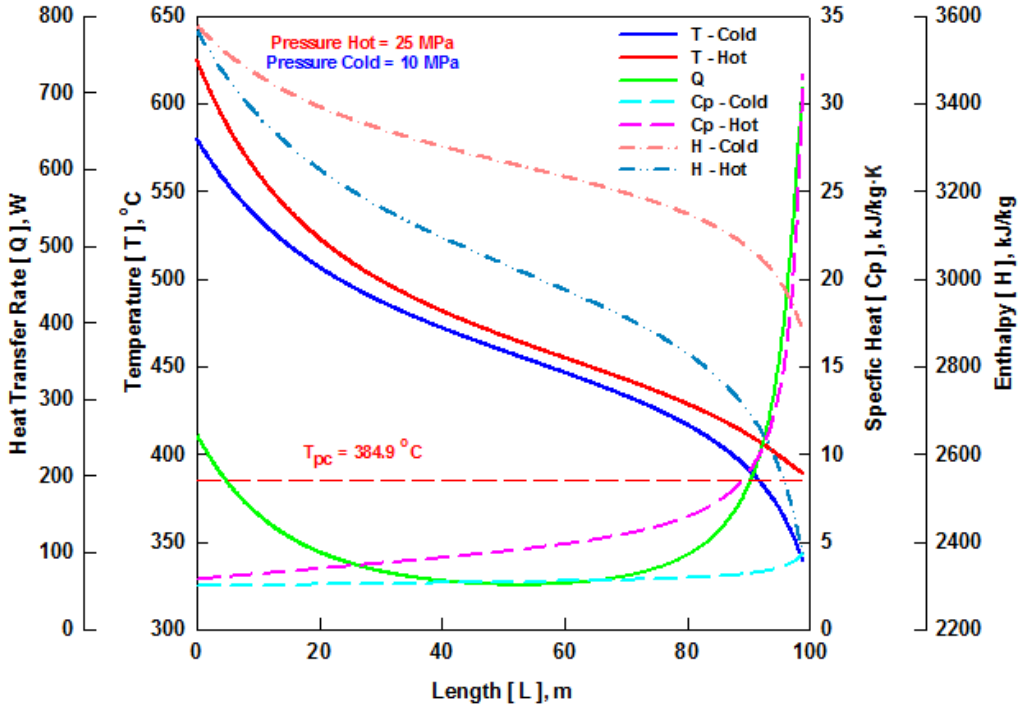

(c)

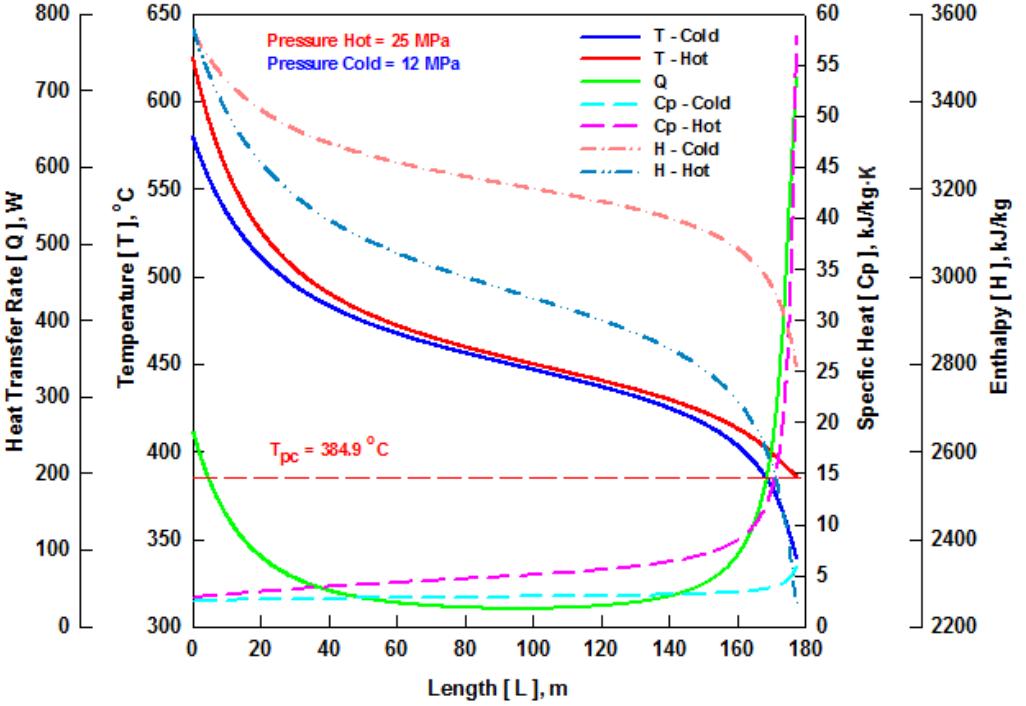

(d)

Figure 6.11: Effect of pressure (cold) on temperature profile and fluid properties along length of double-pipe HX2: P_{cold} = (a) 4 MPa, (b) 8 MPa, (c) 10 MPa, and (d) 12 MPa

Figure 6.12 shows the effect of change in cold side pressure on the heat transfer area. The heat-transfer-surface area increases by approximately 3.5 times with a pressure increase from 4 to 12 MPa. Figure 6.12 also shows that the heat transfer rate increases with the increase of pressure on the cold side from 4 to 12 MPa. The higher pressure on the cold side is better for the overall cycle efficiency, but it tends to increase the heat transfer surface area of HX. It will be advantageous to have the pressure on cold side between 6 to 10 MPa, where the increase in heat transfer surface area of HX is much smaller compared to the pressure increase from 10 to 12 MPa.

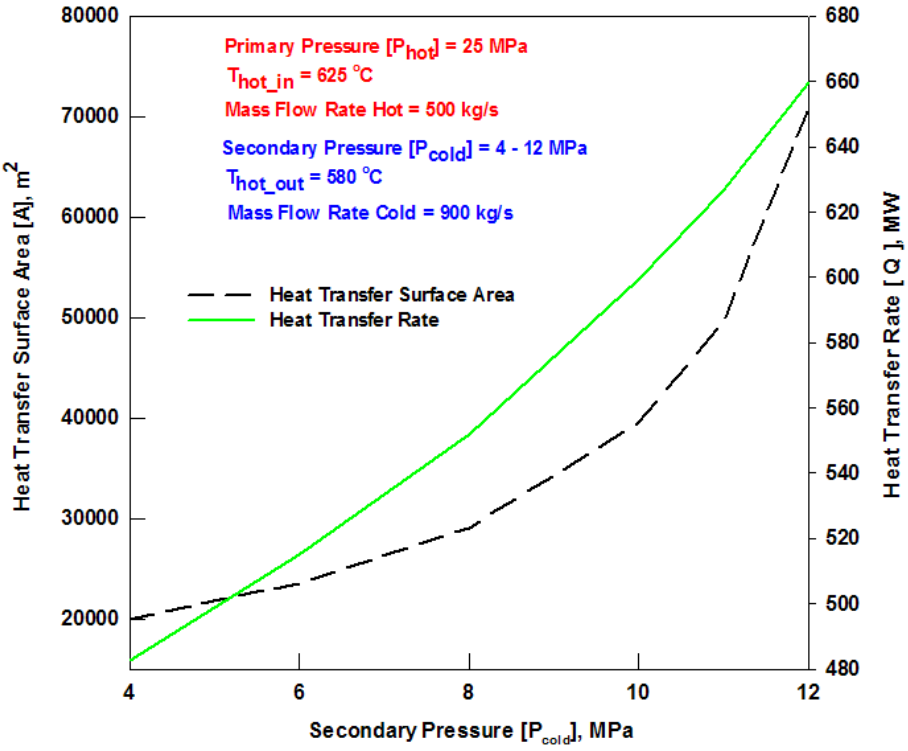

Figure 6.12: Effect of pressure (cold) on heat-transfer-surface area and heat transfer rate.

6.2.2 Effect of Temperature

Heat-transfer analysis was performed by varying the temperature on the cold side. The inlet temperature on the hot side is kept constant at 625 ^{o}C and the outlet temperature on the cold side is varied from 540 ^{o}C to 590 ^{o}C. The pressure on the hot and cold side is kept constant at 25 MPa and 8 MPa respectively. Table 6.7 shows the operating parameters selected for analysis and results obtained, when temperature on the cold side is varied. Figure 6.13 shows the temperature profiles and variations in fluid properties of the hot and cold sides along the length of the double-pipe HX with variation in the outlet temperature on the cold side.

The heat transfer rate is directly proportional to temperature difference between hot and cold side. When temperature difference between hot (in) and cold (out) side is higher, the heat transfer rate is higher as shown in Figure 6.13. Due to higher heat transfer rate and temperature difference in Figure 6.13a the temperature on hot side approaches pseudocritical region much earlier as compared to Figure 6.13d. The temperature difference increases as the hot side temperature approaches closer to the pseudocritical region, effect was more noticeable in Figure 6.13b-d. The temperature drop on the hot side was less as compared to cold side in pseudocritical region due to higher specific heat capacity of the fluid on hot side. The overall HTC increases due to significant change in thermophysical properties on hot side in pseudocritical region leading to much fast temperature drop on cold side.

Table 6.7: Parameters and results for outlet temperature variation on cold side.

Input Parameters						
No. of Pipes	5000	5000	5000	5000	5000	5000
Hot Side						
Pressure (MPa)	25	25	25	25	25	25
Inlet Temperature (^oC)	625	625	625	625	625	625
Total mass flow rate (kg/s)	500	500	500	500	500	500
Outer diameter of pipe (mm)	25.4	25.4	25.4	25.4	25.4	25.4
Cold Side						
Pressure (MPa)	8	8	8	8	8	8
Outlet Temperature (^oC)	540	550	560	570	580	580
Total mass flow rate (kg/s)	860	860	860	860	860	860
Code Output						
Total Q (MW)	469.9	490.7	511.9	529.94	551.9	571.5
Q/Pipe (MW)	0.094	0.098	0.102	0.106	0.110	0.114
Heat Transfer Area/Pipe (m^2)	1.81	2.23	2.84	3.82	5.81	13.6
Total Heat Transfer Area (m^2)	9096	11171	14203	19111	29085	67747
Length of Pipe (m)	22.8	28	35.6	47.9	72.9	169.8
Total Length of Pipe (m)	114000	140000	178000	239500	364500	849000
Hot Side						
Outlet Temperature (^oC)	**403.7**	**400.3**	**397.2**	**395**	**392.7**	**390.9**
Mass flow rate/Pipe (kg/s)	0.1	0.1	0.1	0.1	0.1	0.1
Mass flux ($kg/m^2 \cdot s$)	237.4	237.4	237.4	237.4	237.4	237.4
Inner diameter of pipe (mm)	22.8	22.8	22.8	22.8	22.8	22.8
Cold Side						
Inlet Temperature (^oC)	340	340	340	340	340	340
Mass flow rate/Pipe (kg/s)	0.172	0.172	0.172	0.172	0.172	0.172
Mass flux ($kg/m^2 \cdot s$)	408.4	408.4	408.4	408.4	408.4	408.4
Outer diameter of pipe (mm)	35.3	35.3	35.3	35.3	35.3	35.3
Inner diameter of pipe (mm)	34.1	34.1	34.1	34.1	34.1	34.1

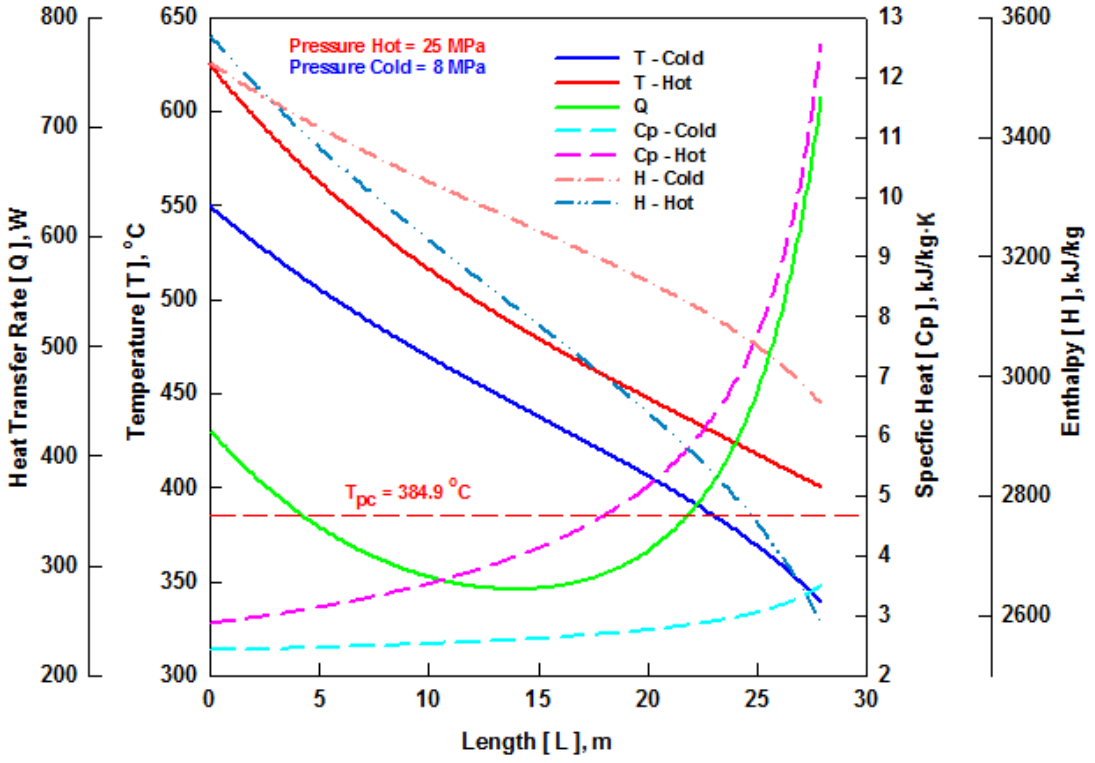
Pressure Hot = 25 MPa
Pressure Cold = 8 MPa
T - Cold
T - Hot
Q
Cp - Cold
Cp - Hot
H - Cold
H - Hot
T_{pc} = 384.9 °C
Heat Transfer Rate [Q], W
Temperature [T], °C
Specific Heat [Cp], kJ/kg·K
Enthalpy [H], kJ/kg
Length [L], m

(a)

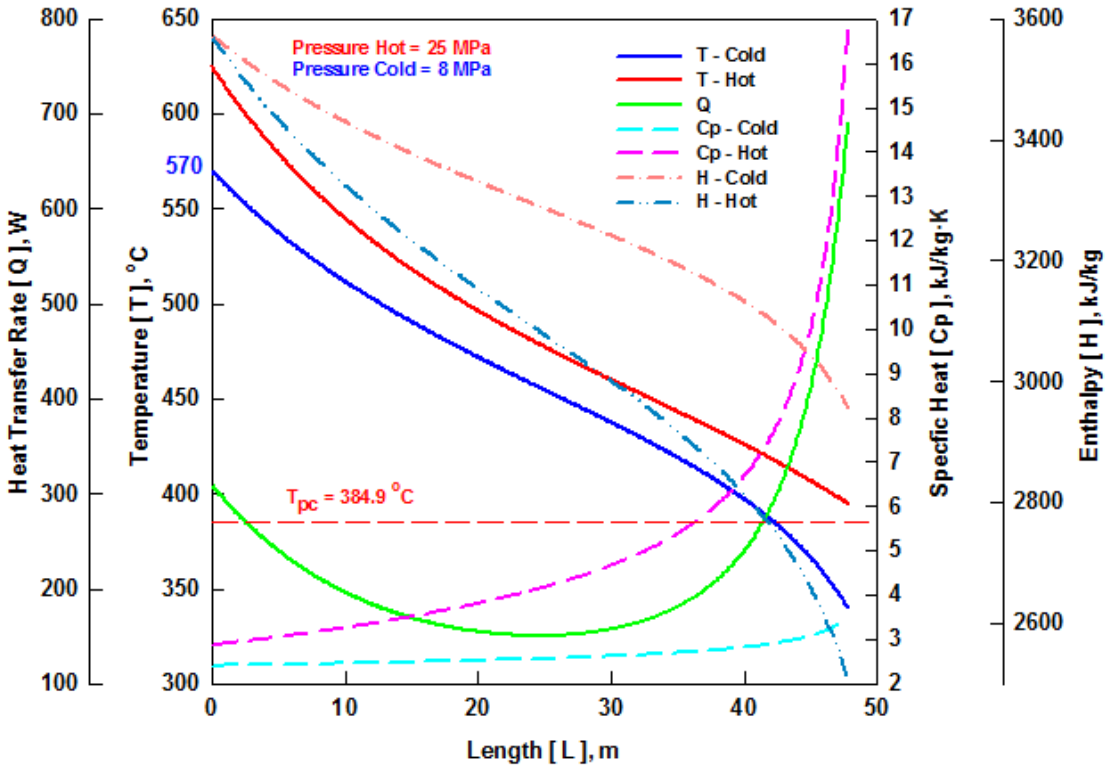
Pressure Hot = 25 MPa
Pressure Cold = 8 MPa
T - Cold
T - Hot
Q
Cp - Cold
Cp - Hot
H - Cold
H - Hot
570
T_{pc} = 384.9 °C
Heat Transfer Rate [Q], W
Temperature [T], °C
Specific Heat [Cp], kJ/kg·K
Enthalpy [H], kJ/kg
Length [L], m

(b)

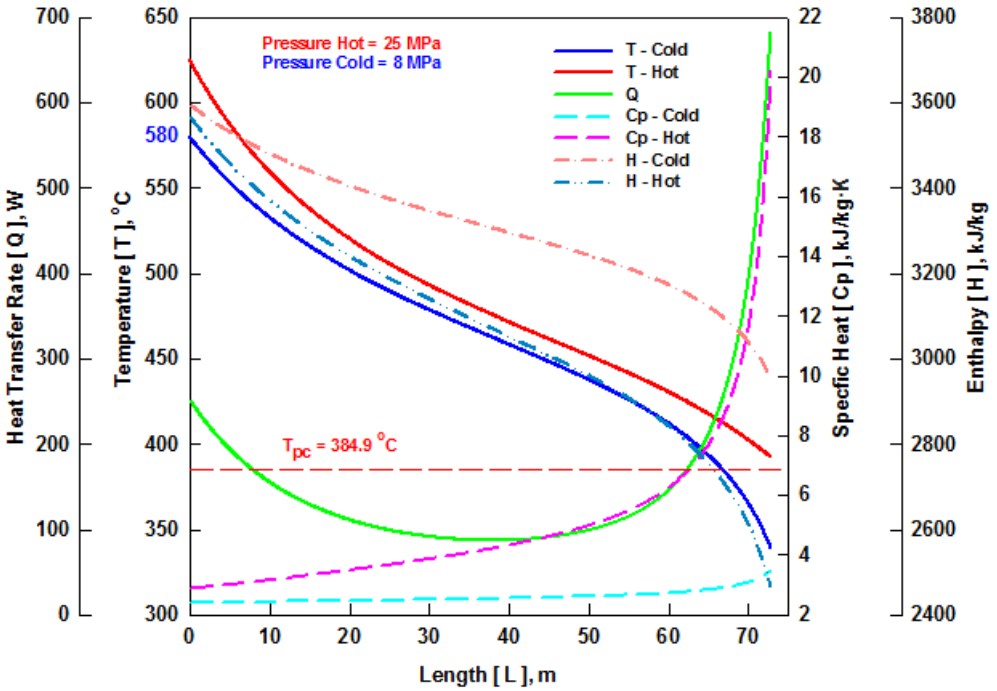

(c)

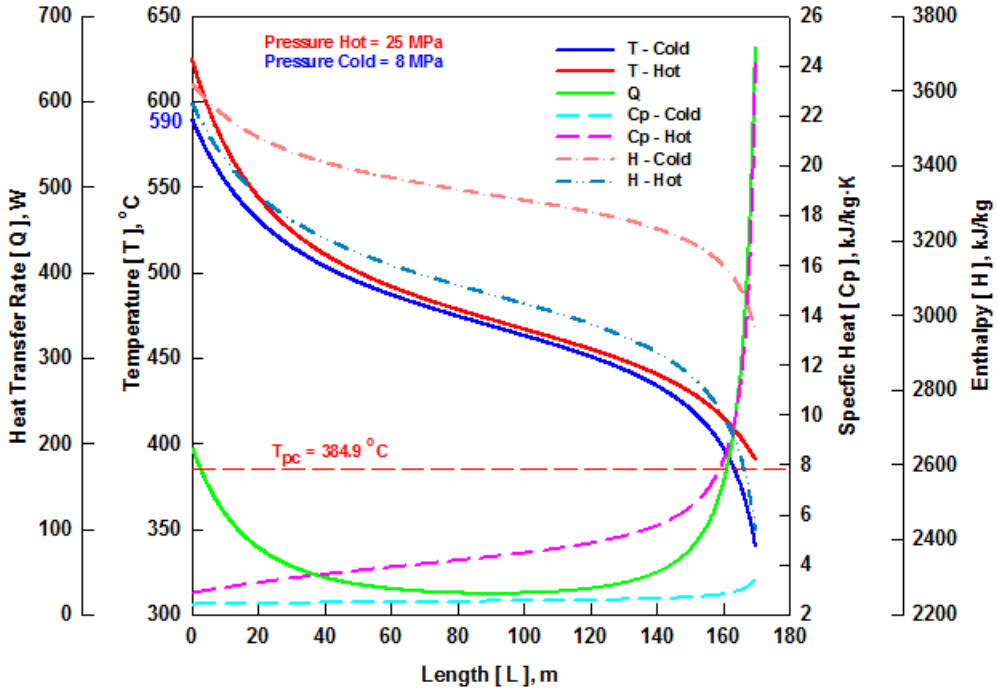

(d)

Figure 6.13: Effect of temperature difference between hot and cold side on temperature profile and fluid properties along length of double-pipe HX: T_{cold_outlet} = (a) 550 °C, (b) 570 °C, (c) 580 °C, and (d) 590 °C.

Figure 6.14 shows the variation in the heat transfer surface area and heat transfer rate with the change in the outlet temperature of the HX on the cold side. The heat transfer surface area increases by approximately 7.5 times as the temperature on the cold side increases from 540 to 590 ^{o}C. The heat transfer rate increases linearly with the increase of temperature, keeping other parameters constant. The temperature range from 550 to 580 ^{o}C gives the optimal efficiency versus the heat transfer area of the HX.

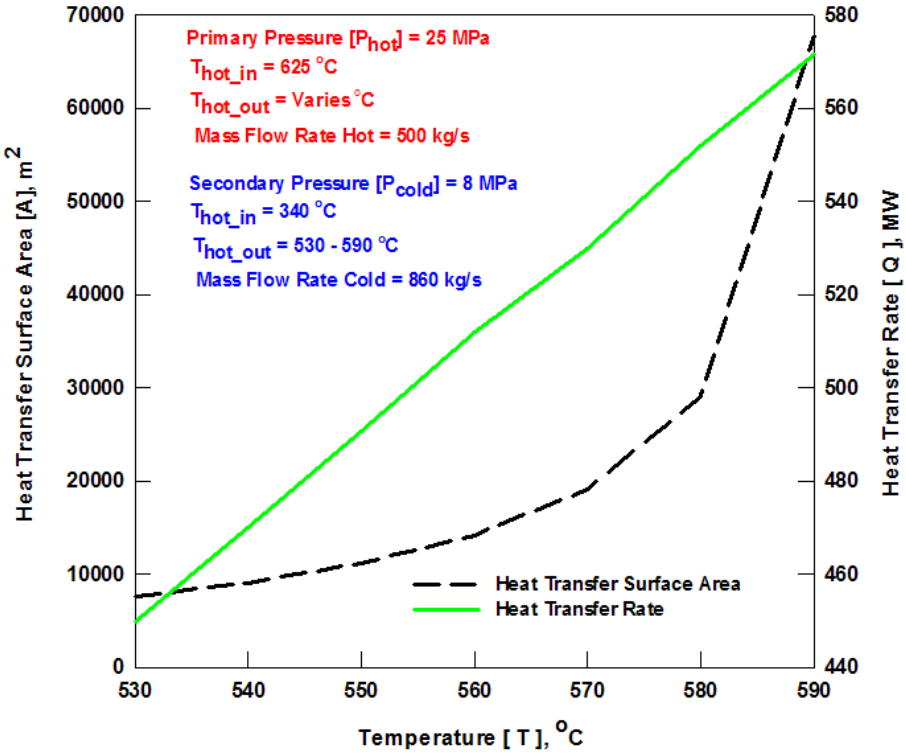

Figure 6.14: Effect of cold outlet temperature on heat-transfer-surface area and heat transfer rate.

6.2.3 Effect of Pipe Variation

Heat-transfer analysis was performed by varying the inner pipe diameter of the double-pipe HX. Table 6.8 shows the operating parameters selected for analysis and results obtained. The pressure and inlet temperature for the hot side is 25 MPa and 625 ^{o}C and for cold side pressure 8 MPa and outlet temperature 580^{o}C are kept constant for the analysis. The number of pipes in a HX are kept constant to 5000. The cross-section area of the inner and outer pipe is kept same. The mass flow rate is kept constant at 500 kg/s and 900 kg/s on the hot and cold side respectively. The mass flux on the hot side varies from 310.1 to 105.5 kg/m^2·s and on the cold side it varies from 558.3 to 189.9 kg/m^2·s. Figure 6.15 shows a temperature profiles and variations in fluid properties of the hot and cold sides along the length of the double-pipe HX with variation in the pipe diameter. The temperature behaviour stays the same for both sides, except the length of the pipe increases with the increase of pipe diameter. The HTC is inversely proportional to the pipe diameter, in Figure 6.15a when pipe diameter is small the temperature drop on hot and cold side is much sharp due to higher HTC as compared to Figure 6.15d when pipe diameter bigger. The heat transfer rate decreases in Figure 6.15 with the increase of pipe diameter from 22.23 mm to 38.1 mm, due to decrease in HTC. In Figure 6.15 the temperature difference increases as the hot side temperature approaches closer to the pseudocritical region. The temperature drop on the hot side was less as compared to cold side in pseudocritical region due to higher specific heat capacity of the fluid on hot side. The overall HTC increases due to significant change in thermophysical properties on hot side in pseudocritical region leading to much fast temperature drop on cold side.

Table 6.8: Parameters and results for pipe diameter variation.

Input Parameters						
No. of Pipes	5000	5000	5000	5000	5000	5000
Hot Side						
Pressure (MPa)	25	25	25	25	25	25
Inlet Temperature (^oC)	625	625	625	625	625	625
Total mass flow rate (kg/s)	500	500	500	500	500	500
Outer diameter of pipe (mm)	22.23	25.4	28.58	31.75	34.93	38.1
Cold Side						
Pressure (MPa)	8	8	8	8	8	8
Outlet Temperature (^oC)	580	580	580	580	580	580
Total mass flow rate (kg/s)	900	900	900	900	900	900
Code Output						
Total Q (MW)	576.5	576.5	576.5	576.5	576.5	576.5
Q/Pipe (MW)	0.115	0.115	0.115	0.115	0.115	0.115
Heat Transfer Area/Pipe (m^2)	6.4	8.2	10.2	12.4	14.9	17.5
Total Heat Transfer Area (m^2)	31838	40895	50989	62141	74390	87616
Length of Pipe (m)	91.2	102.5	113.6	124.6	135.6	146.4
Total Length of Pipe (m)	456000	512500	568000	623000	678000	732000
Hot Side						
Outlet Temperature (^oC)	390.5	390.6	390.5	390.5	390.5	390.6
Mass flow rate/Pipe (kg/s)	0.1	0.1	0.1	0.1	0.1	0.1
Mass flux ($kg/m^2 \cdot s$)	310.1	237.4	187.6	151.9	125.6	105.5
Inner diameter of pipe (mm)	20	22.8	25.7	28.5	31.4	34.2
Cold Side						
Inlet Temperature (^oC)	340	340	340	340	340	340
Mass flow rate/Pipe (kg/s)	0.18	0.18	0.18	0.18	0.18	0.18
Mass flux ($kg/m^2 \cdot s$)	558.3	427.5	337.7	273.5	226.1	189.9
Outer diameter of pipe (mm)	30.9	35.3	39.7	44.1	48.5	52.9
Inner diameter of pipe (mm)	29.9	34.1	38.4	42.7	46.9	51.2

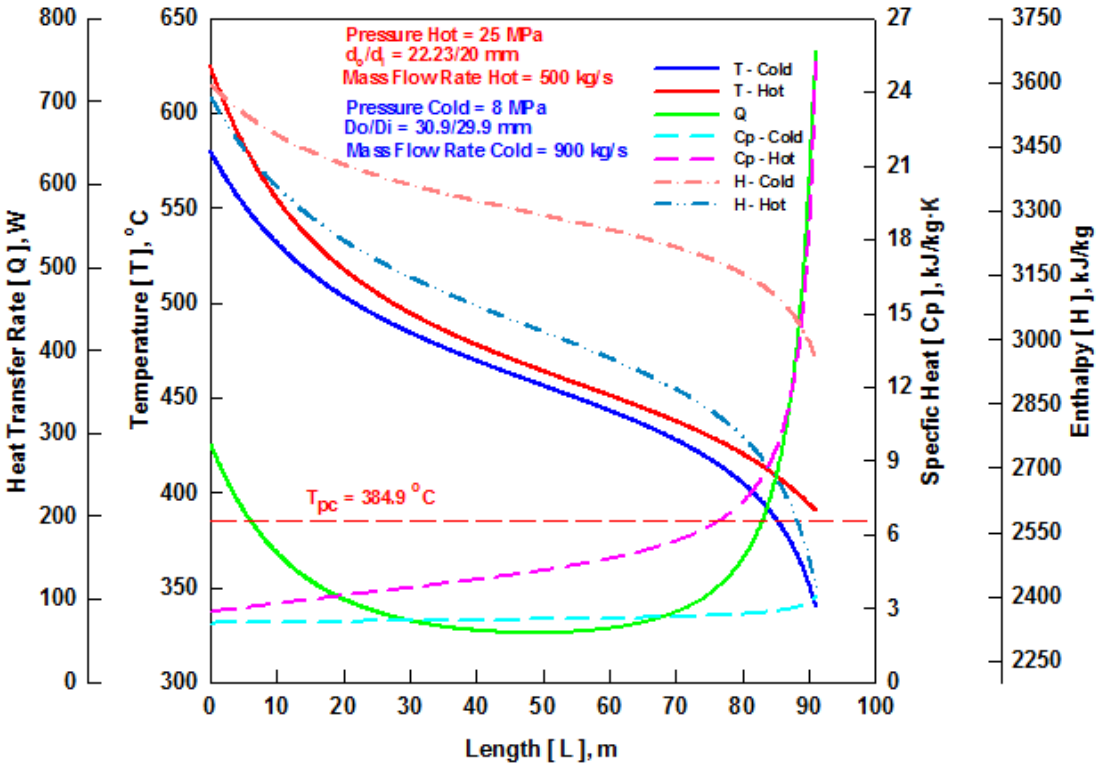
Pressure Hot = 25 MPa
d_o/d_i = 22.23/20 mm
Mass Flow Rate Hot = 500 kg/s
Pressure Cold = 8 MPa
Do/Di = 30.9/29.9 mm
Mass Flow Rate Cold = 900 kg/s
T - Cold
T - Hot
Q
Cp - Cold
Cp - Hot
H - Cold
H - Hot
T_{pc} = 384.9 °C
Heat Transfer Rate [Q], W
Temperature [T], °C
Specific Heat [Cp], kJ/kg·K
Enthalpy [H], kJ/kg
Length [L], m

(a)

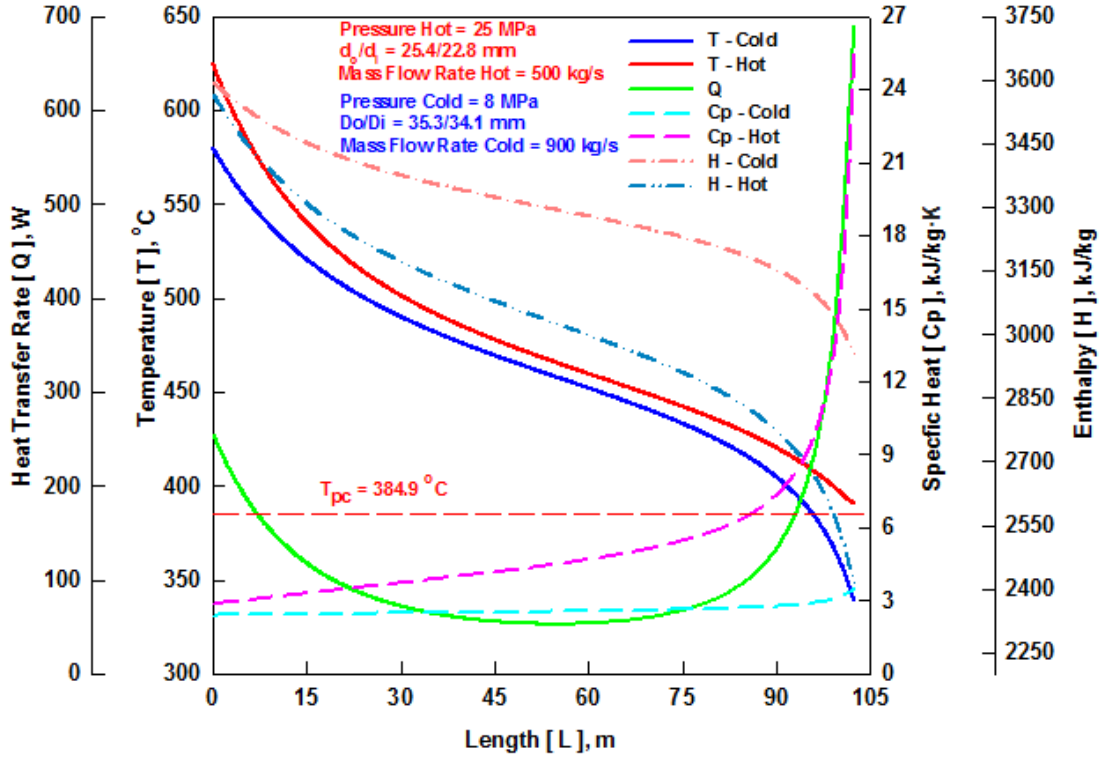
Pressure Hot = 25 MPa
d_o/d_i = 25.4/22.8 mm
Mass Flow Rate Hot = 500 kg/s
Pressure Cold = 8 MPa
Do/Di = 35.3/34.1 mm
Mass Flow Rate Cold = 900 kg/s
T - Cold
T - Hot
Q
Cp - Cold
Cp - Hot
H - Cold
H - Hot
T_{pc} = 384.9 °C
Heat Transfer Rate [Q], W
Temperature [T], °C
Specific Heat [Cp], kJ/kg·K
Enthalpy [H], kJ/kg
Length [L], m

(b)

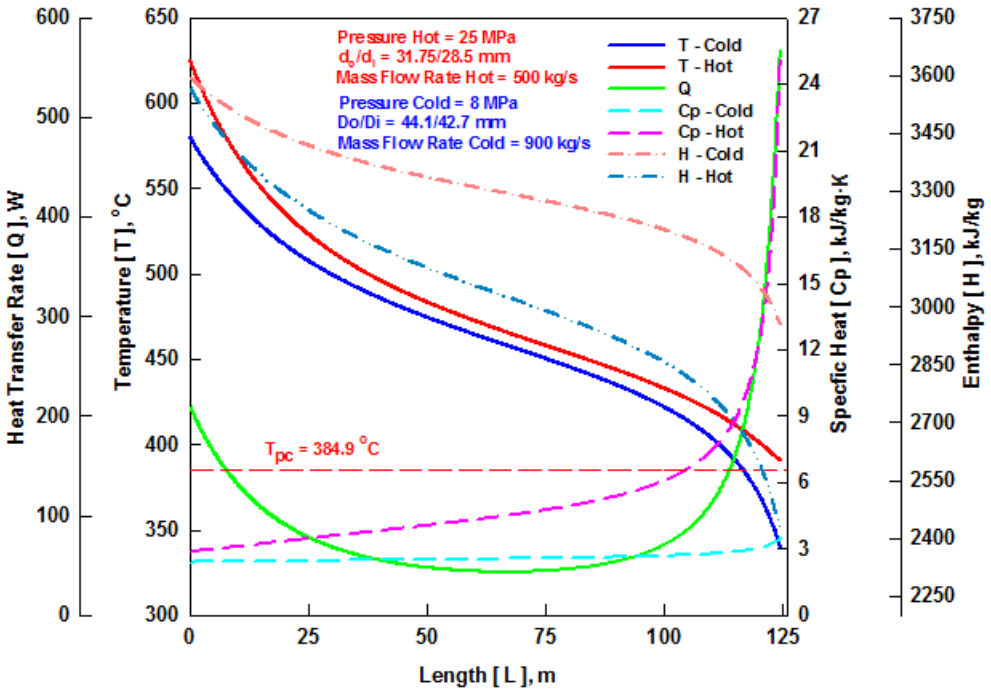

(c)

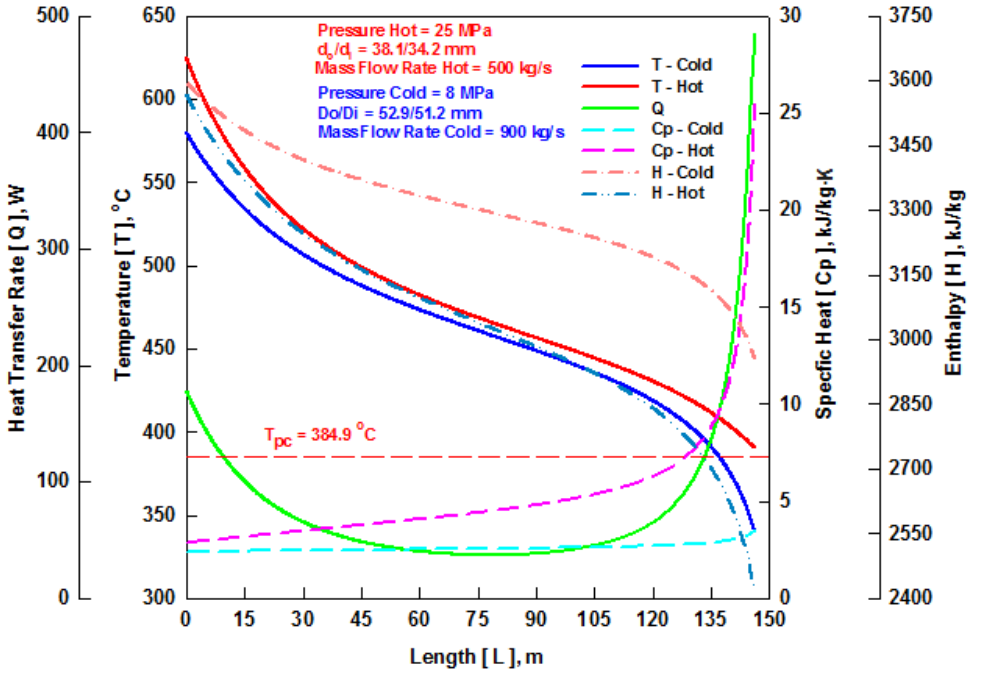

(d)

Figure 6.15: Effect of inner pipe diameter on temperature profile and fluid properties along length of double-pipe HX: d_o = (a) 22.23mm, (b) 25.4mm, (c) 31.75, and (d) 38.1mm.

Figure 6.16 shows the variation in the heat transfer surface area and behavior of the heat transfer rate with the change in the pipe diameter. The heat transfer surface area increases by ~2.8 times as the inner pipe diameter (d_o) increases from 22.23 mm to 38.1 mm. Since the total mass flow rate and the mass flow rate in each pipe is kept constant, the mass flux changes with the change in the pipe diameter. The heat transfer rate stays constant with the change in the pipe diameter. The smaller diameter is better to keep the heat transfer surface area of the HX low, but other factors such as fouling, friction, velocity and power losses may also influence the selection of the optimal pipe diameter of the HX.

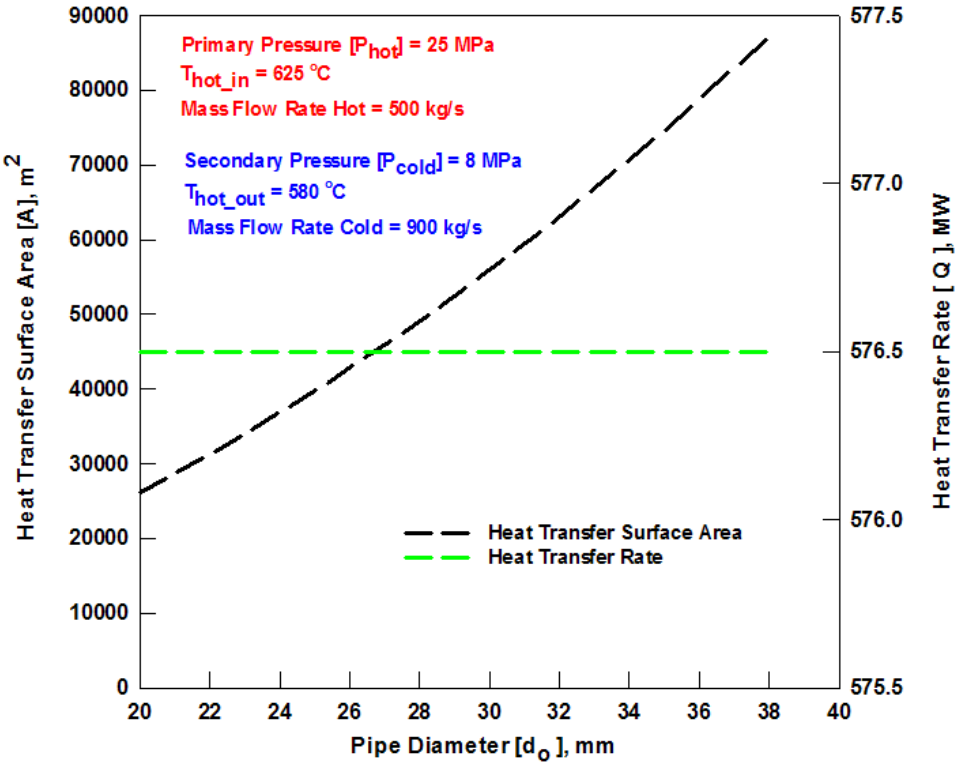

Figure 6.16: Effect of inner pipe diameter on heat-transfer-surface area and heat transfer rate.

6.2.4 Effect of Mass Flow Rate Variation

The mass flow rate on the hot side was kept constant and the mass flow rate on the cold side is changed from 700 kg/s to 1150 kg/s on the cold side. Table 6.9 shows the operating parameters selected for analysis and the results obtained. In Figure 6.17a, when the mass flow rate is 700 kg/s, the temperature difference on the hot and cold side stays constant. In Figure 6.17d when the mass flow rate is 1150 kg/s on the cold side the temperature difference on the hot and cold side decreases due to higher HTC. The temperature difference between hot and cold side increases as hot fluid approaches pseudocritical region. In Figure 6.17 the temperature drop on the hot side was less as compared to cold side in pseudocritical region due to higher specific heat capacity of the fluid on hot side. The overall HTC increases due to significant change in thermophysical properties on hot side in pseudocritical region leading to much fast temperature drop on cold side.

Table 6.9: Parameters and results for mass flow rate variation on cold side.

Input Parameters						
No. of Pipes	5000	5000	5000	5000	5000	5000
Hot Side						
Pressure (MPa)	25	25	25	25	25	25
Inlet Temperature (^oC)	625	625	625	625	625	625
Total mass flow rate (kg/s)	500	500	500	500	500	500
Outer diameter of pipe (mm)	25.4	25.4	25.4	25.4	25.4	25.4
Cold Side						
Pressure (MPa)	8	8	8	8	8	8
Outlet Temperature (^oC)	550	550	550	550	550	550
Total mass flow rate (kg/s)	700	860	900	1000	1100	1150
Code Output						
Total Q (MW)	399.5	490.7	512.2	570.2	624.9	654.6
Q/Pipe (MW)	0.079	0.098	0.102	0.114	0.125	0.131
Heat Transfer Area/Pipe (m^2)	1.5	2.2	2.5	3.4	5.4	7.9
Total Heat Transfer Area (m^2)	7580	11171	12448	17116	26971	39459
Length of Pipe (m)	19	28	31.2	42.9	67.6	98.9
Total Length of Pipe (m)	95000	140000	156000	214500	338000	494500
Hot Side						
Outlet Temperature (^oC)	419.4	400.2	397.1	391	387.5	386.3
Mass flow rate/Pipe (kg/s)	0.1	0.1	0.1	0.1	0.1	0.1
Mass flux ($kg/m^2 \cdot s$)	237.5	237.5	237.5	237.5	237.5	237.5
Inner diameter of pipe (mm)	25.4	25.4	25.4	25.4	25.4	25.4
Cold Side						
Inlet Temperature (^oC)	340	340	340	340	340	340
Mass flow rate/Pipe (kg/s)	0.14	0.172	0.18	0.2	0.22	0.23
Mass flux ($kg/m^2 \cdot s$)	332.5	408.5	427.5	474.9	522.5	546.2
Outer diameter of pipe (mm)	35.3	35.3	35.3	35.3	35.3	35.3
Inner diameter of pipe (mm)	34.1	34.1	34.1	34.1	34.1	34.1

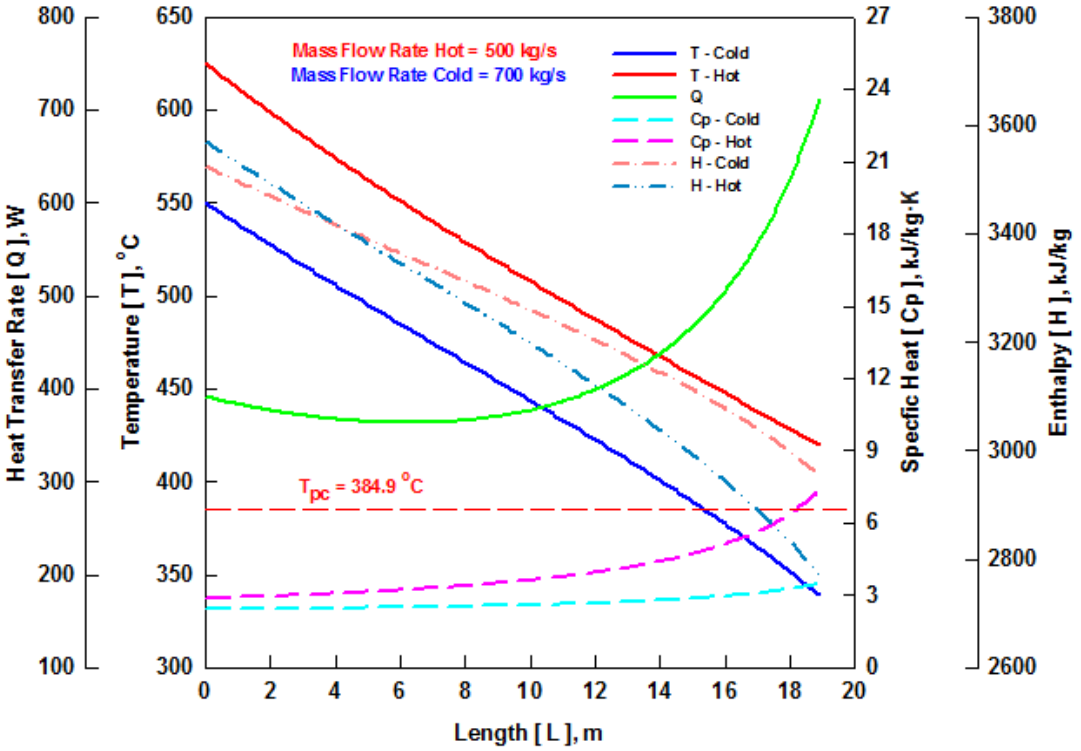
Mass Flow Rate Hot = 500 kg/s
Mass Flow Rate Cold = 700 kg/s
T - Cold
T - Hot
Q
Cp - Cold
Cp - Hot
H - Cold
H - Hot
T_{pc} = 384.9 °C
Heat Transfer Rate [Q], W
Temperature [T], °C
Specific Heat [Cp], kJ/kg·K
Enthalpy [H], kJ/kg
Length [L], m

(a)

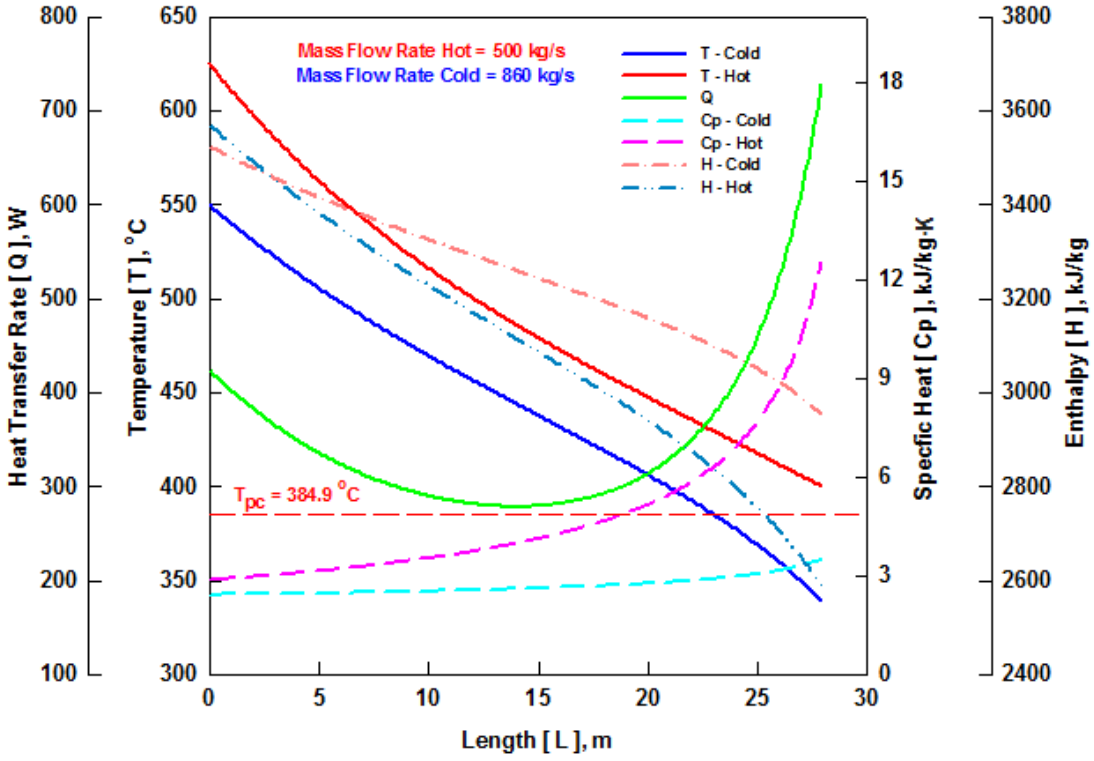
Mass Flow Rate Hot = 500 kg/s
Mass Flow Rate Cold = 860 kg/s
T - Cold
T - Hot
Q
Cp - Cold
Cp - Hot
H - Cold
H - Hot
T_{pc} = 384.9 °C
Heat Transfer Rate [Q], W
Temperature [T], °C
Specific Heat [Cp], kJ/kg·K
Enthalpy [H], kJ/kg
Length [L], m

(b)

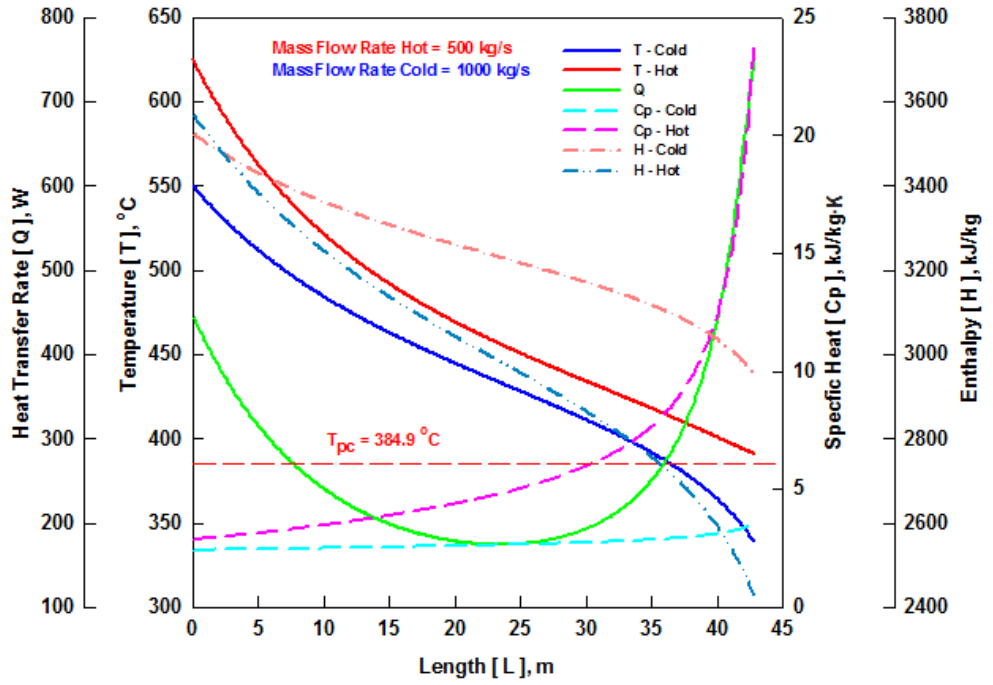

(c)

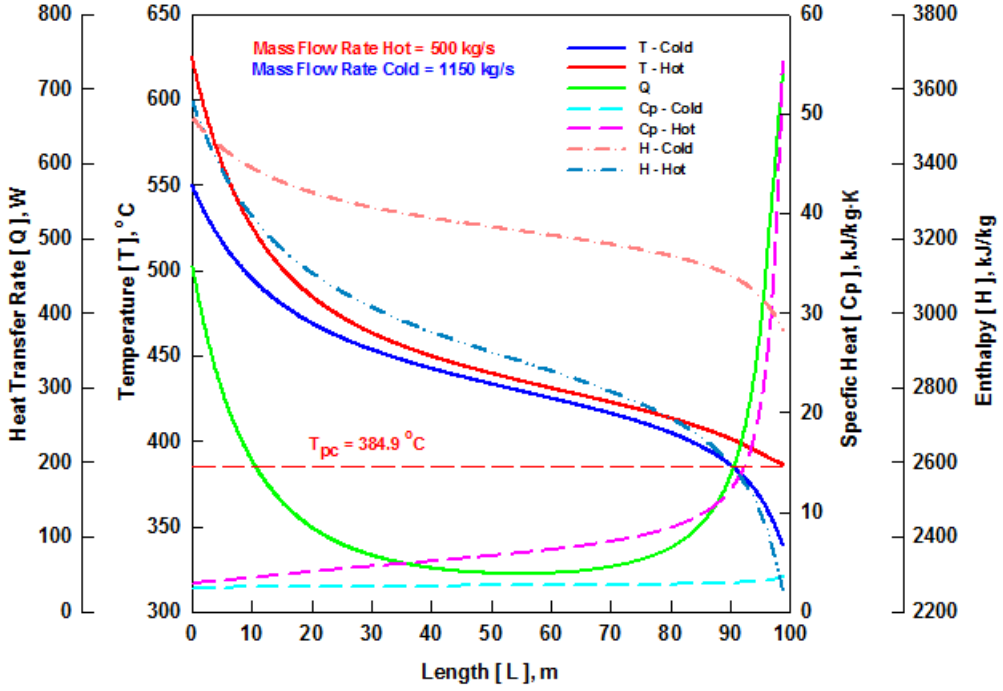

(d)

Figure 6.17: Effect of mass flow rate on temperature profile and fluid properties along length of double-pipe HX: $\dot{m}_o$ (a) 700 kg/s, (b) 860 kg/s, (b) 1000 kg/s, and (c) 1150 kg/s.

Figure 6.18 shows the variation in the heat transfer surface area and heat transfer rate with the change in the mass flow rate on the cold side of the HX. The heat transfer surface area increases by ~5.2 times as the mass flow rate on the cold side increases from 700 to 1150 kg/s. The heat transfer rate increases linearly with the increase of mass flow rate on cold side, keeping other parameters constant. The graph also shows the ratio of mass flow rate difference on the hot and cold side. The heat transfer surface area increases with the higher mass flow rate ratio between the cold and hot side. As noted the higher mass flow rate on the cold side may not seem a good idea for the heat transfer surface area of the HX, but it will help to increase the overall efficiency of the plant.

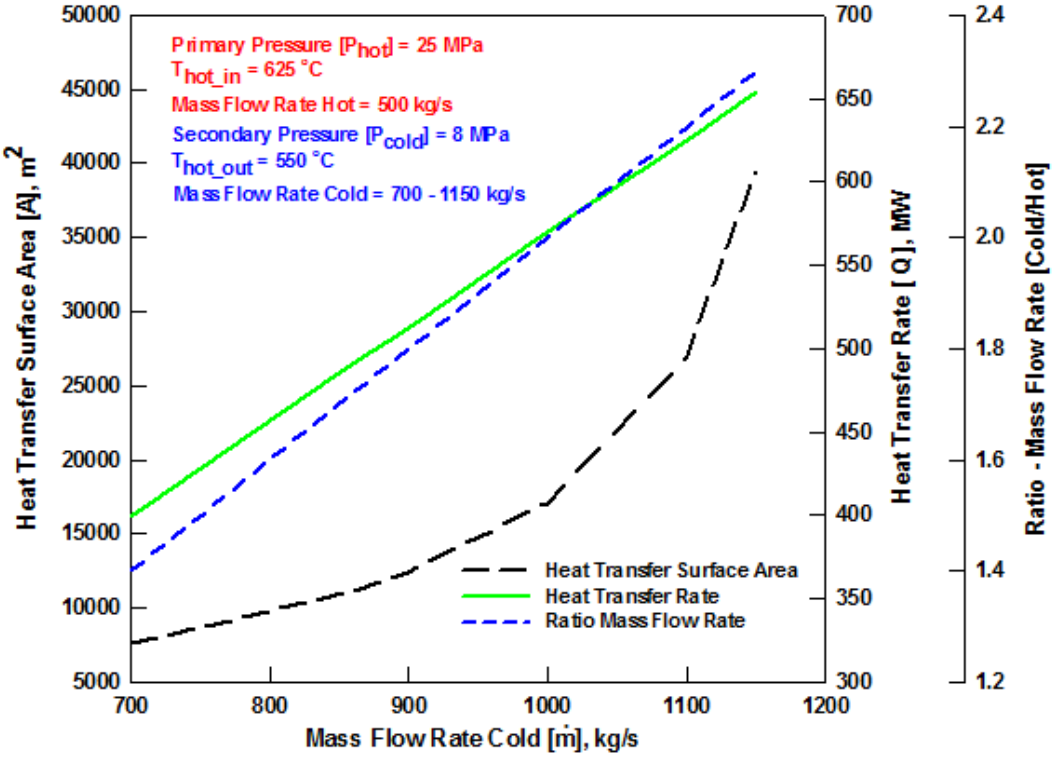

Figure 6.18: Effect of mass flow rate (cold side) on heat-transfer-surface area, heat transfer rate, and ratio of mass flow rate (hot and cold side).

CHAPTER 7 - CONCLUSIONS

The main objective of this work is to develop double pipe HX concepts for SCW applications. This study analyzed the heat transfer from a SCW primary (hot) loop to a SCW and a SHS secondary (cold) loop using double-pipe intermediate HX. The numerical model is developed with MATLAB and NIST REFPROP (NIST, 2010) software. Water from the primary loop flows throw the inner pipe, and water from the secondary loop flows through the annulus in counter direction of the double-pipe HX. The analysis on the double-pipe HX shows temperature and thermophysical properties profiles along the heated length of the HX.

Single-reheat cycle is a proven technology in fossil-fuel thermal power plants. The vast majority of the modern and upcoming SC turbines are single reheat turbines. It will be practical to use similar technology for SCWR NPP layouts.

Various indirect-cycle thermodynamic configurations are proposed for PT and PV reactors to keep the nuclear activities within the reactor-containment building and to reduce probability for radioactive contamination of equipment in the turbine building, thus reducing the chances of human interaction with radioactive materials. SCW HX can be implemented for the single reheat option in both PV and PT reactor concepts (PT reactors core design will be less complex). A double-pipe HX can be used to operate the indirect-cycle configuration.

The Swenson et al. (1965) correlation was selected for the heat transfer calculations.

It was found that the pseudocritical region has a significant effect on the temperature profiles and heat-transfer area of the HX. A sensitivity analysis shows the effect of variation in pressure, temperature, mass flow rate and pipe size on pseudocritical region and heat-transfer area of the HX. The results from the numerical model can be used to optimize the heat-transfer area of the HX.

It was noted that, for the SCW to SCW HX when the pressure on the hot side is higher compared to the cold side, the operating parameters like mass flow rate, temperature, and

pipe sizes are more forgiving than the pressure on the hot side is lower compared to the cold side. Although it looks obvious to increase the pressure on the primary (reactor) side to reduce the heat-transfer-surface area of the HX, it might add complexity to the reactor core design. The higher temperature and mass flow rate difference on the hot side and cold sides reduces the pseudocritical region duration. This decreases the heat-transfer surface area of the HX.

On SCW to SHS HX, it was noted that the thermophysical properties on the SCW (hot) side had significant changes when the temperature approaches the pseudocritical region compared to the SHS (cold) side. The higher pressure and temperature difference on the hot and cold sides reduces the heat transfer area, whereas higher mass flow rate differences on the hot and cold sides increases the heat transfer area.

CHAPTER 8 - FUTURE WORK

The HTC enhancement techniques, for example, spiral tubes, fins, and static mixer inserts etc., for pipes needs to be studied in the future work to determine any potential for increasing the HTC and reducing the overall size of the HX.

Parameters on primary (hot) and secondary (cold) sides need to be optimized to reduce the heat transfer area of the HX.

Other types of HXs, e.g., shell and tube type, needs to be investigated as an intermediate HX.

In future work, the heat losses to the environment, pressure losses, and fouling factors needs to be considered along the length of the HX.

REFERENCES

Bishop, A.A., Sandberg, R.O. and Tong, L.S., 1964. Forced convection heat transfer to water at near-critical temperatures and super-critical pressures, Report WCAP-2056, Westinghouse Electric Corporation, Atomic Power Division, Pittsburgh, PA, USA, December, 85 pages.

Buongiorno, J. and MacDonald, Ph.E., 2003a. Supercritical water reactor (SCWR). Progress report for the FY-03 Generation-IV R&D activities for the development of the SCWR in the U.S., Report INEEL/EXT-03-01210, Idaho National Engineering and Environmental Laboratory, USA, September, 38 pages.

Bringer, R.P. and Smith, J.M., 1957. Heat transfer in the critical region, AIChE Journal, Vol. 3, Issue 1, pp. 49–55.

British Stainless Steel Association. (n.d.). Elevated temperature properties of stainless steels. Retrieved December 2, 2008, http://www.bssa.org.uk/topics.php?article=139.

Cheng, X., Yang, Y.H., and Huang, S.F., 2009, A Simple Heat Transfer Correlation for SC Fluid Flow in Circular Tubes, In NURETH-13, Kanazawa City, Ishikawa Prefecture, Japan, September 27-October 2.

Cengel, A. Y., Boles A. M., 2008, 6th edition. Thermodynamics An Engineering Approach. McGraw Hill, New York, USA.

Chow, C. K., and Khartabil, H. F., "Conceptual Fuel Channel Designs for CANDU-SCWR," Nuclear Engineering and Technology, Vol. 40, Issue 1, 200, 8 pages.

Clifford, Tony., 1999. Fundamentals of Supercritcal Fluids, Oxford University Press Inc., New York, USA, 210 pages.

Dittus, F.W. and Boelter, L.M.K., 1930. Heat Transfer in Automobile Radiators of the Tubular Type, University of California, Berkeley, Publications in Engineering, Vol. 2, Issue 13, pp. 443-461.

Domin, G, 1963. Wärmeübergang in kritischen und überkritischen Bereichen von Wasser in Rohren, Brennstoff-Warme-Fraft (BWK), Vol. 15, Issue 11, pp. 527–532.

Duffey, R., and Hedges, K., 1999. Future CANDU reactor development, In Proceeding of 7th International Conference on Nuclear Engineering (ICONE-7), ASME, Tokyo, Japan, April 19-23, 14 pages.

Duffey, R.B., Pioro, I.L. and Kuran, S., 2008a. Advanced Concepts for Pressure-Channel Reactors: Modularity, Performance and Safety, JSME, Journal of Power and Energy Systems, Vol. 2, pp. 112-121.

Duffey, R.B., Pioro, I., Zhou, T., Zirn, U., Kuran, S., Khartabil, H. and Naidin, M., 2008b. Supercritical Water-Cooled Nuclear Reactors (SCWRs): Current and Future Concepts - Steam-Cycle Options, In Proceedings of the 16th International Conference on Nuclear Engineering (ICONE-16), ASME, Orlando, Florida, USA, May 11-15, Paper #48869, 9 pages.

Filippov, G.A., Avdeev, A.A., Bogoyavlensky, R.G. et al., 2003. Case micro-fuel-element nuclear reactor with supercritical pressure of light water coolant for single-loop power units of NPP, In International Scientific-Engineering Conference "Nuclear Power Engineering and Fuel Cycles", Moscow-Dimitrovgrad, Russia, December 1–5, 7 pages.

GIF – Generation IV International Forum, 2002. A Technology Roadmap for Generation IV Nuclear Energy Systems, Issued by the Generation IV international Forum and the U.S. DOE Nuclear Energy Research Advisory Board, 97 pages. http://www.gen-4.org/PDFs/GenIVRoadmap.pdf

Gospodinov, Ye., Mokry, S., Pioro, I., and Kirillov, P.L., 2008. Supercritical Water Heat Transfer in a Vertical Bare Tube, Proc. ICONE-16, ASME, Orlando, Florida, USA, May 11–15, Paper No. 48546.

Gnielinski, V., 1976. New equation for heat and mass transfer in turbulent pipe and channel flow, International Chemical Engineering, Vol. 16, Issue 2, pp. 359–368.

Grande, L., Peiman, W., Villamere, B., Rodriguez-Prado, A., Mikhael, S., Allison, L., and Pioro, I., 2011. Effect of Heat Transfer Coefficient on Sheath and Fuel Centreline Temperature, In Proceedings of the 19th International Conference on Nuclear Engineering (ICONE-19), ASME, Chiba, Japan, May 16-19, Paper#44082, 9 pages.

Griem, H., 1996. A new procedure for the prediction of forced convection heat transfer at near- and supercritical pressure, Heat and Mass Transfer (Warme- und Stoffubertragung), Springer-Verlag Publishing House, Vol. 31, Issue 5, pp. 301–305.

Hadaller, G., and Banerjee, S., 1969, Heat Transfer to Superheated Steam in Round Tubes, AECL Report.

Harrison, G. and Watson, A., 1976. A experimental investigation of forced convection to supercritical pressure water in heated small bore tubes, In Proceedings of the Institute of Mechanical Engineers, Vol. 190, Issue 40-76, pp. 429–435.

Hore-Lacy, Ian., 2003. Nuclear Energy in the 21st Century, World Nuclear University Press, Carlton House, London, United Kingdom, 167 Pages.

Incropera, F. P., Dewitt, D. P., Bergman, T. L., & Lavine, A. S. , 2006. Fundamentals of Heat and Mass Transfer. John Wiley & Sons, USA.

Jackson, J.D., 2002. Consideration of the heat transfer properties of supercritical pressure water in connection with the cooling of advanced nuclear reactors, In Proceedings of the 13th Pacific Basin Nuclear Conference, Shenzhen City, China, October 21–25.

Kakac, S., Pramuanjaroenkij, A., and Liu, H., 2002, Second Edition, Heat Exchangers: Selection, Rating, and Thermal Design, CRC Press, USA, pp 283-341.

Kirillov, P.L., Lozhkin, V.V. and Smirnov, A.M., 2003. Investigation of borders of deteriorated regimes of a channel at supercritical pressures, (In Russian), State Scientific Center of Russian Federation Institute of Physics and Power Engineering by the name of A.I. Leypunskiy, FEI-2988, Obninsk, Russia, 20 pages.

Krasnoshchekov, E. A., and Protopopov, V. S., 1966, Experimental Study of Heat Exchange in Carbon Dioxide in the Supercritical Range at High Temperature Drops, Teplofizika Vysokikh Tempraturi (High Temp.), Vol. 4, Issue 3.

Kuang, B., Zhang, Y., and Cheng, X., 2008, A New, Wide-Ranged Heat Transfer Correlation of Water at Supercritical Pressures in Vertical Upward Ducts, NUTHOS-7, Seoul, Korea, October 5–9.

Lee, R.A. and Haller, K.H., 1974. Supercritical water heat transfer developments and applications, In Proceedings of the 5th International Heat Transfer Conference, Tokyo, Japan, September 3–7, Vol. 4, Paper #B7.7, pp. 335–339.

LU, Wang., XiaoDong, Feng., and Qiang, Sunjing., 2011. Study on Comprehensive and Coordination Construction and Operation Mode of Nuclear Power Plant to Power Grid, 19th International Conference on Nuclear Engineering (ICONE-19), ASME, Chiba, Japan, May 16-19, Paper #43397, 5 pages.

Matweb. (n.d.). Material Property Data. Retrieved December 2, 2008, from http://www.matweb.com/index.aspx.

McAdams, W.H., 1942. Heat Transmission, 2nd edition, McGraw-Hill, New York, NY, USA, 459 pages.

Mokry, S., Naidin, M., Baig F., Gospodinov, Ye., Zirn U., Bakan K., Pioro, I. and Naterer G., 2008. Conceptual Thermal-Design Options for Pressure-Tube SCWR'S with Thermochemical Co-generation of Hydrogen, In Proceedings of the 16th International Conference on Nuclear Engineering (ICONE-16), ASME, Florida, USA, May 11-15, Paper #48313, 13 pages.

Mokry, S., Gospodinov, Ye., Pioro, I. and Kirillov, P., 2009. Supercritical Water Heat-Transfer Correlation for Vertical Bare Tubes, In proceedings of the 17th International Conference on Nuclear Engineering (ICONE-17), ASME, Brussels, Belgium, July 12-16, Paper #76010, 8 pages.

Mokry, S., Farah, A., King, A. and Pioro, I., 2011. Updated Heat Transfer Correlations for SuperCritical Water Cooled Reactor Applications, In Proceedings of the 19th International Conference on Nuclear Engineering (ICONE-19), ASME, Chiba, Japan, May 16-19, Paper #43876, 13 pages.

Naidin, M., Mokry, S., Monichan, R., Chophla, K., Pioro, I., Naterer, G., and Gabriel, K., 2009. Thermodynamic Analysis of SCW NPP Cycles with Thermo-Chemical Co-generation of Hydrogen. In International Conference on Hydrogen Production, Oshawa, Canada, May 03-06, 15 pages.

National Institute of Standards and Technology (NIST), 2010. NIST Standard Reference Database 23: Reference Fluid Thermodynamic and Transport Properties–REFPROP, Version 9.0. Boulder, CO, U.S., Department of Commerce.

Ornatskiy, A.P., Dashkiev, Yu.G. and Perkov, V.G., 1980. Supercritical Steam Generators, (In Russian), Vyshcha Shkola Publishing House, Kiev, Ukraine, 287 pages.

Peiman, W., Gabriel, K., Pioro, I.L., 2009. Thermal Design Options for New Pressure Channel for SCWRs. In Proceedings of the 17th International Conference on Nuclear Engineering (ICONE-17), ASME, Brussels, Belgium, July 12-16, Paper #75514.

Pioro, I., Saltanov, Eu., Naidin, M., King, K., Farah, A., Peiman, W., Mokry, S., Grande, L., Thind, H., Samuel, J. and Harvel, G., 2010. Steam-Reheat Option in SCWRs and Experimental BWRs, Report for NSERC/NRCan/AECL Generation IV Energy Technologies Program (NNAPJ) entitled "Alternative Fuel-Channel Design for SCWR" with Atomic Energy of Canada Ltd., Version 1, UOIT, Oshawa, ON, Canada, March, 128 pages.

Pioro, I. and Duffey, R., 2007. Heat Transfer and Hydraulic Resistance at Supercritical Pressures in Power Engineering Applications, ASME Press, New York, NY, USA, 334 pages.

Pioro, I., Zirn U., Duffey, R., Naidin, M., Mokry, S., Gospodinov Ye., and Baig F., 2008. Supercritical Water-Cooled Nuclear Reactors: Thermodynamic-Cycles Options, In 6th International Conference on Heat Transfer, Fluid Mechanics and Thermodynamics, Pretoria, South Africa, June 30 – July 2, 10 pages.

Ribando, R.J., O'Leary, G.W., and Carlson-Skalak, S., 1997. General Numerical Scheme for Heat Exchanger Thermal Analysis and Design, Journal of Computer Applications in Engineering Education. Vol. 5, Issue 4, pp. 231-242.

Samuel, J., Harvel, G., and Pioro, I., 2010. Design Concept and Heat Transfer Analysis for a Double Pipe Fuel Channel for SCWR Type Reactor, In Proceeding of the 18th International Conference on Nuclear Engineering (ICONE-18), ASME, Xi'an, China, May 17−21, Paper #29956, 10 pages.

Schnurr, N.M., Sastry, V.S. and Shapiro, A.B., 1976. A numerical analysis of heat transfer to fluids near the thermodynamic critical point including the thermal entrance region. Journal of Heat Transfer, Transactions of the ASME, pp. 609–615.

Shah, R. K., and Sekulic, D. P., 2003, Fundamentals of Heat Exchanger Design, John Wiley & Sons, Inc., Hoboken, New Jersey, USA, 931 pages.

Seider, N. M., and Tate, G. E., 1936, Heat Transfer and Pressure Drop of Liquids in Tubes, Ind. Eng. Chem. Vol. 28, Issue 12, pp. 1429–1435.

Swenson, H.S., Carver, J.R. and Kakarala, C.R., 1965. Heat transfer to supercritical water in smooth-bore tubes, Journal of Heat Transfer, Transactions of the ASME, Series C, Vol. 87, Issue 4, pp. 477–484.

Thind, H., Pioro, I., and Harvel G., 2010. Supercritical Water-Cooled Nuclear Reactor with Intermediate Heat Exchangers, Proceeding of the 18th International Conference on Nuclear Engineering (ICONE-18), ASME, Xi'an, China, May 17−21, Paper #30104, 10 pages.

Timoshenko S. P. and Gere J., 1961. Theory of Elastic Stability, McGraw-Hill College.

Watts, M. J., and Chou, C-T., 1982, Mixed Convection Heat Transfer to Supercritical Pressure Water, Proc. 7th, IHTC, Munich, Germany, pp. 495–500.

World Nuclear Association – June 2010 - http://www.world-nuclear.org/info/inf16.html.

Yamaji, A., Kamei, K., Oka, Yo. and Koshizuka, S., 2004. Improved core design of high temperature supercritical-pressure light water reactor, In Proceedings of the International Congress on Advances in Nuclear Power Plants (ICAPP'04), Pittsburgh, PA, USA, June 13–17, Paper #4331, pp. 509–517.

Zahlan, H., Groeneveld, D. and Tavoularis, S., 2010. Look-Up Table for Trans-Critical Heat Transfer, The 2nd Canada-China Joint Workshop on Supercritical Water-Cooled Reactors (CCSC), Toronto, Ontario, Canada, April 25-28, Paper #P036, 18 pages.

APPENDIX A : THERMOPHYSCIAL PROPERTY PROFILES OF HX1 AND HX2 ALONG THE LENGTH OF PIPE

In this section valid operating parameters for the heat transfer analysis are selected based on the analysis in Chapter 6, and operating parameters of the CANDU SCWR discussed in chapter 4. Table A.1 shows the parameters of the SCW to SCW HX1 and Table A.2 shows the parameters of the SCW to SHS HX2. The intent of this section is to show the various thermophysical properties of the fluid on the hot and the cold side along the length of the HX pipe.

Table A.1: Summary of thermodynamic parameters of HX1 for analysis.

Parameters	Primary Loop (Hot Side)	Secondary Loop (Cold Side)
HX1 (SCW – SCW)		
Thermal Power (MW)	2540	-
Pressure (MPa)	25	25.5
Inlet Temperature (^{o}C)	625	340
Outlet Temperature (^{o}C)	350	600
Mass Flow Rate (kg/s)	1320	1240
Outer diameter of pipe (mm)	25.4	38.1
Inner diameter of pipe (mm)	22.8	34.1

Figure A.1 shows the temperature, specific heat, heat transfer rate, and enthalpy profiles of fluid on the hot and cold sides along the length of the double-pipe HX. The heat transfer is enhanced or deteriorated due to the change in fluid properties depending on the exact fluid conditions. The value of specific heat on the hot and cold sides is high in pseudocritical range. In this region the most of the heat is used up due to a higher specific heat capacity of the fluid, resulting in small temperature change between the hot and cold sides. The heat transfer rate is low in the pseudocritical range and starts rising as

the fluid exits the pseudocritical range along the length of the pipe. The enthalpy change follows the temperature profile along the length of the pipe. It drops significantly as the heat is transferred from hot to cold side at the beginning and at the end of pipe, the enthalpy change slows down as it approaches the pseudocritical range. Nusset number, Reynolds number, and average Prandtl number profiles shown in Figure A.2 are dependent on the thermal conductivity, viscosity, enthalpy, and density of the fluid along the length of the pipe. Figure A.3 shows the viscosity, density, and temperature profiles along the length of the pipe. For example viscosity in Figure A.3 drops in the beginning for the first ~90 m, then rises slowly up to 400 m and from 400 to 460 m it rises rapidly fast. Since the Reynolds number is inversely proportional to viscosity, similar behavior is noticed in Figure A.2 for the Reynolds number, but in opposite direction. Also to be noted, the Swenson et al. correlation relies on the average fluid properties in a pipe at given cross-section, thus in Figures A.2 to A.4, the pseudocritical peak is off from the actual peak as the bulk fluid temperature is different than to the wall temperature. In Figure A.4 heat transfer coefficient peaks as it approaches the pseudocritical point for both the hot and cold side respectivley. The resistance is inversely proportional to the heat transfer coefficient, and it drops to a minimum at the pseudocritical point.

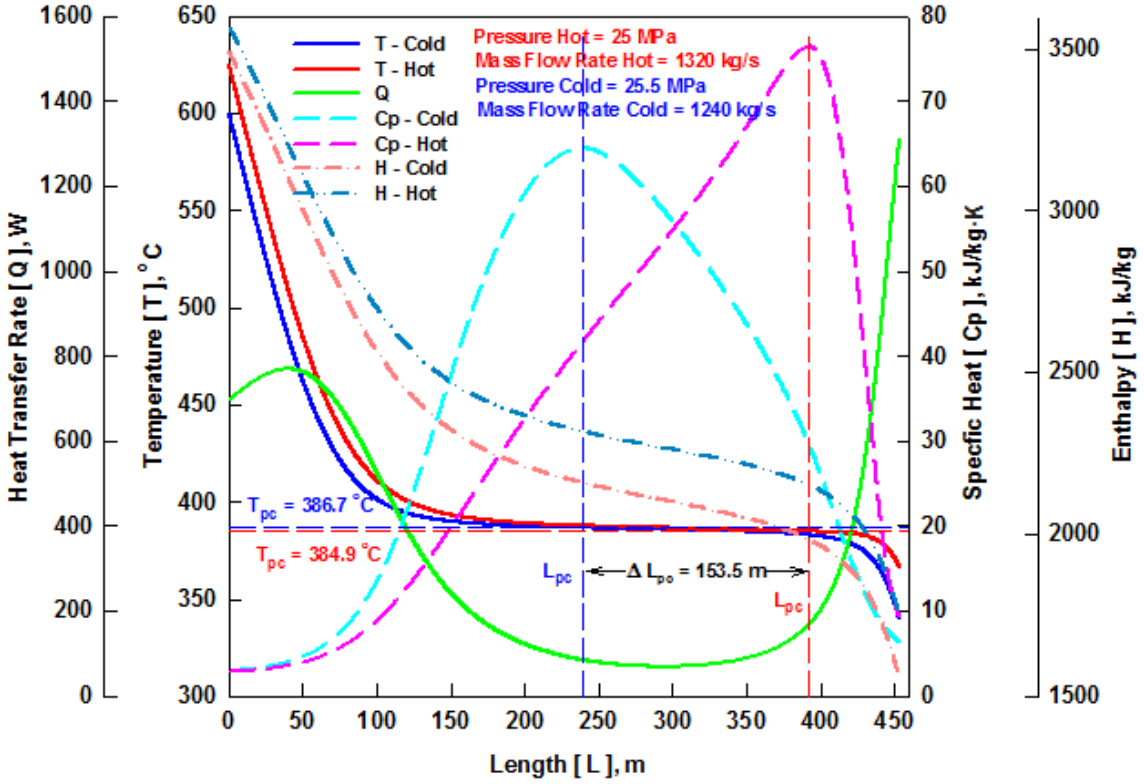

Figure A.1: Temperature profile, Heat Transfer Rate, Specific Heat, and Enthalpy along length of double-pipe HX.

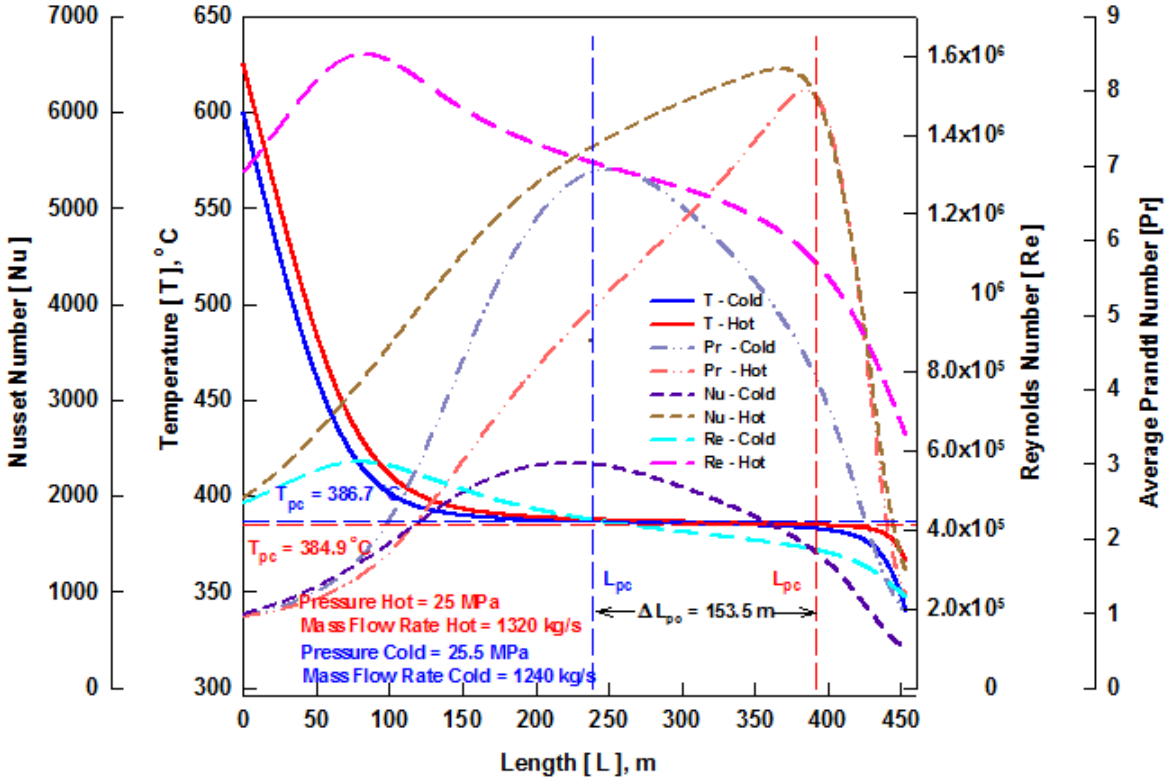

Figure A.2: Temperature profile, Nusset, Reynolds, and Average Prandtl numbers along length of double-pipe HX.

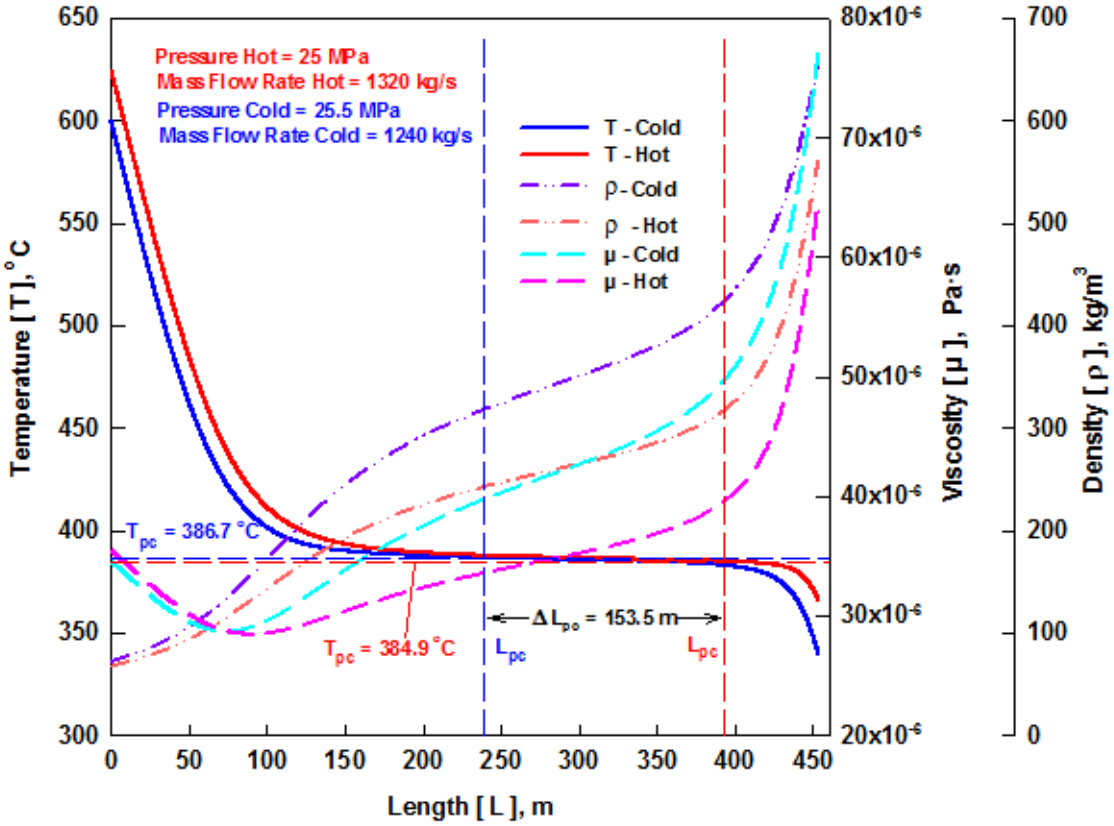

Figure A.3: Temperature profile, Viscosity, and Density along length of double-pipe HX.

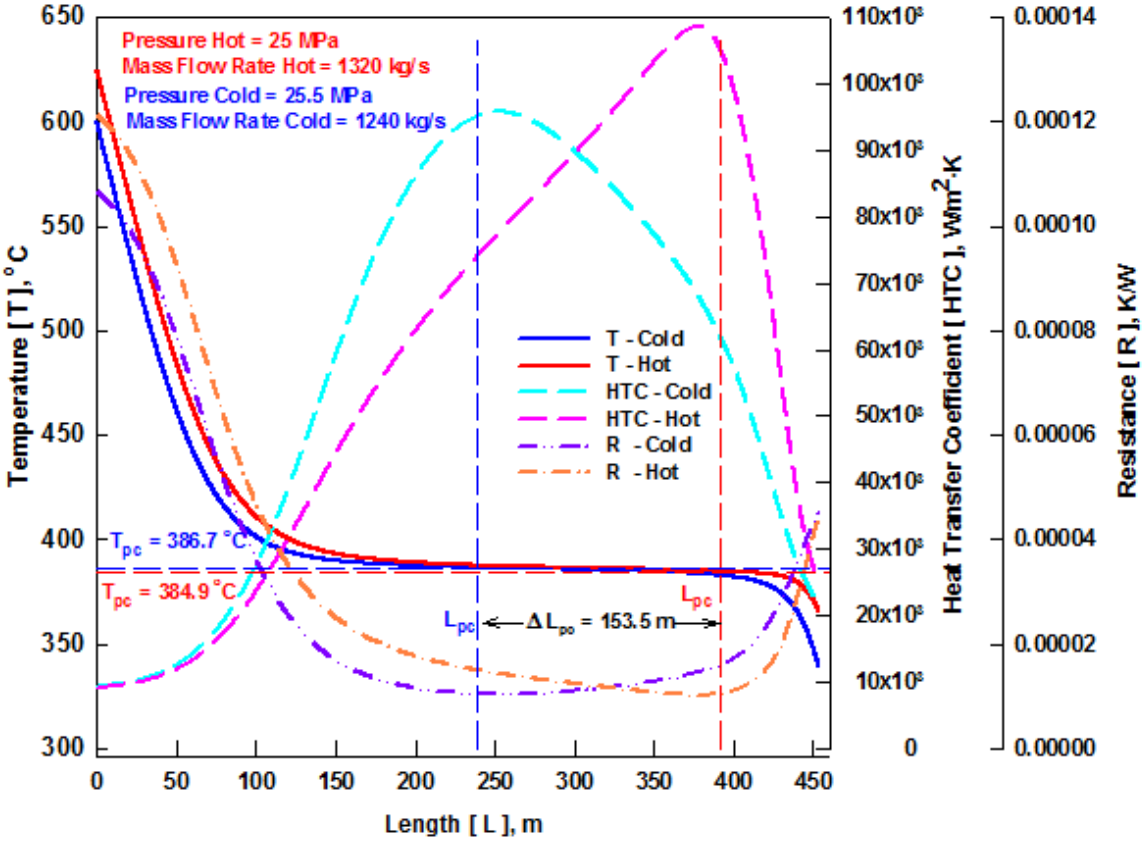

Figure A.4: Temperature profile, Heat transfer coefficient, and Resistance along length of double-pipe HX.

Table A.2: Summary of thermodynamic parameters of HX2 for analysis.

Parameters	Primary Loop (Hot Side)	Secondary Loop (Cold Side)
HX1 (SCW – SHS)		
Thermal Power (MW)	566	-
Pressure (MPa)	25	8
Inlet Temperature (^{o}C)	625	340
Outlet Temperature (^{o}C)	350	590
Mass Flow Rate (kg/s)	500	850
Outer diameter of pipe (mm)	25.4	35.3
Inner diameter of pipe (mm)	22.8	34.1

Figure A.5 shows the temperature, specific heat, heat transfer rate, and enthalpy profiles of the fluid on the hot and cold sides along the length of the double-pipe HX. The fluid on hot side leaves slightly above the pseudocritical temperature. The temperature of the cold side increases drastically as fluid enters the HX, due to the hot side reaches the pseudocritical region at the exit of the HX. This corresponds to the HTC in Figure A.8, the HTC increases drastically on hot side as it approaches pseudocritical region, which brings the overall HTC higher. Figure A.8 also shows the thermal resistance of the hot and cold side, which inversely corresponds to the heat transfer coefficient at given cross-section of the pipe. The changes in the thermophysical properties on the cold side are not as significant as on the hot side, given the absence of a pseudocritical region. In Figure A.7 on the cold side the fluid viscosity decrease produces a drop in the Reynolds number seen in Figure A.6, whereas the average Prandtl number does not change much along the length of the HX pipe. On the hot side, the most significant changes occur in pseudocritical region. In figure A.7 the viscosity and density increases drastically in the pseudocritical region. Increase in viscosity produces a sudden increase in the Prandtl number and the decrease in the Reynolds number in Figure A.6.

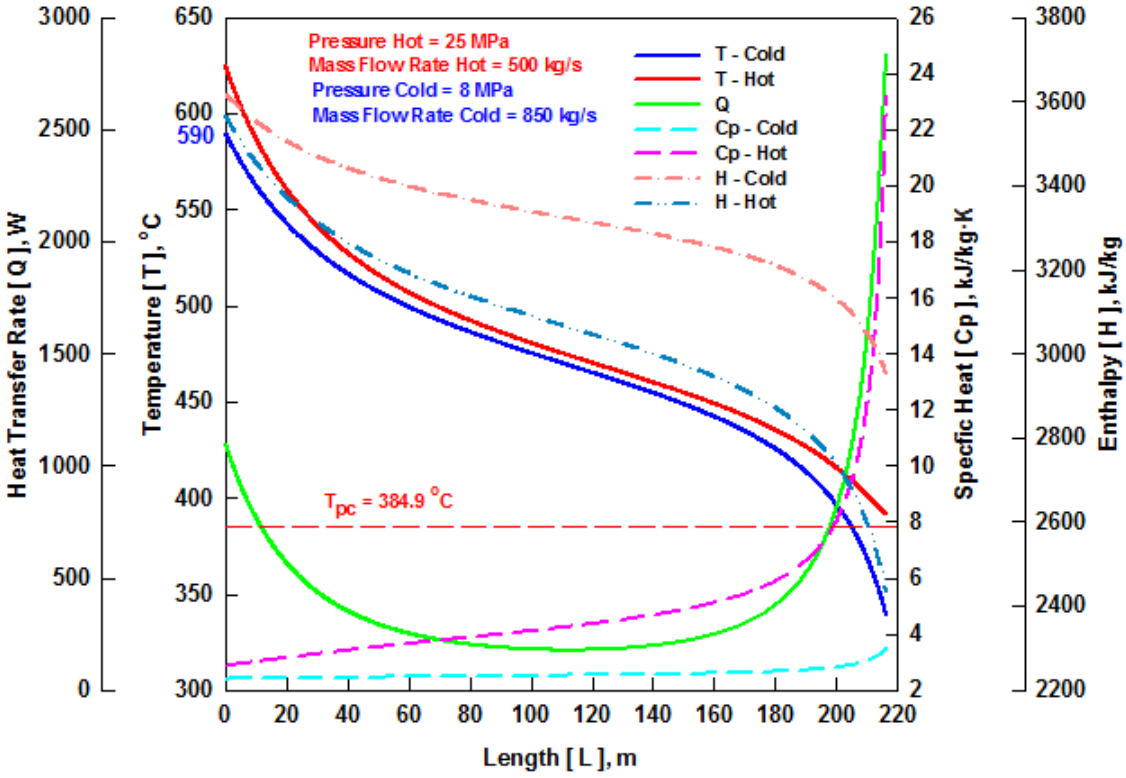

Figure A.5: Temperature profile, Heat Transfer Rate, Specific Heat, and Enthalpy along length of double-pipe HX.

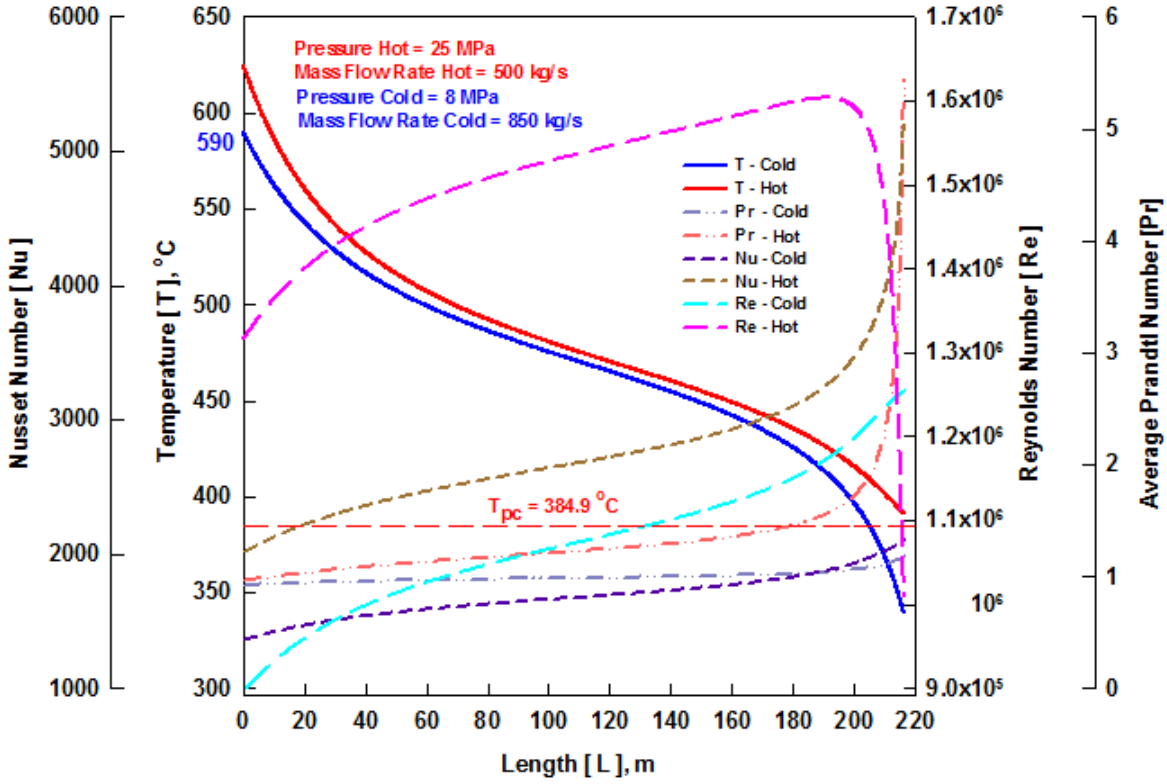

Figure A.6: Temperature profile, Nusset, Reynolds, and Average Prandtl numbers along length of double-pipe HX.

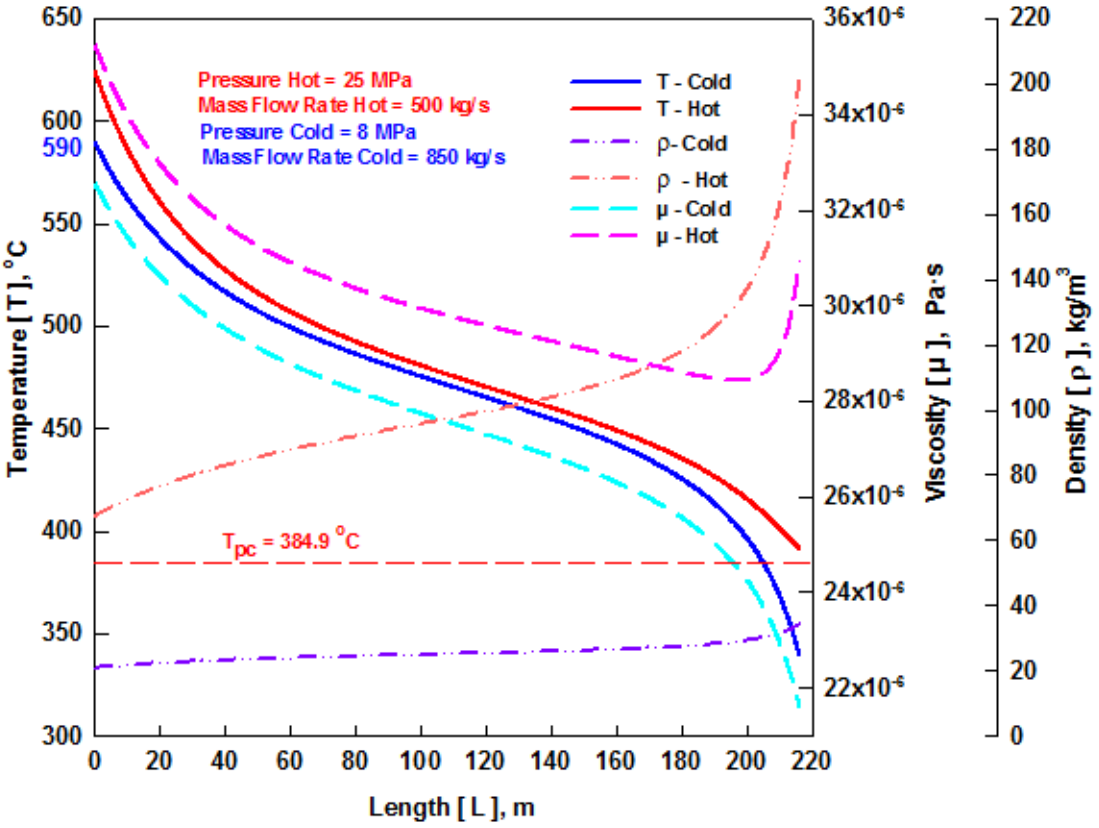

Figure A.7: Temperature profile, Viscosity, and Density along length of double-pipe HX.

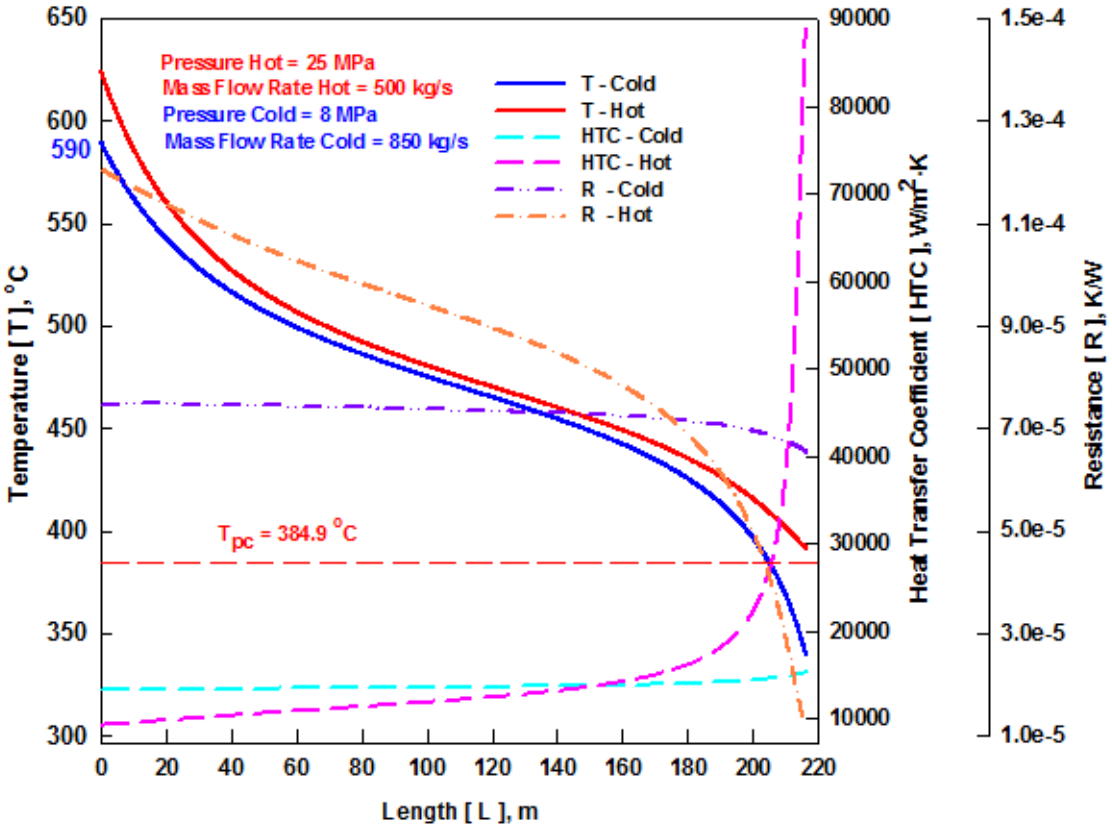

Figure A.8: Temperature profile, Heat transfer coefficient, and Resistance along length of double-pipe HX.

APPENDIX B : PRELIMNARY CALCULATIONS FOR DOUBLE-PIPE HEAT EXCHANGER AND SHELL & TUBE HEAT EXCHANGER

In chapter 2 initial investigations suggested the shell and tube, and double-pipe type HX were the most suitable for the operating parameters of SCW nuclear reactor system. Shell and tube heat exchangers can be designed on a custom basis for any capacity and operating conditions. The double-pipe heat exchanger gives us the added safety due to their capabilities of operation, when both fluids are under high pressure. In this appendix preliminary calculations are performed on both double-pipe HX and shell and tube HX by log mean temperature difference method.

Based on the analysis of different SCW correlations in chapter 3, it was found that the correlation predicted different HTC in the pseudocritical (±25 ^{o}C) region. However at the bulk-fluid temperature of 450 ^{o}C and higher, HTC values calculated with different correlations are close to each other. As a larger percentage of the operation of the HX is above 450 ^{o}C, the simplest of the four correlations is used for preliminary heat transfer calculations, i.e., the Dittus-Boelter correlation, which does not require iterations, when doing manual calculations.

B.1 Major Parameters of Primary and Secondary Loop for Double-Pipe and Shell & Tube Heat Exchanger

Table B.1 shows the parameters for the HX1 and HX2 for the preliminary calculations. The water in primary loop for HX1 (SCW-SCW) is at pressure 25 MPa, enters into the HX at temperature 625 ^{o}C and exit at 350 ^{o}C. The pressure on the secondary side is 25.5 MPa, the water enters HX at 340 ^{o}C and exits at 600 ^{o}C. For HX2 (SCW – SHS) the water in primary loop is at 25 MPa, enters into HX at temperature 625 ^{o}C and exit at 350 ^{o}C. The pressure on the secondary side is 5 MPa, the water enters HX at 340 ^{o}C and exits at 600 ^{o}C. Mass-flow rates on both primary and secondary sides are assumed to be the same.

Table B.1: Heat exchanger parameters for preliminary calculations.

Parameters	Primary Loop (Hot Side)	Secondary Loop (Cold Side)
HX1 (SCW – SCW)		
Pressure (MPa)	25	25.5
Inlet Temperature (^oC)	350	340
Outlet Temperature (^oC)	625	600
Mass Flow Rate (kg/s)	1320	1320
HX2 (SCW – SHS)		
Pressure (MPa)	25	5
Inlet Temperature (^oC)	350	340
Outlet Temperature (^oC)	625	600
Mass Flow Rate (kg/s)	1320	1320

Thermal Power – Q = 2500 MW

Mass Flux – G = 2000 kg/m^2·s

Thermal Conductivity – k = 17.4 W/m·K (Stainless Steel SS-304)

Assumptions:

- Negligible heat loss to the surroundings;
- Negligible kinetic and potential energy changes;
- Constant properties;
- Fully developed conditions for the water on both sides;
- Negligible fouling factor; and
- Thermal conductivity, Young's modulus of elasticity, Tensile Strength, Poisson's Ratio of stainless steel (SS-304) is taken at the average temperature of 450 °C.

Analysis:

(Incropera *et al*., 2006)

$$\bar{T}_h = \frac{(T_{h,i}+T_{h,o})}{2} \quad \text{(B.1)}$$

$$\bar{T}_c = \frac{(T_{c,i}+T_{c,o})}{2} \quad \text{(B.2)}$$

$$Q = U \cdot A_s \cdot \Delta T_{lm} \quad \text{(B.3)}$$

$$\Delta T_{lm} = \frac{\Delta T_1 - \Delta T_2}{ln\,(\Delta T_1/\Delta T_2)} \quad \text{(B.4)}$$

$$\Delta T_1 = (T_{h,i} - T_{c,o}) \quad \text{(B.5)}$$

$$\Delta T_2 = (T_{h,o} - T_{c,i}) \quad \text{(B.6)}$$

$$\frac{1}{U} = \frac{d_o}{d_i \cdot h_i} + \frac{d_o \cdot ln(d_o/d_i)}{2k} + \frac{1}{h_o} \quad \text{(B.7)}$$

Dittus-Boelter correlation (1930):

$$\mathrm{Nu_b} = 0.0243\ \mathrm{Re_b^{0.8}Pr_b^{0.4}} \quad \text{(B.8)}$$

Minimum required wall thickness of pipes and shell is calculated with the safety factor of 25% on operating pressure for both double-pipe heat exchanger and shell and tube heat exchanger

d_o – assumed

Burst pressure (inner pipe):

(Pioro and Duffey, 2007)

$$P = \frac{2S \cdot \delta}{d_o} \quad \text{(B.9)}$$

Collapse pressure (inner tube):

(Timoshenko and Gere, 1961)

$$P_{cr} = \frac{2E}{(1-\nu^2)}\left(\frac{\delta}{d_o}\right)^3 \quad \text{(B.10)}$$

Whichever burst or collapse pressure calculations gives higher wall thickness value for the pipe is selected. Based on this higher value, the next standard available size for the pipe is selected.

$$d_i = d_o - 2\delta \quad \text{(B.11)}$$

$$A_{c,i} = \frac{(\pi \cdot d_i^2)}{4} \quad \text{(B.12)}$$

$$\dot{m} = G \cdot A_{c,i} \quad \text{[Mass flow rate in one pipe]} \quad \text{(A.13)}$$

$$N = \frac{\dot{m}_h}{\dot{m}} \quad \text{(B.14)}$$

B.2 Double-Pipe Heat Exchanger

(Incropera et al., 2006).

Based on the assumption that mass-flow rate is the same on both hot and cold sides. We can find the inside diameter of the annulus pipe.

$$D_i = \sqrt{d_i^2 + d_o^2} \quad \text{(B.15)}$$

Burst pressure (annulus pipe):

$$p = \frac{2S \cdot \delta}{(D_i + 2\delta)} \quad \text{(B.16)}$$

$$D_o = (D_i + 2\,\delta) \quad \text{(B.17)}$$

For hot side:

$$Re_h = \frac{\mathrm{G \cdot d_i}}{\mu_h} \quad \text{(B.18)}$$

$$\mathrm{Nu_b} = 0.0243\ \mathrm{Re_b^{0.8} Pr_b^{0.4}}$$

$$h_i = \frac{Nu_h \cdot k_h}{d_i} \quad \text{(B.19)}$$

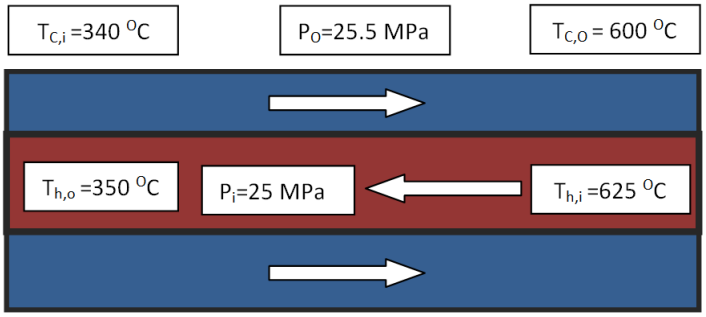

(a)

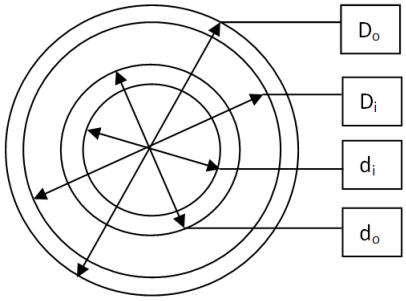

(b)

Figure B.1: Hot-Side and Cold-Side Arrangement of Double-Pipe Heat Exchanger. (a) Schematic of flow, (b) Cross-section of channel.

For cold side:

$$D_{hy} = D_i - d_o \tag{B.20}$$

$$Re_c = \frac{G \cdot D_{hy}}{\mu_c} \tag{B.21}$$

$$\mathrm{Nu_b} = 0.0243\ \mathrm{Re_b^{0.8}Pr_b^{0.4}}$$

$$h_o = \frac{Nu_c \cdot k_c}{D_{hy}} \tag{B.22}$$

Calculate "U"

$$A_s = \frac{Q/N}{U\ .\ \Delta T_{lm}} \quad \text{[Heat-transfer surface area for one pipe]} \tag{B.23}$$

$$L = \frac{A_s}{\pi \cdot d_o} \tag{B.24}$$

B.3 Shell and Tube Heat Exchanger

(Kakac et al., 2002)

L = Assumed for the initial trial

$$A_s = \pi \cdot d_o \cdot N \cdot L \tag{B.25}$$

Tube Count Constant (TCC) = 0.93 [one pass]

Tube Layout Constant (TLC) = 1.0 [for 90^o and 45^o]

Tube Pitch Ratio (PR) = Pitch/d_o [Recommended between1.25 – 1.5]

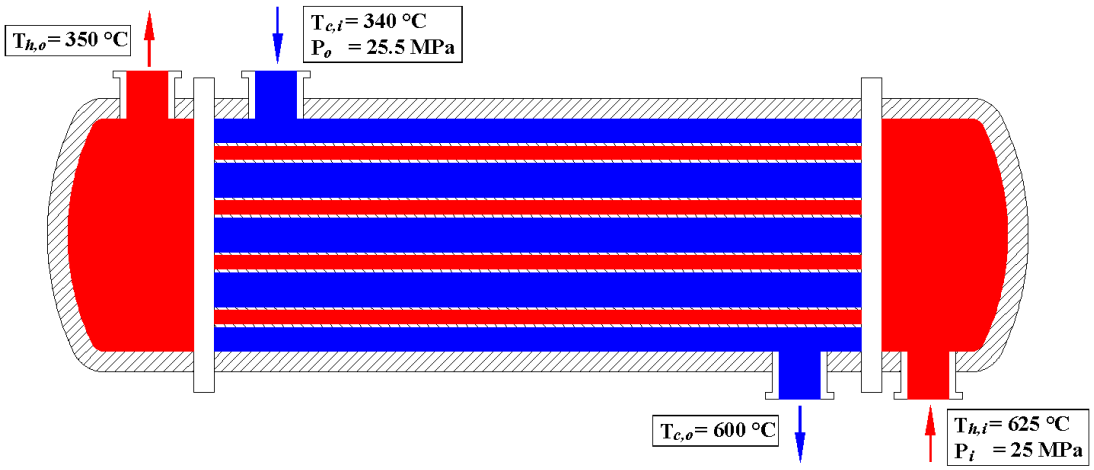

(a)

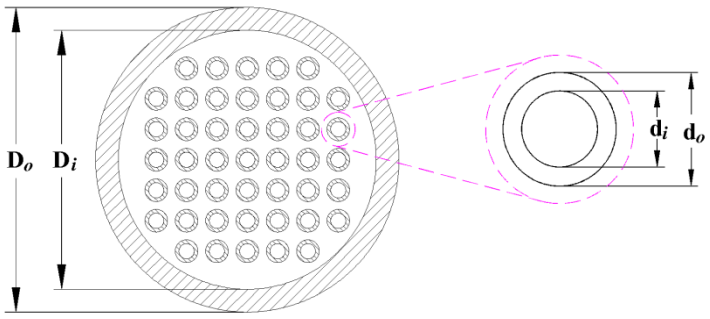

(b)

Figure B.2: Hot-Side and Cold-Side Arrangement of Shell and Tube Heat Exchanger.

(a) Schematic of flow, (b) Cross-section of shell and channels.

$$D_i = 0.637\sqrt{\frac{TCC}{TLC}\left[\frac{A_s \cdot PR^2 \cdot d_O}{L}\right]} \quad \text{(B.26)}$$

Burst pressure (Shell):

$$P = \frac{2S \cdot \delta}{(D_i + 2\delta)} \quad \text{(B.27)}$$

$$D_{o,shell} = (D_{i,shell} + 2\,\delta) \quad \text{(B.28)}$$

For hot side:

$$Re_h = \frac{\mathrm{G \cdot d_i}}{\mu_h} \quad \text{(B.29)}$$

$$\mathrm{Nu_b} = 0.0243\ \mathrm{Re_b^{0.8} Pr_b^{0.4}}$$

$$h_i = \frac{Nu_h \cdot k_h}{d_i} \quad \text{(B.30)}$$

For cold side (Shell side):

$$Re_c = \frac{\mathrm{G \cdot D_e}}{\mu_c} \quad \text{(B.31)}$$

$$D_e = \frac{4 \cdot \text{free-flow area}}{\text{wetted perimeter}} = \frac{4\left(\mathrm{Pitch^2} - \pi \cdot (\mathrm{d_o^2}/4)\right)}{\pi \cdot \mathrm{d_o}} \quad \text{[for square pitch]} \quad \text{(B.32)}$$

$$\mathrm{Nu_b} = 0.0243\ \mathrm{Re_b^{0.8} Pr_b^{0.4}}$$

$$h_o = \frac{Nu_c \cdot k_c}{D_e} \quad \text{(B.33)}$$

Calculate "U"

$$Q_{calculated} = U \cdot A_s \cdot \Delta T_{lm} \quad \text{(B.34)}$$

B.4 Results from preliminary Calculations

The results from the preliminary calculations are shown in Table B.2. The HX is divided into 4 equal units to resemble CANDU-6 steam generators. The heat transfer surface area for the double-pipe HX is higher compared to the shell and tube HX. It is 17% higher for SCW to SCW heat exchanger and 22% for SCW to SHS heat exchanger. Although the double-pipe heat transfer surface area is higher, the double-pipe HX is selected for further analysis in this study due to added safety provided by double-pipe HX under high pressure and simplicity of the design. The analysis on shell and tube HX will be carried out in future work. The results also show that the indirect cycle can be combination of double-pipe for SCW to SCW HX and shell and tube for SCW to SHS heat exchanger.

Table B.2: Comparison of Double-Pipe and Shell and Tube heat exchangers results.

Calculated Values	SCW-SCW		SCW-SHS	
	Double-Pipe HX	Shell and Tube HX	Double-Pipe HX	Shell and Tube HX
Number of Units	4	4	4	4
Height (m)	8	18	8	18.5
Width (m)	8	4.5 (dia)	8	4.5 (dia)
Length (m)	12	4.5 (dia)	15	4.5 (dia)
Number of pipes per unit	434	434	434	434
Outer diameter of inner pipe (mm)	25.4	25.4	25.4	25.4
Inner diameter of inner pipe (mm)	22	22	22	22
Outer diameter of outer pipe	38.1 (mm)	4.5 (shell)(m)	34.3 (mm)	4.5 (shell)(m)
Inner diameter of outer pipe	33.6 (mm)	4.0 (shell)(m)	33.6 (mm)	4.4 (shell)(m)
Annulus gap (mm)	4.1		4.1	
Tube material	SS-304	SS-304	SS-304	SS-304
Total heated length per unit (m)	186186	154504	238700	186620
Heat transfer area per unit (m^2)	14868	12330	19057	14892
Heat flux (kW/m^2)	42	51	33	42
Mass flux ($kg/s \cdot m^2$)	2000	2000	2000	2000
Dry weight per unit (tonnes)	540	655	323	297

APPENDIX C: HEAT EXCHANGER MATERIAL

The material for SCW HX should exhibit good thermal conductivity, and high corrosion resistance, and mechanical strength. The operating parameters of the SCW HX are the same as the SCWR outlet temperature and pressure. Figure C.1 shows the thermal conductivity of the Inconel-600, Inconel-718, Inconel-800, SS-304, and Zirconium. The thermal conductivity of the Inconel-600, Inconel-718, Inconel-800, and SS-304 increases linearly with the increase of the temperature, where as the Zirconium thermal conductivity is steady in the 300 ^{o}C range and starts increasing from ~300 ^{o}C onwards. The Inconel-600, SS-304, and Zirconium has shown better results compared to Inconel-718 and Inconel-800 in the HX operating range. However the corrosion rate of Zirconium increases significantly when the temperature reaches 500 ^{o}C (Duffey and Hedges, 1999). Since the maximum operating temperature of SCW HX is 625 ^{o}C, Zirconium is not considered for the HX construction.

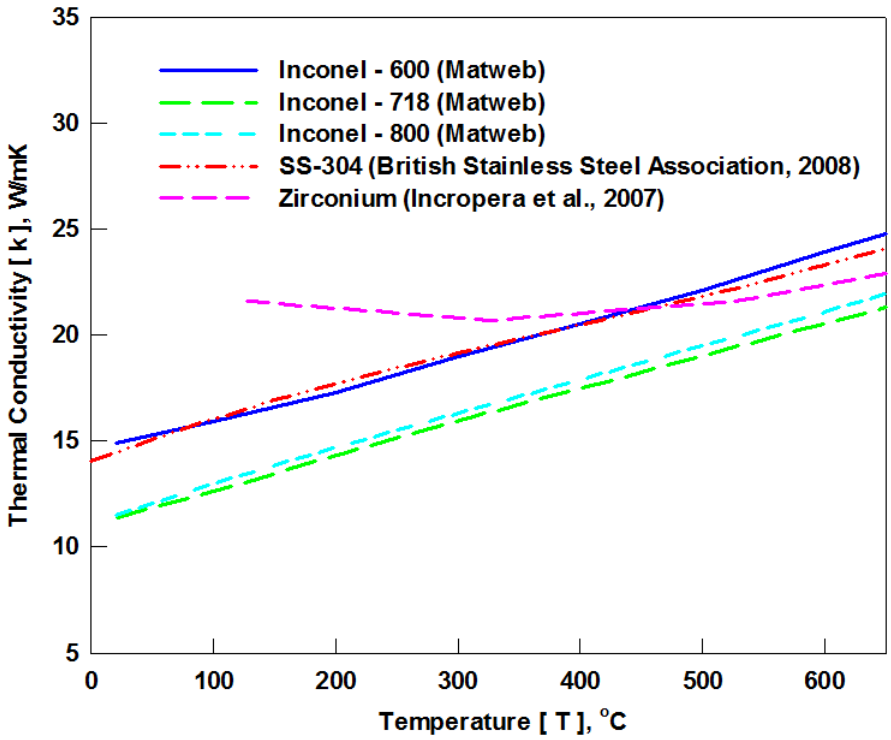

Figure C.1: Thermal conductivity vs. temperature for Inconel-600, Inconel-718, Inconel-800, SS-304, and Zirconium.

Table C.1 shows the Young's Modulus of Elasticity, Ultimate Strength, and Poisson's ratio of Inconel-600, Inconel-718, Inconel-800, and SS-304. The properties are taken at 650 ^{o}C above the upper operating temperature limit (625 ^{o}C). The objective is to determine minimum tube thickness required to withstand SCW pressure of 25 MPa to prevent from both collapsing and bursting. For the case study, the 1 inch outer pipe diameter is selected. Table C.2 shows the minimum thickness required for both collapsing and bursting. The design stress of the pressure boundary component should be less than 1/3 of the Ultimate Strength of Material (UTS) as per ASME standards (Chow & Khartabil, 2008). For purpose of this work SS-304 is selected as the HX pipe material. Further tests/analysis needs to be conducted before finalizing the tube material for HX.

Table C.1: Young's Modulus, Ultimate Strength and Poisson's Ratio of Inconel-600, Inconel-718, Inoconel-800 and SS-304 at 650 ^{o}C. (Inconels (Matweb) and SS-304 (British Stainless Steel Association)).

Material	Young's Modulus, MPa	Ultimate Tensile Strength, MPa	Poisson's Ratio
Inconel-600	176000	450	0.32
Inconel-718	163500	1100	0.32
Inconel-800	155800	378	0.31
SS-304	147500	305	0.31

Table C.2: Minimum tube thickness for Inconel-600, Inconel-718, Inconel-800 and SS-304 at temperature 650 ^{o}C and pressure 25 MPa for 1" pipe OD.

Tube Material	Minimum collapsing thickness, mm	Minimum bursting thickness, mm
Inconel-600	1.0	2.2
Inconel-718	1.0	0.8
Inconel-800	1.1	2.6
SS-304	1.1	3.2

APPENDIX D: NUMERICAL MODEL IN MATLAB

```
clear all;
clc

pi = 3.14159265358979;          % Value of pi
fluid = 'water';                % Coolant

Q=2540 * (10^6);                % Total Power [MW]

%%%%%%%%%%%%%%%%%%%%%%%%%%%%%%%%%%%%%%%%%%%%%%%%%%%%%%%%%%%%%%%%%%%%%%%%%%%%%%%
% Tube Material Parameters At 650 °C
%%%%%%%%%%%%%%%%%%%%%%%%%%%%%%%%%%%%%%%%%%%%%%%%%%%%%%%%%%%%%%%%%%%%%%%%%%%%%%%

S=305 * (1000);                 % Tube tensile strength [MPa]
E=147500 * (1000);              % Youngs modulus of elasticity [MPa]
v=0.31;                         % Poisson's ratio

%%%%%%%%%%%%%%%%%%%%%%%%%%%%%%%%%%%%%%%%%%%%%%%%%%%%%%%%%%%%%%%%%%%%%%%%%%%%%%%
% Hot Side Parameters
%%%%%%%%%%%%%%%%%%%%%%%%%%%%%%%%%%%%%%%%%%%%%%%%%%%%%%%%%%%%%%%%%%%%%%%%%%%%%%%

T_hot_in=625 + (273.15);        % Inlet temperature of hot side [C]
T_hot_out=350 + (273.15);       % Outlet temperature of hot side [C]
G_hot = 2000;                   % Mass flux hot side [kg/s.m^2]
m_dot_hot=1320;                 % Mass flow rate hot side [kg/s]
p_tube_hot=25 * (1000);         % Pressure in tube on hot side [MPa]

%%%%%%%%%%%%%%%%%%%%%%%%%%%%%%%%%%%%%%%%%%%%%%%%%%%%%%%%%%%%%%%%%%%%%%%%%%%%%%%
% Hot Side Tube Diameters
%%%%%%%%%%%%%%%%%%%%%%%%%%%%%%%%%%%%%%%%%%%%%%%%%%%%%%%%%%%%%%%%%%%%%%%%%%%%%%%

do=25.4 / (1000);               % inside diameter of inner tube [mm]

% inner tube thickness based on burst pressure
inner_tube_thickness_b=((p_tube_hot*1.25)*do)/(2*S);

% inner tube thickness based on collapse pressure
inner_tube_thickness_c=(((p_tube_hot*1.25)*(1-v^2)/(2*E))^(1/3)) * do;

if (inner_tube_thickness_b > inner_tube_thickness_c);
    inner_tube_thickness = inner_tube_thickness_b;
else
    inner_tube_thickness = inner_tube_thickness_c;
end

di=do-2*inner_tube_thickness;       % outer diameter of inner tube
Ac_innertube=(pi/4)*di^2;           % crossection area of inner tube
m_dot_tube_hot= G_hot*Ac_innertube; % mass flow rate in one inner tube
N=m_dot_hot/m_dot_tube_hot;         % Total number of tubes
```

```
%%%%%%%%%%%%%%%%%%%%%%%%%%%%%%%%%%%%%%%%%%%%%%%%%%%%%%%%%%%%%%%%%%%%%%%%%%%%
% Cold Side Parameters
%%%%%%%%%%%%%%%%%%%%%%%%%%%%%%%%%%%%%%%%%%%%%%%%%%%%%%%%%%%%%%%%%%%%%%%%%%%%

T_cold_in=340+ (273.15);       % Inlet temperature of cold side [C}
T_cold_out=600 + (273.15);     % Outlet temperature of cold side [C]
m_dot_cold=1250;               % mass flow rate cold side [kg/s]
p_tube_cold=25.5* (1000);      % pressure in tube on cold side [MPa]

%%%%%%%%%%%%%%%%%%%%%%%%%%%%%%%%%%%%%%%%%%%%%%%%%%%%%%%%%%%%%%%%%%%%%%%%%%%%
% Cold Side Tube Diameters
%%%%%%%%%%%%%%%%%%%%%%%%%%%%%%%%%%%%%%%%%%%%%%%%%%%%%%%%%%%%%%%%%%%%%%%%%%%%

Di=1*((di^2+do^2)^(1/2));          % inside diameter of outside tube
Ac_annulus =(pi/4)*(Di^2-do^2);    % crossection area of annulus tube
m_dot_tube_cold=m_dot_cold/N;
G_cold = m_dot_tube_cold/Ac_annulus; % Mass flux cold [kg/s.m^2]

% outer tube thickness based on burst pressure
outer_tube_thickness_b=(-1.25*p_tube_cold*Di)/2*(1.25*p_tube_cold-S);

Do=(Di+2*outer_tube_thickness_b);   % outer diameter of outside tube
P_wet = pi*(Di+do);                 % Wet perimeter for outer tube
D_hy = (4*Ac_annulus)/P_wet;        % Hydraulic diameter of outer tube
P_ht = pi*do;
D_ht = (4*Ac_innertube)/P_ht;

q_tube=Q/N;       % Initial heat transfer rate or power for each tube

%%%%%%%%%%%%%%%%%%%%%%%%%%%%%%%%%%%%%%%%%%%%%%%%%%%%%%%%%%%%%%%%%%%%%%%%%%%%
% Intial Value
%%%%%%%%%%%%%%%%%%%%%%%%%%%%%%%%%%%%%%%%%%%%%%%%%%%%%%%%%%%%%%%%%%%%%%%%%%%%

calculate =1;
if (calculate == 1)
   inc = .10;
   iternumber = 20000;
   hxlength = iternumber*inc;
   As = inc*pi*do;

   position = zeros(iternumber, 1);
   position(1,1) = 0;

   T_h_actual = zeros(iternumber, 1);
   T_h_actual(1,1) = T_hot_in;

   T_c_actual = zeros(iternumber, 1);
   T_c_actual(1,1) = T_cold_out;

for i = 2:1:iternumber
   position(i,1) = inc*i-inc;
```

```
%%%%%%%%%%%%%%%%%%%%%%%%%%%%%%%%%%%%%%%%%%%%%%%%%%%%%%%%%%%%%%%%%%%%%%%%%%%%
"while loop" calculate new wall temperature using hot and cold side
thermophysical properties from NIST and comparing it with assumed
values
%%%%%%%%%%%%%%%%%%%%%%%%%%%%%%%%%%%%%%%%%%%%%%%%%%%%%%%%%%%%%%%%%%%%%%%%%%%%

delta_walltemp = 1;
Tw_assume = T_h_actual(i-1,1)-0.10;
Tw(i,1)= Tw_assume;
counterwall(i,1) = 1;

while(abs(delta_walltemp)>0.01)

%%%%%%%%%%%%%%%%%%%%%%%%%%%%%%%%%%%%%%%%%%%%%%%%%%%%%%%%%%%%%%%%%%%%%%%%%%%%
% Hot side
%%%%%%%%%%%%%%%%%%%%%%%%%%%%%%%%%%%%%%%%%%%%%%%%%%%%%%%%%%%%%%%%%%%%%%%%%%%%

% Density bulk
rho_hb_intial(i,1) = refpropm('D','T',T_h_actual(i-
1,1),'P',p_tube_hot,'water');

% Viscosity bulk
mu_hb_intial(i,1) = refpropm('V','T',T_h_actual(i-
1,1),'P',p_tube_hot,'water');

% Thermal conductivity bulk
k_hb_intial(i,1) = refpropm('L','T',T_h_actual(i-
1,1),'P',p_tube_hot,'water');

% Enthalpy bulk
H_hb_intial(i,1) = refpropm('H','T',T_h_actual(i-
1,1),'P',p_tube_hot,'water');

% Cp bulk
Cp_hb_intial(i,1) = refpropm('C','T',T_h_actual(i-
1,1),'P',p_tube_hot,'water'); % Cp bulk

% Density wall
rho_hw_intial(i,1) = refpropm('D','T',Tw(i,1),'P',p_tube_hot,'water');

% Viscosity wall
mu_hw_intial(i,1) = refpropm('V','T',Tw(i,1),'P',p_tube_hot,'water');

% Thermal conductivity wall
k_hw_intial(i,1) = refpropm('L','T',Tw(i,1),'P',p_tube_hot,'water');

% Enthalpy wall
H_hw_intial(i,1) = refpropm('H','T',Tw(i,1),'P',p_tube_hot,'water');

% Average specific heat
Cp_avg_h_intial(i,1) = (H_hw_intial(i,1)-H_hb_intial(i,1))/(Tw(i,1)-
T_h_actual(i-1,1));

% Average Prandtl number
Pr_h_intial(i,1) =
(mu_hw_intial(i,1)*Cp_avg_h_intial(i,1))/k_hw_intial(i,1);
```

```
% Reynolds number
Re_h_intial(i,1) = (4*m_dot_tube_hot)/(pi*di*mu_hw_intial(i,1));

% Swenson et al.(1965)
Nu_h_intial(i,1) = (0.00459 * Re_h_intial(i,1)^0.923 *
Pr_h_intial(i,1)^0.613 * (rho_hw_intial(i,1)/rho_hb_intial(i,1))^0.23);

% Heat transfer coefficient
htc_h_intial(i,1) = (Nu_h_intial(i,1)*k_hw_intial(i,1))/di;

% Resistance
Rconv_h(i,1) = do/(htc_h_intial(i,1)*di);

%%%%%%%%%%%%%%%%%%%%%%%%%%%%%%%%%%%%%%%%%%%%%%%%%%%%%%%%%%%%%%%%%%%%%%%%%%%%
% Tube
%%%%%%%%%%%%%%%%%%%%%%%%%%%%%%%%%%%%%%%%%%%%%%%%%%%%%%%%%%%%%%%%%%%%%%%%%%%%

% Thermal Conductivity
k_tube(i,1) = 0.00000002*(Tw(i,1))^3 - 0.00004*(Tw(i,1))^2 +
0.0398*(Tw(i,1))+ 5.728;

% Resistance of flow tube
Rcond(i,1) = ((do)*(log(do/di)))/(2*k_tube(i,1));

%%%%%%%%%%%%%%%%%%%%%%%%%%%%%%%%%%%%%%%%%%%%%%%%%%%%%%%%%%%%%%%%%%%%%%%%%%%%
% Cold side
%%%%%%%%%%%%%%%%%%%%%%%%%%%%%%%%%%%%%%%%%%%%%%%%%%%%%%%%%%%%%%%%%%%%%%%%%%%%

% Density bulk
rho_cb_intial(i,1) = refpropm('D','T',T_c_actual(i-
1,1),'P',p_tube_cold,'water');

% Viscosity bulk
mu_cb_intial(i,1) = refpropm('V','T',T_c_actual(i-
1,1),'P',p_tube_cold,'water');

% Thermal conductivity bulk
k_cb_intial(i,1) = refpropm('L','T',T_c_actual(i-
1,1),'P',p_tube_cold,'water');

% Enthalpy bulk
H_cb_intial(i,1)= refpropm('H','T',T_c_actual(i-
1,1),'P',p_tube_cold,'water');

% Cp bulk
Cp_cb_intial(i,1) = refpropm('C','T',T_c_actual(i-
1,1),'P',p_tube_cold,'water');

% Density wall
rho_cw_intial(i,1) = refpropm('D','T',Tw(i,1),'P',p_tube_cold,'water');

% Viscosity wall
mu_cw_intial(i,1) = refpropm('V','T',Tw(i,1),'P',p_tube_cold,'water');
```

```
% Thermal conductivity wall
k_cw_intial(i,1) = refpropm('L','T',Tw(i,1),'P',p_tube_cold,'water');

% Enthalpy wall
H_cw_intial(i,1)= refpropm('H','T',Tw(i,1),'P',p_tube_cold,'water');

% Average specific heat
Cp_avg_c_intial(i,1) = (H_cw_intial(i,1)-H_cb_intial(i,1))/(Tw(i,1)-
T_c_actual(i-1,1));

% Average Prandtl number
Pr_c_intial(i,1) =
(mu_cw_intial(i,1)*Cp_avg_c_intial(i,1))/k_cw_intial(i,1);

% Reynolds number
Re_c_intial(i,1) = (4*m_dot_tube_cold)/(pi*(Di+do)*mu_cw_intial(i,1));

% Swenson et al.(1965)
Nu_c_intial(i,1) = (0.00459 * Re_c_intial(i,1)^0.923 *
Pr_c_intial(i,1)^0.613 * (rho_cw_intial(i,1)/rho_cb_intial(i,1))^0.23);

% Heat transfer coefficient
htc_c_intial(i,1) = (Nu_c_intial(i,1)*k_cw_intial(i,1))/D_hy;

% Resistance
Rconv_c(i,1) = 1/(htc_c_intial(i,1));


store_Tw = Tw(i,1);
Tw(i,1) = ((T_h_actual(i-1,1)/Rconv_h(i,1)) + (T_c_actual(i-
1,1)/Rconv_c(i,1)))/(1/Rconv_h(i,1) + 1/Rconv_c(i,1));

delta_walltemp = Tw(i,1)-store_Tw;

if (delta_walltemp == 0.01 || delta_walltemp > 0.01)
    Tw(i,1) = Tw(i,1) - abs(delta_walltemp)/2;
    counterwall(i,1) = counterwall(i,1) + 1;
end

if (delta_walltemp < -0.01)
   Tw(i,1) = Tw(i,1) + abs(delta_walltemp)/2;
   counterwall(i,1) = counterwall(i,1) + 1;
end

if (counterwall(i,1) == 100)
    disp('Error - Iteration Maximum (100) reached')
  break
end

end

U(i,1)  = 1/(Rconv_h(i,1) + Rcond(i,1) + Rconv_c(i,1));
UAs(i,1) = U(i,1)*As;
```

```
%%%%%%%%%%%%%%%%%%%%%%%%%%%%%%%%%%%%%%%%%%%%%%%%%%%%%%%%%%%%%%%%%%%%%%%%%%%%
"while loop" to calculate hot side outlet temperature and cold side
inlet %temperature of a Node
%%%%%%%%%%%%%%%%%%%%%%%%%%%%%%%%%%%%%%%%%%%%%%%%%%%%%%%%%%%%%%%%%%%%%%%%%%%%


delta_mcpdt = 1;
T_c_assume = T_c_actual(i-1,1)-0.10;
T_c_actual(i,1) = T_c_assume;
countertemp(i,1) = 1;

hot_mdotcp(i,1)=m_dot_tube_hot*refpropm('C','T',T_h_actual(i-
1,1),'P',p_tube_hot,'water');
cold_mdotcp(i,1)=m_dot_tube_cold*refpropm('C','T',T_c_actual(i-
1,1),'P',p_tube_cold,'water');

while (abs(delta_mcpdt)>0.01)

T_h_actual(i,1) = ((hot_mdotcp(i,1)-0.5*UAs(i,1))*T_h_actual(i-1,1) +
0.5*UAs(i,1)*(T_c_actual(i,1)...
+ T_c_actual(i-1,1))) / (hot_mdotcp(i,1) + 0.5*UAs(i,1));

storeT_c_actual = T_c_actual(i,1);

T_c_actual(i,1)  = (T_c_actual(i-1,1)*(cold_mdotcp(i,1)+0.5*UAs(i,1))-
0.5*UAs(i,1)*(T_h_actual(i-1,1)...
+ T_h_actual(i,1))) / (cold_mdotcp(i,1) - 0.5*UAs(i,1));

hot_mdotcp_deltatemp(i,1) = hot_mdotcp(i,1)*(T_h_actual(i-1,1) -
T_h_actual(i,1));

cold_mdotcp_deltatemp(i,1) = cold_mdotcp(i,1)*(T_c_actual(i,1) -
T_c_actual(i-1,1));

% Find the difference in Heat Transfer rates
delta_mcpdt = hot_mdotcp_deltatemp(i,1) + cold_mdotcp_deltatemp(i,1);
delta_T_c_actual = storeT_c_actual - T_c_actual(i,1);

if (delta_mcpdt == 0.01 || delta_mcpdt > 0.01)
   T_c_actual(i,1) = T_c_actual(i,1) - abs(delta_T_c_actual)/2;
   countertemp(i,1) = countertemp(i,1) + 1;
end

if (delta_mcpdt < -0.01)
   T_c_actual(i,1) = T_c_actual(i,1) + abs(delta_T_c_actual)/2;
   countertemp(i,1) = countertemp(i,1) + 1;
   end

 if(countertemp(i,1) == 100)
      disp('Heat Balance Error - Iteration Maximum (100) reached'),
      disp(position(i))
   break
 end

end
```

```
% total heat transfer rate taken on hot side (gain to cold side)
q_hot_trans(i,1) = sum(hot_mdotcp_deltatemp);

% total heat transfer rate taken on cold side (loss on hot side)
q_cold_trans(i,1)   = sum(cold_mdotcp_deltatemp);

% Heat flux of a node
q_flux(i,1)=q_hot_trans(i,1)/As;

% if cold side temperature reaches the cold side inlet temperature--end

 if(T_c_actual(i,1)< T_cold_in)
   break
 end

% if q transfer reaches the total q_tube--end
if (q_hot_trans(i,1) > q_tube)
  break
end

end

hxlength_actual = i*inc;
total_hxlength = N*hxlength_actual;

end

 hx_pipe_area = i*As;
 actual_inc = position(i,1);
 total_hx_area = N*hx_pipe_area;
 actual_total_Q = N*max(q_hot_trans);
 T_c_last = min(T_c_actual(i,1));
 T_h_last = min(T_h_actual(i,1));

%%%%%%%%%%%%%%%%%%%%%%%%%%%%%%%%%%%%%%%%%%%%%%%%%%%%%%%%%%%%%%%%%%%%%%%%%%%%%%%
Plotting and Printing of values into EXCEL
%%%%%%%%%%%%%%%%%%%%%%%%%%%%%%%%%%%%%%%%%%%%%%%%%%%%%%%%%%%%%%%%%%%%%%%%%%%%%%%

graph_T_hot=T_h_actual(1:i,:)-273.15;
graph_T_cold=T_c_actual(1:i,:)-273.15;

figure(1);
plot(position(1:i,:),graph_T_hot,'-r', position(1:i,:),graph_T_cold,'-
.b');
hold
xlabel('Length of Hx[m]'); ylabel ('Temperatures[c]');title('Final
Estimate');
```

```
%%%%%%%%%%%%%%%%%%%%%%%%%%%%%%%%%%%%%%%%%%%%%%%%%%%%%%%%%%%%%%%%%%%%%%%%%%%%

columnHeader = {'', 'Node', 'Overall HTC', '',...
    'T Coolant Cold Side', 'T Coolant Hot Side', 'T Wall Outer ', 'Th
Wall Inner', 'T Wall avg', 'q', 'q_sum', 'q"','q"_sum', '',...
    'Cold Fluid Properties','Cp_Avg','Cp_bulk','H wall','H bulk','k
bulk','mu bulk','rho wall','rho bulk','Pr','Re','Nu','h','R
Conv','',...
    'Hot Fluid Properties','Cp_Avg','Cp_bulk','H wall','H bulk','k
bulk','mu bulk','rho wall','rho bulk','Pr','Re','Nu','h','R
Conv','',...
    'k_tube', '', 'Surface Area(m^2)'};


% write data to Excel File, specifying the placement

xlswrite('harwinderinc.xlsx',  columnHeader ,'Sheet1','A1');
xlswrite('harwinderinc.xlsx',  position(1:i,:),'Sheet1','B2');
xlswrite('harwinderinc.xlsx',  U,'Sheet1','C2');

xlswrite('harwinderinc.xlsx',  T_c_actual(1:i,:)-273.15,'Sheet1','E2');
xlswrite('harwinderinc.xlsx',  T_h_actual(1:i,:)-273.15,'Sheet1','F2');
xlswrite('harwinderinc.xlsx',  Tw-273.15,'Sheet1','H2');
xlswrite('harwinderinc.xlsx',  hot_mdotcp_deltatemp,'Sheet1','J2');
xlswrite('harwinderinc.xlsx',  q_hot_trans,'Sheet1','K2');
xlswrite('harwinderinc.xlsx',  q_flux_node,'Sheet1','L2');
xlswrite('harwinderinc.xlsx',  q_flux,'Sheet1','M2');

xlswrite('harwinderinc.xlsx',  Cp_avg_c_intial,'Sheet1','P2');
xlswrite('harwinderinc.xlsx',  Cp_cb_intial,'Sheet1','Q2');
xlswrite('harwinderinc.xlsx',  H_cw_intial,'Sheet1','R2');
xlswrite('harwinderinc.xlsx',  H_cb_intial,'Sheet1','S2');
xlswrite('harwinderinc.xlsx',  k_cb_intial,'Sheet1','T2');
xlswrite('harwinderinc.xlsx',  mu_cb_intial,'Sheet1','U2');
xlswrite('harwinderinc.xlsx',  rho_cw_intial,'Sheet1','V2');
xlswrite('harwinderinc.xlsx',  rho_cb_intial,'Sheet1','W2');
xlswrite('harwinderinc.xlsx',  Pr_c_intial,'Sheet1','X2');
xlswrite('harwinderinc.xlsx',  Re_c_intial,'Sheet1','Y2');
xlswrite('harwinderinc.xlsx',  Nu_c_intial,'Sheet1','Z2');
xlswrite('harwinderinc.xlsx',  htc_c_intial,'Sheet1','AA2');
xlswrite('harwinderinc.xlsx',  Rconv_c,'Sheet1','AB2');

xlswrite('harwinderinc.xlsx',  Cp_avg_h_intial,'Sheet1','AE2');
xlswrite('harwinderinc.xlsx',  Cp_hb_intial,'Sheet1','AF2');
xlswrite('harwinderinc.xlsx',  H_hw_intial,'Sheet1','AG2');
xlswrite('harwinderinc.xlsx',  H_hb_intial,'Sheet1','AH2');
xlswrite('harwinderinc.xlsx',  k_hb_intial,'Sheet1','AI2');
xlswrite('harwinderinc.xlsx',  mu_hb_intial,'Sheet1','AJ2');
xlswrite('harwinderinc.xlsx',  rho_hw_intial,'Sheet1','AK2');
xlswrite('harwinderinc.xlsx',  rho_hb_intial,'Sheet1','AL2');
xlswrite('harwinderinc.xlsx',  Pr_h_intial,'Sheet1','AM2');
xlswrite('harwinderinc.xlsx',  Re_h_intial,'Sheet1','AN2');
xlswrite('harwinderinc.xlsx',  Nu_h_intial,'Sheet1','AO2');
xlswrite('harwinderinc.xlsx',  htc_h_intial,'Sheet1','AP2');
xlswrite('harwinderinc.xlsx',  Rconv_h,'Sheet1','AQ2');
```

```
xlswrite('harwinderinc.xlsx',  Rcond,'Sheet1','AS2');
xlswrite('harwinderinc.xlsx',  total_hx_area,'Sheet1','AU2');

%%%%%%%%%%%%%%%%%%%%%%%%%%%%%%%%%%%%%%%%%%%%%%%%%%%%%%%%%%%%%%%%%%%%%%%%%%%%%%%

rowHeader = {''; 'Total Q (MW)'; 'q_tube(MW)'; 'No. of Pipe'; 'Heat
Transfer Area Pipe (m^2)'; 'Total Heat Transfer Area (m^2)';,...
'Length of Pipe (m)';'Total Length of Pipe (m)';,...
''; 'Hot Side (SCW)'; 'Pressure (MPa)'; 'Inlet Temperature (C)';
'Outlet Temperture (C)'; 'Total mass flow rate (kg/s)'; 'Mass flow rate
pipe (kg/s)';,...
'Mass flux (kg/s.m^2)';'Max flow speed';'Outer diameter-do (m)';'Inner
diameter-di (m)';'Crossection Area Inner (m^2)';,...
''; 'Cold Side (SHS)'; 'Pressure (MPa)'; 'Inlet Temperature (C)';
'Outlet Temperture (C)'; 'Total mass flow rate (kg/s)'; 'Mass flow rate
pipe (kg/s)';,...
'Mass flux (kg/s.m^2)';'Max flow speed';'Outer diameter-Do (m)';'Inner
diameter-Di (m)';'Crossection Area Annulus (m^2)'};

xlswrite('harwinderinc.xlsx',  rowHeader ,'Sheet2','A1');
xlswrite('harwinderinc.xlsx',  actual_total_Q/1000000,'Sheet2','B2');
xlswrite('harwinderinc.xlsx',  max(q_hot_trans)/1000000,'Sheet2','B3');
xlswrite('harwinderinc.xlsx',  N,'Sheet2','B4');
xlswrite('harwinderinc.xlsx',  hx_pipe_area,'Sheet2','B5');
xlswrite('harwinderinc.xlsx',  total_hx_area,'Sheet2','B6');
xlswrite('harwinderinc.xlsx',  hxlength_actual,'Sheet2','B7');
xlswrite('harwinderinc.xlsx',  total_hxlength,'Sheet2','B8');

xlswrite('harwinderinc.xlsx',  p_tube_hot/1000,'Sheet2','B11');
xlswrite('harwinderinc.xlsx',  T_hot_in-273.15,'Sheet2','B12');
xlswrite('harwinderinc.xlsx',  T_h_last-273.15,'Sheet2','B13');
xlswrite('harwinderinc.xlsx',  m_dot_hot,'Sheet2','B14');
xlswrite('harwinderinc.xlsx',  m_dot_tube_hot,'Sheet2','B15');
xlswrite('harwinderinc.xlsx',  G_hot,'Sheet2','B16');
xlswrite('harwinderinc.xlsx',  max(hottubespeed),'Sheet2','B17');
xlswrite('harwinderinc.xlsx',  do,'Sheet2','B18');
xlswrite('harwinderinc.xlsx',  di,'Sheet2','B19');
xlswrite('harwinderinc.xlsx',  Ac_innertube,'Sheet2','B20');

xlswrite('harwinderinc.xlsx',  p_tube_cold/1000,'Sheet2','B23');
xlswrite('harwinderinc.xlsx',  T_c_last-273.15,'Sheet2','B24');
xlswrite('harwinderinc.xlsx',  T_cold_out-273.15,'Sheet2','B25');
xlswrite('harwinderinc.xlsx',  m_dot_cold,'Sheet2','B26');
xlswrite('harwinderinc.xlsx',  m_dot_tube_cold,'Sheet2','B27');
xlswrite('harwinderinc.xlsx',  G_cold,'Sheet2','B28');
xlswrite('harwinderinc.xlsx',  max(coldtubespeed),'Sheet2','B29');
xlswrite('harwinderinc.xlsx',  Do,'Sheet2','B30');
xlswrite('harwinderinc.xlsx',  Di,'Sheet2','B31');
xlswrite('harwinderinc.xlsx',  Ac_annulus,'Sheet2','B32');
```

APPENDIX E: PUBLICATIONS AND CONFERENCES

Four papers have been prepared for participation in international conferences, out of which two conferences have been attended.

Thind, H., Pioro, I., and Harvel, G., 2010. Supercritical Water-cooled Nuclear Reactor with Intermediate Heat Exchangers, Proceedings of the 18th International Conference on Nuclear Engineering (ICONE-17), Xi'an, China, May 17-21. Paper #30104. 10 Pages.

H. Thind, S. Gupta, I. Pioro, and G. Harvel., 2011. Heat-Transfer Analysis of SCW to SCW Double-Pipe Heat Exchanger for Indirect-Cycle SCW NPPS, Proceedings of the 5th Int. Sym. SCWR (ISSCWR-5), Vancouver, British Columbia, Canada, March 13-16, P84, 14 Pages.

Pioro, I., Naidin, M., Mokry, S., Saltanov, Eu., Peiman W., King, K., Farah, A. and **Thind, H**., 2010. General Layouts of SuperCritical-Water NPPS, Proceedings of the 18th International Conference on Nuclear Engineering (ICONE-17), Xi'an, China, May 17-21. Paper #29993, 9 Pages.

I. Pioro, S. Mokry, W. Peiman, E. Saltanov, **H. Thind**, L. Grande, J. Samuel, and G. Harvel., 2010. SuperCritical Water-Cooled Nuclear Reactors: Thermodynamic-Cycles Plant Layouts and Thermal Aspects of Pressure-Channel Design, Proceedings of the European Nuclear Conference (ENC 2010), Barcelona, Spain, May 30 – June 2. 11 Pages.